

---

Final Report

November 2008

UF Project No. 00059422  
Contract No. BD545-64

---

**DEVELOPMENT OF CONCRETE MIXTURES  
CONTAINING HIGHLY REACTIVE POZZOLANS FOR  
IMPROVED DURABILITY IN FLORIDA  
ENVIRONMENTS**

---

Principal Investigator: H. R. (Trey) Hamilton III, P.E., PhD  
Research Engineer: Tanya Nash  
Graduate Research Assistant: Edward Roske  
Project Manager: Charles A. Ishee, P.E.

---

Department of Civil & Coastal Engineering  
College of Engineering  
University of Florida  
Gainesville, Florida 32611

Engineering and Industrial Experiment Station

---



## **DISCLAIMER**

The opinions, findings, and conclusions expressed in this publication are those of the authors and not necessarily those of the State of Florida Department of Transportation.

1. Report No.		2. Government Accession No.		3. Recipient's Catalog No.	
4. Title and Subtitle Development of Concrete Mixtures Containing Highly Reactive Pozzolans for Improved Durability in Florida Environments				5. Report Date November 2008	
				6. Performing Organization Code	
7. Author(s) Edward Roske, Tanya Nash, and H. R. Hamilton III				8. Performing Organization Report No. 00059422	
9. Performing Organization Name and Address University of Florida Department of Civil & Coastal Engineering P.O. Box 116580 Gainesville, FL 32611-6580				10. Work Unit No. (TRAIS)	
				11. Contract or Grant No. BD545-64	
12. Sponsoring Agency Name and Address Florida Department of Transportation Research Management Center 605 Suwannee Street, MS 30 Tallahassee, FL 32301-8064				13. Type of Report and Period Covered Final Report	
				14. Sponsoring Agency Code	
15. Supplementary Notes					
16. Abstract <p>Part 1 of this report describes research that evaluated the use of supplementary cementitious materials (SCM) to improve the service life of bridges constructed in severe marine environments. The SCM studied included ultra-fine fly ash, ground granulated blast furnace slag, silica fume, and metakaolin, in conjunction with fly ash. The plastic, mechanical, and durability properties of concrete made with these SCM were tested. Additionally, mixtures using these SCMs were optimized for use in the precast, prestressed piling for the Key Royale Drive Bridge Replacement Project.</p> <p>Thirteen trial mixtures were prepared using varying proportions of portland cement, fly ash and selected SCM. One of the two control mixtures contained only portland cement and the second contained 18% fly ash cement replacement by weight. The remaining eleven mixtures contained 18% fly ash with varying portions of SCM.</p> <p>Using results from laboratory testing, a decision matrix was created to select the mixture proportions that exhibited the best overall performance for each SCM tested. One mixture from each SCM was selected to be used in the production of piles for the Key Royale Drive Bridge Replacement Project. The decision matrix included ratings for cost, mechanical properties, and durability. Although the costs of several mixtures were considerably higher than the controls, each mixture showed an overall improvement in mechanical and durability properties over that of the controls. Proportions determined to provide the most effective mixtures were those with 30% ground granulated blast furnace slag, 10% metakaolin, 12% ultra-fine fly ash, or 9% silica fume by weight of cement replacement.</p> <p>Part 2 of this report presents research in which microscopy techniques were used to measure chloride concentration in concrete. The experimental program involved preparing portland cement and water pastes that had known quantities of chlorides introduced during mixing. It was found that scanning electron microscope with energy dispersive spectroscopy (SEM/EDS) (using mineral standards) was able to measure chloride content that was within 23% of the titration values in quantities down to 800 ppm. It is recommended that Microprobe (EPMA) with wavelength dispersive spectrometer (WDS) be further evaluated for low values of chlorides.</p>					
17. Key Word Supplementary cementitious materials, pozzolans, concrete durability, microscopy, chloride contamination.			18. Distribution Statement No restrictions. This document is available to the public through the National Technical Information Service, Springfield, VA, 22161		
19. Security Classif. (of this report) Unclassified		20. Security Classif. (of this page) Unclassified		21. No. of Pages 187	22. Price

## **ACKNOWLEDGMENTS**

The authors would like to acknowledge and thank the Florida Department of Transportation for funding this project. We would also like to thank Charles Ishee for his contribution of knowledge and assistance and Richard Delorenzo for making his laboratory expertise available. In addition, the authors would like to thank Kerry Siebein and Amelia Dempere for their microscopy expertise and contribution.

Thanks are also due to Sal Depolis and Wayne Allick Jr. for their assistance in laboratory testing and to Mahir Dham, Christopher Ferraro, Samuel Smith, Yu Chen, Beyoung Il Kim and Xiaoyan Zheng who contributed their time and effort to this research project.

## EXECUTIVE SUMMARY

Part 1 of this report describes research that evaluated the use of supplementary cementitious materials (SCM) to improve the service life of bridges constructed in severe marine environments. The SCM studied included ultra-fine fly ash, ground granulated blast furnace slag, silica fume, and metakaolin, in conjunction with fly ash. The plastic, mechanical, and durability properties of concrete made with these SCM were tested. Additionally, mixtures using these SCMs were optimized for use in the precast, prestressed piling for the Key Royale Drive Bridge Replacement Project.

Thirteen trial mixtures were prepared using varying proportions of portland cement, fly ash and selected SCM. One of the two control mixtures contained only portland cement and the second contained 18% fly ash cement replacement by weight. The remaining eleven mixtures contained 18% fly ash with varying portions of SCM.

Plastic property tests were conducted on temperature, air content, slump, bleeding, and setting times. Mechanical tests included compressive strength, flexural strength, splitting tensile strength, modulus of elasticity, and Poisson's ratio. Several durability tests were also performed including surface resistivity, rapid migration test, volume of voids, absorption, water permeability, shrinkage, sulfate expansion, and corrosion of embedded steel reinforcement.

Using results from laboratory testing, a decision matrix was created to select the mixture proportions that exhibited the best overall performance for each SCM tested. One mixture from each SCM was selected to be used in the production of piles for the Key Royale Drive Bridge Replacement Project. The decision matrix included ratings for cost, mechanical properties, and durability. Although the costs of several mixtures were considerably higher than the controls, each mixture showed an overall improvement in mechanical and durability properties over that of the controls. Proportions determined to provide the most effective mixtures were 30% ground granulated blast furnace slag, 10% metakaolin, 12% ultra-fine fly ash, and 9% silica fume by weight of cement replacement.

Based on the decision matrix, each mixture showed consistent mechanical properties. The silica fume and metakaolin mixtures, however, performed the best overall in the durability tests. Silica fume mixtures showed improvement in the durability over the cement only control ranging from 21% to 23%. Metakaolin also showed improvements of 17% to 20%.

Part 2 of this report presents research in which microscopy techniques were used to measure chloride concentration in concrete. It is the ultimate goal to be able to use microscopy techniques to generate the chloride profile and diffusion coefficient in concrete that has been exposed to salt water. The experimental program involved preparing portland cement and water pastes that had known quantities of chlorides introduced during mixing. The hardened pastes were analyzed with several instruments. It was found that scanning electron microscope with energy dispersive spectroscopy (SEM/EDS) (using mineral standards) was able to measure chloride content that was within 23% of the titration values in quantities down to 800 ppm. SEM/EDS may not have the sensitivity needed to detect the level of chlorides needed for analysis of chloride contaminated concrete below these levels. It is recommended that Microprobe (EPMA) with wavelength dispersive spectrometer (WDS) be further evaluated for low values of chlorides.

# TABLE OF CONTENTS

<b>EXECUTIVE SUMMARY .....</b>	<b>v</b>
<b>PART I - DEVELOPMENT OF MIXTURE DESIGNS FOR KEY ROYALE BRIDGE.....</b>	<b>1</b>
<b>1 INTRODUCTION.....</b>	<b>2</b>
<b>2 LITERATURE REVIEW.....</b>	<b>4</b>
2.1 UNHYDRATED CEMENT CHEMISTRY.....	4
2.2 HYDRATION CHEMISTRY.....	6
2.3 EFFECT OF CEMENT AND SCM ON CONCRETE PROPERTIES.....	7
<b>3 MIXTURE DESIGN.....</b>	<b>21</b>
3.1 MATERIALS .....	21
3.2 PROPORTIONS.....	26
3.3 PREPARATION OF CONCRETE MIXTURES.....	31
3.4 SPECIMEN FABRICATION.....	32
3.5 CURING CONDITIONS.....	32
3.6 ADDITIONAL MIXTURES .....	33
<b>4 LABORATORY TESTING .....</b>	<b>34</b>
4.1 PLASTIC PROPERTIES TESTS .....	34
4.2 MECHANICAL TESTS .....	37
4.3 DURABILITY TESTS .....	43
<b>5 RESULTS AND DISCUSSION .....</b>	<b>53</b>
5.1 PLASTIC PROPERTIES TESTS .....	53
5.2 MECHANICAL TESTS.....	54
5.3 DURABILITY TESTS .....	70
<b>6 SELECTION OF MIXTURE DESIGNS FOR PILES .....</b>	<b>89</b>
6.1 SELECTION APPROACH .....	89
6.2 SELECTION CRITERION I – COST .....	89
6.3 SELECTION CRITERION II – MECHANICAL PROPERTIES.....	90
6.4 SELECTION CRITERION III – DURABILITY.....	91
6.5 IMPORTANCE FACTORS .....	91
<b>7 CONCLUSIONS AND RECOMMENDATIONS .....</b>	<b>93</b>
<b>8 REFERENCES.....</b>	<b>95</b>
<b>PART 2 – DETECTING CHLORIDE CONCENTRATION USING MICROSCOPY.....</b>	<b>100</b>
<b>1 INTRODUCTION.....</b>	<b>101</b>
<b>2 INSTRUMENT THEORY AND BACKGROUND.....</b>	<b>102</b>
2.1 SCANNING ELECTRON MICROSCOPE.....	102
2.2 X-RAY MICROSCOPE .....	106
2.3 COMPOSITIONAL IDENTIFICATION .....	106
<b>3 PILOT STUDY.....</b>	<b>110</b>
3.1 MATERIAL AND SAMPLE PREPARATION .....	110
3.2 EXPERIMENTAL .....	111
3.3 RESULTS AND DISCUSSION .....	114
<b>4 ALTERNATIVE TECHNIQUES AND INSTRUMENTATION .....</b>	<b>116</b>

4.1	MICHIGAN TECH UNIVERSITY .....	116
4.2	MATERIALS .....	116
4.3	SAMPLE PREPARATION .....	117
4.4	CHLORIDE PROFILING .....	119
4.5	RESULTS AND CALIBRATION.....	123
4.6	ALTERNATIVE APPROACH.....	132
<b>5</b>	<b>SENSITIVITY STUDY .....</b>	<b>135</b>
<b>6</b>	<b>CONCLUSIONS .....</b>	<b>138</b>
<b>7</b>	<b>FUTURE RESEARCH.....</b>	<b>140</b>
<b>8</b>	<b>REFERENCES.....</b>	<b>141</b>
	<b>APPENDIX A – LABORATORY MIXTURE TESTING DATA .....</b>	<b>142</b>
	PLASTIC PROPERTIES TESTS .....	142
	MECHANICAL PROPERTIES TESTS .....	142
	DURABILITY TESTS .....	146
	RELATIVE HUMIDITY IN DRY CURING ROOM.....	148
	TEMPERATURE IN DRY CURING ROOM .....	149
	CORROSION OF EMBEDDED STEEL REINFORCEMENT .....	150
	<b>APPENDIX B – LABORATORY MIXTURE NORMALIZED DATA .....</b>	<b>155</b>
	COST .....	155
	MECHANICAL TESTS .....	155
	DURABILITY TESTS .....	156
	SUMMARY.....	156
	<b>APPENDIX C – SAMPLE PREPARATION FOR XGT AND SEM ANALYSIS.....</b>	<b>157</b>
	<b>APPENDIX D - PILOT STUDY SEM/EDS DATA.....</b>	<b>167</b>

# **PART I - DEVELOPMENT OF MIXTURE DESIGNS FOR KEY ROYALE BRIDGE**

by Edward Roske and H. R. Hamilton III

## 1 INTRODUCTION

The Florida Department of Transportation (FDOT) has set a goal to build bridges that will last at least 100 years. Currently, the acceptance criteria consist of measuring the plastic properties, water-to-cementitious ratio and compressive strength. None of these acceptance criteria can be used to predict the ultimate service life of the structure. By performing more durability-related tests on local materials, the Department can develop a better understanding of how long a structure can be expected to last.

Current FDOT design standards (FDOT Structures Manual [2008]) allow only silica fume for improving the chloride resistance of concrete. Silica fume is currently specified in Florida concretes under certain conditions: “[W]hen the environmental classification is Extremely Aggressive due to the presence of chloride in the water, specify silica fume in the splash zone of all piles, columns or walls.” (Section 1.4.3) Silica fume is typically used for the entire pile, column or wall. The splash zone is the vertical distance from 4 feet below MLW to 12 feet above MHW. Under new specifications proposed by AASHTO, other materials could be allowed in place of silica fume for concrete placed under such conditions.

Mixtures containing highly-reactive supplementary cementitious materials (SCM) such as metakaolin and superfine fly ash are purported to provide similar strength and durability as silica fume, while avoiding the detrimental workability issues. Currently, the availability and cost of the highly reactive SCM designated in this study are sometimes better than that of silica fume. Newer materials, however, require investigation to determine which mixture design criteria should be implemented in order to provide the desired service life to FDOT structures.

The present research evaluated the durability and mechanical properties of concrete made with highly reactive SCM other than silica fume. Four of these concrete mixture designs were selected for use in fabricating piles for a bridge structure to be built in a severely aggressive environment. The field project was funded by the Federal Highway Administration through their Innovative Bridge Research & Construction (IBRC) program.

This investigation tested several alternative materials to provide the FDOT with the means to assess the applicability for utilization in the splash zone of a Florida concrete in a severely aggressive environment. These materials include slag, metakaolin, and ultrafine fly ash. Research was conducted on the effects of implementing these highly reactive pozzolanic materials in conjunction with fly ash to the plastic, mechanical, and durability properties of

portland cement concrete. Additionally, this study provided the FDOT with a recommendation of the most effective mixtures containing various SCM for the utilization in the piling of the Key Royale bridge replacement project.

## 2 LITERATURE REVIEW

Presently, the Florida Department of Transportation (FDOT) only allows the use of silica fume in the splash zone of concretes in a severely aggressive environment. There are, however, several other Supplementary Cementitious Materials (SCM) that provide improvement in the mechanical and durability characteristics of a concrete. Many researchers have presented data relating to the effects of SCM on the plastic, mechanical, and durability properties of a concrete. Therefore, this chapter presents a comprehensive review of the currently available literature.

### 2.1 UNHYDRATED CEMENT CHEMISTRY

Portland cement is hydraulic cement which is typically produced by initially heating limestone with clay in 2500 to 2900°F kiln to produce clinker (Mindess et al. 2003). The clinker is then ground to a specific fineness. Small amounts of gypsum are interground with the clinker to control the hydration rate of the finished cement product.

Shorthand notation used to represent the actual chemical formulas for oxides found in cements and SCM are shown in Table 1. Chemical compounds that are the major constituents in cement are formed from these oxides in the calcining process of cement manufacturing. The chemical name, chemical formula and shorthand notation for the five most abundant compounds are found in Table 2.

Table 1 - Typical oxides and their shorthand notations

Common Name	Chemical Formula	Shorthand Notation
Lime	CaO	C
Silica	SiO <sub>2</sub>	S
Alumina	Al <sub>2</sub> O <sub>3</sub>	A
Ferric Oxide	Fe <sub>2</sub> O <sub>3</sub>	F
Magnesia	MgO	M
Alkali	K <sub>2</sub> O	K
Alkali	Na <sub>2</sub> O	N
Sulfur Trioxide	SO <sub>3</sub>	Ŝ
Carbon Dioxide	CO <sub>2</sub>	Ĉ
Water	H <sub>2</sub> O	H

Table 2 - Typical chemical compounds and their shorthand notations

Chemical Name	Chemical Formula	Shorthand Notation
Tricalcium Silicate	$3\text{CaO}\cdot\text{SiO}_2$	$\text{C}_3\text{S}$
Dicalcium Silicate	$2\text{CaO}\cdot\text{SiO}_2$	$\text{C}_2\text{S}$
Tricalcium Aluminate	$2\text{CaO}\cdot\text{Al}_2\text{O}_3$	$\text{C}_3\text{A}$
Tetracalcium Aluminoferrite	$4\text{CaO}\cdot\text{Al}_2\text{O}_3\cdot\text{Fe}_2\text{O}_3$	$\text{C}_4\text{AF}$
Calcium Sulfate Dihydrate (gypsum)	$\text{CaSO}_4\cdot 2\text{H}_2\text{O}$	$\text{C}\hat{\text{S}}\text{H}_2$

Estimations of the quantity of these compounds can be made through equations found by R.H. Bogue and others (Neville 1995). These calculations, known as Bogue equations, are used to predict the properties of cement, such as rate of strength development and heat liberation. Moreover, manipulation of the cement, based on results of these equations, can be made to modify certain properties to make it more appropriate to a particular application (Mindess et al. 2003). The formula is shown in Table 3. A/F represents the % mass ratio of alumina to ferric oxide.

Table 3 – Bogue equations

<b>Case A:</b>	<b>A/F ≥ 0.64</b>
	$\text{C}_3\text{S} = 4.071\text{C} - 7.600\text{S} - 6.718\text{A} - 1.430\text{F} - 2.852\hat{\text{S}}$
	$\text{C}_2\text{S} = 2.867\text{S} - 0.7544 \text{C}_3\text{S}$
	$\text{C}_3\text{A} = 2.650\text{A} - 1.692\text{F}$
	$\text{C}_4\text{AF} = 3.043\text{F}$
<b>Case B:</b>	<b>A/F &lt; 0.64</b>
	$\text{C}_3\text{S} = 4.071\text{C} - 7.600\text{S} - 4.479\text{A} - 2.859\text{F} - 2.852\hat{\text{S}}$
	$\text{C}_2\text{S} = 2.867\text{S} - 0.7544 \text{C}_3\text{S}$
	$\text{C}_3\text{A} = 0$
	$\text{C}_4\text{AF} = 2.100\text{A} + 1.702\text{F}$

Each cement and mineral admixture is composed of some or all of these compounds and oxides. A more detailed analysis of the typical compositions for each material is discussed in the following section.

## 2.2 HYDRATION CHEMISTRY

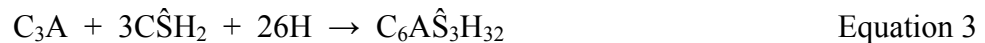
### 2.2.1 CEMENT HYDRATION

The hydration of the calcium silicates in portland cement produces calcium silicate hydrate and calcium hydroxide. The  $C_3S$  and  $C_2S$  reactions are very similar, with the only difference being the quantity of calcium hydroxide (CH) formed. The following equations provide a summary of the primary reactions with some of the intermediate reactions omitted for clarity.



The composition of this calcium silicate hydrate product can vary widely—typically in water content. Presented here, the product is in its saturated state. In contrast, CH has a fixed composition.

Hydration of  $C_3A$  occurs in the presence of sulfate ions supplied by the dissolution of gypsum. These ions react with  $C_3A$  to form a calcium sulfoaluminate hydrate, or more commonly, ettringite:



The ettringite can transform to a different form of calcium sulfoaluminate hydrate if the sulfate is consumed before the  $C_3A$  is completely hydrated as indicated in the following equation:



This form is called monosulfoaluminate. If a new source of sulfate ions comes in contact with this product, ettringite can be reformed:



## 2.2.2 POZZOLANIC HYDRATION

Pozzolans are not cementitious, but rather amorphous silica which will react with CH and water to form a cementitious product, C-S-H:



If the silica content in the pozzolan is very high, a secondary reaction will occur:



When the pozzolan has large quantity of reactive alumina, the CH will react with alumina to form a calcium aluminate hydrate (C-A-H):



Other compounds besides C-A-H may form depending on the composition of the pozzolan such as  $\text{C}_2\text{AH}$ ,  $\text{C}_2\text{ASH}_8$ , or monosulfoaluminate.

## 2.3 EFFECT OF CEMENT AND SCM ON CONCRETE PROPERTIES

### 2.3.1 PORTLAND CEMENT

Portland cements are produced with a specific composition and fineness to ensure a satisfactory performance for a particular application, such as high early strength or low heat of hydration. ASTM created a cement classification to standardize cements so that a more consistent product can be manufactured. These standardized cements are designated ASTM Types I, II, III, IV, and V.

The ASTM Type I is the most commonly used cement, as it is general purpose. It has average strength gain and heat of hydration. However, if a more specialized application, such as sulfate resistance or high early strength development, is needed, a different type should be selected. Type V cements was developed to combat sulfate attack. Sulfate attack involves the hydration products formed from  $\text{C}_3\text{A}$ . Therefore, lowering the percentage of  $\text{C}_3\text{A}$  will serve to increase the sulfate resistance of cement. Type III cement was developed to create a high early strength concrete. This was accomplished by increasing the proportions of  $\text{C}_3\text{S}$  or, more

effectively, grinding the cement finer. However, much heat is generated during the hydration process because of the increase surface area of  $C_3S$ . Therefore, this cement cannot be used where high temperatures create adverse effects, such as in mass concrete, where thermal cracking can become a problem. It is for this reason that Type IV was created. Type IV cement was developed to create a low heat of hydration product. The proportions of the highly exothermic compounds,  $C_3A$  and  $C_3S$ , were reduced. However, there are problems associated with this cement also. Because of the lower  $C_3S$  composition, this cement has a slow strength gain; therefore, a Type II cement was developed. The  $C_3S$  proportion remains the same, while  $C_3A$  is slightly lowered. This cement has a better strength development, as well as being fairly sulfate resistant. Table 4 was recreated from Mindess (et al. 2003), detailing typical chemical compositions and properties of ASTM Types I to V cements.

Table 4 - Typical chemical compositions and properties of ASTM Type I to V cements

	<b>I</b>	<b>II</b>	<b>III</b>	<b>IV</b>	<b>V</b>
$C_3S$	55	55	55	42	55
$C_2S$	18	19	17	32	22
$C_3A$	10	6	10	4	4
$C_4AF$	8	11	8	15	12
$C\bar{S}H_2$	6	5	6	4	4
Fineness ( $m^2/kg$ )	365	375	550	340	380

### 2.3.2 FLY ASH

Fly ash is precipitated from the exhaust gases of a coal burning power station. The majority of particles are spherical, glassy, and either hollow or solid in shape and have a high fineness. Typically, particles have a diameter range of 1  $\mu m$  to 100  $\mu m$  and a specific surface between 250 to 600  $m^2/kg$  (Neville 1995). The main components in the composition of fly ash are oxides of silicon, aluminum, iron, and calcium. The varying calcium content in fly ash composition led to the creation of ASTM C 618. This standard created two classes of fly ash—Class C and Class F. ASTM C 618 requires a Class F fly ash to be composed of a minimum of 70% silicon oxide ( $SiO_2$ ) plus aluminum oxide ( $Al_2O_3$ ) plus iron oxide ( $Fe_2O_3$ ), while a Class C has a minimum of 50%. Derived from the burning of subbituminous coal or lignite, Class C fly ash has a high lime ( $CaO$ ) content. Because of this, it is also slightly cementitious. Problems arise with high water demand, early stiffening, and rapid setting. Class F fly ash is derived from the burning of bituminous coal or anthracite. Its calcium content is lower than a Class C fly ash.

Because fly ash is a pozzolan, the silica and alumina will react with CH to form a cementitious compound, C-S-H and C-A-H, respectively. The reactions depend on the breakdown and dissolution of silica and alumina by the hydroxide ions and heat generated by the hydration of portland cement. The glass material in fly ash is only broken down when the pH value of the pore water is at least 13.2 (Neville 1995). In other words, the fly ash will consume CH and form a hydration product as long as enough CH is present in the pore solution and there is sufficient void space present for the hydration product to fill.

Fly ash influences the properties of a fresh concrete in a variety of ways. Workability, bleeding, and time of setting are all affected by the addition of fly ash. For the most part, the changes due to the addition of fly ash are because of the shape and size of the particles and its chemical composition.

A reduction in water demand and an increase in workability is attributed to the spherical shape of the particles. The particle shape reduces the interparticle friction within the mixture, effectively increasing the workability. This also allows for a reduction in water to keep the same workability for a concrete mixture. Neville (1995) indicates that another mechanism of fly ash may be dominant in decreasing the water demand. The finer fly ash particle may become electrically charged and cover the surface of the cement particles. This defloculates the cement particles, thus reducing the water demand for a given workability. Another benefit of fly ash is the small particle size, which allows them to pack between the cement particles. This is known as particle packing; it reduces bleeding, lowers the mean size of the capillary pores, and can reduce water requirements (Mindess et al. 2003).

The composition of fly ash also extends setting times and decreases the overall heat liberated during hydration. Delayed setting times are ascribed to the slow pozzolanic reactions of fly ash. As mentioned above, the glassy fraction of fly ash will only breakdown when sufficient hydroxide ions are present in the pore solution. This process takes place only after a certain amount of hydration of portland cement has taken place (Neville 1995). A consequence of the delay in the cement hydration is the slow pattern of heat evolution. Much of the heat is generated during the early stages of hydration of the  $C_3S$  and  $C_3A$  within the paste. The delayed setting time allows the concrete to slowly liberate the heat generated. In addition, when fly ash is used as a cement replacement, smaller quantities of the high heat generating compounds,  $C_3S$  and  $C_3A$ , are present. Therefore, the overall heat of hydration is reduced.

Fly ash influences the properties of a hardened concrete in a variety of ways. Compressive strength and rate of strength gain, modulus of elasticity, permeability, sulfate resistance, and drying shrinkage are all affected by the addition of fly ash. For the most part, the changes due to the addition of fly ash are because of the shape and size of the particles and its chemical composition.

The rate of strength gain is reduced by the addition of a Class F fly ash. As mentioned above, the pozzolanic reactions of fly ash depend on a high pH pores solution. Because this takes time to occur, the early hydration of mixtures containing fly ash is slow. Consequently, the early age compressive strengths are low. However, over time, the Class F fly ash will react to produce a stronger concrete than that of the same mixture containing only portland cement (ACI 232.2R-03). Conversely, Class C fly ash concrete often exhibit higher rate of reaction at early ages, but lower strength gain at late ages when compared to a Class F fly ash concrete (ACI 232.2R-03).

ACI (232.2R-03) has found that the effects of fly ash on the modulus of elasticity are not as significant as the effects on compressive strength. Furthermore, they suggest that cement and aggregate characteristics will have a greater effect on modulus of elasticity than the use of fly ash. Similar to modulus of elasticity, creep strain is more affected by compressive strength than fly ash. Lower compressive strengths result in higher creep strains (ACI 232.2R-03).

The consequence of using the slow reacting fly ash is that the initial permeability is higher than that of the same concrete containing only portland cement (Neville 1995). However, over time the fly ash concrete will develop a very low permeability through pozzolanic reactions (ACI 232.2R-03). CH is susceptible to leaching, leaving voids in which deleterious solution can ingress. However, fly ash chemically combines with CH to form a cementitious product, C-S-H. This action reduces the risk of leaching, and further reduces permeability as the pore structure becomes occupied with C-S-H. Consequently, the durability of a concrete exposed to aggressive environments containing sulfates and chlorides is improved because of the reduction in permeability (Neville 1995). In addition, sulfate resistance is further improved through the removal of CH (Mindess et al. 2003).

### 2.3.3 ULTRA-FINE FLY ASH

Ultrafine Fly ash, similar to ordinary fly ash, is precipitated from the exhaust gases of a coal burning power station. The larger particles are removed through filters or separators and

they are spherical, glassy, and either hollow or solid in shape and have a very high fineness. Boral (2003) states that the average particle diameter is 3  $\mu\text{m}$  and the distribution of particle size are minimum of 50% of particle sizes less than 3.25 microns and minimum of 90% of particle sizes less than 8.50 microns.

Little research has been conducted on the effects of ultrafine fly ash on the durability and mechanical properties of a concrete. However, estimations on the behavior can be made through relations with ordinary fly ash based upon chemical composition and particle size. The addition of ultrafine fly ash will influence the properties of a fresh concrete similarly to ordinary fly ash. Differences in workability and bleeding from that of ordinary fly ash are attributed to the smaller average particle size.

The higher surface area of the ultrafine particles increases water demand. Therefore, the addition of ultrafine fly ash reduces workability when compared to ordinary fly ash. However, workability is increased when using ultrafine fly ash as a replacement for portland cement (Boral 2003). Bleeding is also affected by the particle size. The ultrafine fly ash particles will pack between cement grains and aggregate. Consequently, the mixture is more cohesive and a reduction in bleeding is achieved.

Jones (et al. 2003) conducted 72 hour heat of hydration experiments on 30% ultrafine fly ash and 30% ordinary fly ash mixtures. Because of the retardation of  $\text{C}_3\text{A}$  hydration, the rate of heat evolution was impeded by 2 hours and 5 hours for the ordinary fly ash and ultrafine fly ash mixtures, respectively. They have shown that both mixtures lower the total heat of hydration when compared to the control. The ultrafine fly ash mixture showed the lowest total heat until 18 hours. Beyond 18 hours, the ordinary fly ash mixture had the lowest total heat.

Because the mineral composition is the same, ultrafine fly ash will have similar chemical reactions to that of ordinary fly ash. However, because the average particle size of ultrafine fly ash is much smaller, the reactivity will increase. Consequently, the strength and durability on the concrete will be higher at early ages.

Boral (2003) found that at 7 days there is an increase in strength activity index of 107% of the control, and 124% at 28 days. Furthermore, they have conducted compressive strength tests on 8% silica fume, 6% ultrafine fly ash, and 9% ultrafine fly ash mixtures with the following characteristics: w/cm of 0.26 – 0.28, cement = 823  $\text{lb}/\text{yd}^3$ , and fly ash = 100  $\text{lb}/\text{yd}^3$ . They have shown that a 6% replacement of ultrafine fly ash has nearly equal compressive strength at 7 and 28 days, and roughly a 5% increase at 91 days when compared to an 8% silica

fume concrete. A 9% replacement showed increases over the 8% silica fume concrete of roughly 6%, 8%, and 11% at 7, 28, and 91 days, respectively. Jones (et al. 2006) researched the effects of 15% and 30% replacements of ordinary and ultrafine fly ash at a 0.50 w/cm on cube strength. They found that at 28 days, the control mixture had the highest strength (Table 5). At 90 and 180 days, both ultrafine fly ash mixtures showed higher strength than the control, while both ordinary fly ash mixtures were lower.

Table 5 - Summary of comparing cube strength (Jones et al 2006)

Mixture	% of Control		
	28 day	90 day	180 day
Control	100	100	100
15% Ordinary Fly Ash	75	85	87
30% Ordinary Fly Ash	54	30	64
15% Ultrafine Fly Ash	96	116	110
30% Ultrafine Fly Ash	87	102	104

At each age, the ultrafine fly ash mixtures showed an improvement over the ordinary fly ash (Table 6). Therefore, it is evident that the decreased particle size of the ultrafine fly ash increases the strength development at early ages.

Table 6 - Percent improvement of ultra-fine fly ash vs. ordinary fly ash

Mixture	% of Ordinary Fly ash		
	28 day	90 day	180 day
15% Ultrafine Fly Ash	27	36	39
30% Ultrafine Fly Ash	61	45	64

Research conducted by Boral (2003) has also shown improvement in concrete mixtures containing ultrafine fly ash in reducing chloride penetration. They measured chloride diffusion coefficients for 8% silica fume, 8% ultrafine fly ash, and 12% ultrafine fly ash mixtures (0.40 w/cm) at 40 days and 2 years. At both ages, the ultrafine fly ash mixtures showed lower coefficients when compared to the control. It appears that the 12% replacement showed slightly better results than the 8% mixture. Neither ultrafine fly ash mixture, however, had lower coefficients than the silica fume mixture.

Jones (et al. 2003) researched the effects of 30% replacement of ordinary fly ash and ultrafine fly ash on the total CH content within a mixture. They found that from age of 3 days to 90 days, the ultrafine fly ash mixtures showed a lower CH content when compared to the ordinary fly ash mixtures. This indicates that ultrafine fly ash is more reactive and has consumed more CH through pozzolanic reactions

#### 2.3.4 SLAG

Blast furnace slag is the residue wastes formed from the production or refinement of iron. Slag is removed from the molten metal and rapidly cooled. The raw slag is then dried and ground to a specific fineness so that it can be used as a cement replacement. ASTM C 989 provides three grades for slag based upon its relative strength to a reference mortar made with pure cement (Table 7).

Table 7 - Slag activity index (ASTM C 989)

<b>Designation</b>	<b>7 day</b>	<b>28 day</b>
Grade 80	---	75%
Grade 100	75%	95%
Grade 120	95%	115%

Typically, silica, calcium, aluminum, magnesium and oxygen constitute over 95% of the chemical composition of slag (ACI 233R-03). Because of the high lime content, slag is a hydraulic admixture, meaning it will react with water to form a cementitious compound.

Concrete containing slag as a portion of the cementitious materials typically have better workability in the fresh state than that of similar concrete with portland cement alone. This is thought to be due to smooth dense surface of the particles that absorb little water during mixing. This results in better particle dispersion and fluidity of the paste. (ACI 233R-03)

Neville (1995) has suggested that slag leads to retardation of setting times at normal temperatures of typically 30 to 60 minutes. ACI (233R-03) has found that setting times of slag mixtures is significantly affected by portland cement setting characteristics and the amount of portland cement within the mixture. They state that setting times are delayed when more than 25% slag is used as a replacement.

Bleeding is typically reduced when slag is ground to a high fineness (finer than portland cement) and used as a replacement for portland cement. If the slag particles are larger than those of portland cement, then the rate and amount of bleeding may increase.

The addition of slag in a mixture increases the silica content and decreases the total lime content. Consequently, more C-S-H is produced resulting in a microstructure that is denser than that of a cement only mixture (Neville 1995). However, the rate of strength gain is initially very slow because of the presence of impervious coatings of amorphous silica and alumina on the slag particles (Mindess et al. 2003). These coatings are broken down in a slow process by hydroxyl ions that are released during the hydration of the portland cement (Neville 1995).

ACI (233R-03) has found that when compared with a portland cement only concrete, the use of Grade 120 slag typically reduces the strength at ages before 7 days; at 7 days and later, Grade 120 slag increases strength. Grade 100 slag reduces strength at ages less than 21 days, while producing equal or greater strength at later ages. Grade 80 slag shows lower strength at ages less than 28 days, and comparable strength at 28 days and later.

Modulus of rupture is generally increased with the addition of slag at ages beyond 7 days (ACI 233R-03). They suggest that the improvement in modulus of rupture is because of an increased density of the paste and improved bond at the aggregate-paste interface. Neville (1995) has stated that the incorporation of slag does not significantly alter the usual relations between compressive strength and modulus of rupture.

The use of slag in concrete that is water cured does not have an effect on early modulus of elasticity. At later ages, however, modulus is increased ACI (233R-03). Conversely, air cured specimen exhibited reductions in modulus, which is attributed to inadequate curing. Because modulus of elasticity is most dominantly affected by porosity, prolonged moist curing is particularly important in a slag concrete in which the low early hydration results in a system of capillary pores which allow for the loss of water under dry conditions (Neville 1995). Consequently, hydration is halted, leaving a porous concrete and reduced modulus of elasticity.

This compound adds to the strength of the mix, while also increasing durability by decreasing the interconnectivity of the voids. In addition, the high silica and alumina content promote pozzolanic reactions. The CH produced from cement hydration will be consumed and transformed into more cementitious compounds. These compounds are in the forms of C-S-H or C-A-H, depending on whether the reactive compound was silica or alumina. These new hydration products are denser and more homogenous than that produced by cement hydration alone.

At early ages, the incorporation of slag in a mixture will increase shrinkage; however, at later ages shrinkage and creep are not adversely affected (Neville 1995). ACI (233R-03) supports the statement in which there is no significant affect on shrinkage or creep.

The heat of hydration has been found by ACI (233R-03) to be lower in a 75% slag replacement concrete than in a 30% fly ash concrete or cement only concrete. Slag reduced the early rate of heat generation and lowered the peak temperature.

One benefit of the addition of slag into a concrete arises from the denser microstructure of hydrated cement paste in which more of the pore space is filled with C-S-H than in a cement only paste (Neville 1995). As a result, the permeability is decreased. ACI (233R-03) has found that as the slag content increases, the permeability decreases. Consequently, the resistance to sulfate attack is increased. The resistance to sulfate attack is further increased through consumption of CH, the major component in sulfoaluminate corrosion (Mindess et al 2003). ACI (233R-03) found that 50% blends of slag with a Type I concrete had the same sulfate resistance as a Type V cement concrete. They have found that the use of slag in a well hydrated concrete reduces the penetrability of chloride ions and the depth of carbonation. However, Neville (1995) presents conflicting opinions regarding improvements in depths of carbonation with the addition of slag. Slag can have a detrimental effect at early ages when there is very little CH present in the concrete. Because of the decreased presence, CH cannot react with carbon dioxide to form calcium carbonate in the pores. Consequently, the depth of carbonation is significantly greater than in a concrete containing only cement. Conversely, the reduced permeability of slag concrete at later ages prevents continued increases in depth of carbonation.

### 2.3.5 METAKAOLIN

Metakaolin is manufacture by calcining kaolin or kaolinite clays at temperatures between 650 and 800°C (Vu 2002). This results in a material that is largely composed of highly reactive amorphous aluminosilicates. Mindess (et al. 2003) has reported that, typically, the reactive silica and alumina content in metakaolin ranges from about 55% and 35 to 45%, respectively. The particles are plate-like and have an average size of 1 to 2  $\mu\text{m}$ , with a surface area of about 15  $\text{m}^2/\text{g}$ . ACI (232.1R-00) has reported an average size of highly reactive metakaolin to range from 1 to 20  $\mu\text{m}$ . Through pozzolanic reactions, CH will react with both silica and alumina to form a cementitious hydration product. These can be in the form of C-S-H or C-A-H, depending on

whether the reactive compound is silica or alumina, which are denser and more homogenous than that produced by cement hydration alone. (Mindess et al. 2003).

Zongjin and Ding (2003) have found that a 10% blend of metakaolin reduces the fluidity of the mixture. They have shown that the water demand was increased by roughly 11%, which is attributed to the plate-like particle shape and its tendencies to absorb water. Setting times were also shown to decrease by 26% and 36% for initial and final setting times. ACI (232.1R-00) has reported lower adiabatic temperatures for 15 and 30% metakaolin replacements over a cement only concrete. Conversely, a 10% replacement showed higher temperatures when compared to the control.

ACI (232.1R-00) has shown improvements in compressive strength of 0.3 and 0.4 w/cm concretes with blends of 8 and 12% metakaolin. At ages up to 45 days, each metakaolin mixture showed higher compressive strengths; compressive strength increased as proportion increased and w/cm decreased. Badogiannis (et al 2005) researched the strength development of 0.4 w/cm concrete with metakaolin replacements rates of 10% and 20%. Compressive strength was tested at ages of 1 to 180 days. They have shown that, at these ages, a 10% replacement will increase the compressive strength. However, 20% replacement has shown that the compressive strength was not higher than the control until ages of 7 days and later. In addition, the 20% replacement concrete showed lower compressive strength than the 10% blend at all ages.

Kim (et al. 2007) conducted research on metakaolin blends of 5, 10, 15, and 20%. They have shown that there is no significant effect on the flexural strength or splitting tensile strength for replacement levels of 5 to 15%. A slight decrease in strength, however, was noted in the 20% blends at ages less than 28 days.

ACI (232.1R-00) has reported improvements in chloride penetration resistance for both 0.3 and 0.4 w/cm concretes with an 8 and 12% blend of metakaolin. Furthermore, they state that the 12% replacement improved the chloride penetration resistance more than reducing the w/cm from 0.4 to 0.3 in a concrete containing no metakaolin. By reducing the w/cm from 0.4 to 0.36, chloride permeability values for a 10% metakaolin concrete were reduced. Research conducted by Kim (et al. 2007) supports the findings by ACI, in which increasing metakaolin contents (5 to 20%), reduce chloride ion penetrability at 28, 60, and 90 days. They have also reported on the effects of increasing metakaolin contents on the depth of carbonation. They have found that increasing metakaolin contents will increase the depth of carbonation at age of 7, 14, 28, and 56 days. This data suggests that decreased in CH present in the concrete because of the pozzolanic

reaction with the additional metakaolin can have a detrimental effect. Because of the decreased presence, CH cannot react with carbon dioxide to form calcium carbonate in the pores (Neville 1995). Consequently, the depth of carbonation is significantly greater in the metakaolin concretes than in a concrete containing only cement. However, the reduced permeability of metakaolin concrete at later ages prevents continued increases in depth of carbonation.

### 2.3.6 SILICA FUME

A by-product of producing silicon metals or ferrosilicone alloys, silica fume is a highly reactive pozzolanic material that is commonly used as a cement replacement in concrete. Escaping gases condense to form a large quantity of highly amorphous silicon dioxide, typically 85 to 98% by weight (ACI 234R-06). Its particle size is very small, typically 0.1 to 0.3 $\mu$ m with a surface area of 15 to 25 m<sup>2</sup>/g, and spherical in shape (Mindess et al 2003). Silica fume is typically supplied in densified or pelletized form.

Because of the large surface area, silica fume has a higher water demand which must be offset in low w/cm mixtures with a superplasticizer (Neville 1995). However, it was found that the effectiveness of the superplasticizer is enhanced in a silica fume mixture. This is because of its spherical shape and small particle size which allow it to pack between cement particles and act as a lubricant (Mindess et al. 2003). Further benefit of the small silica fume particles packing between cement grains is the reduction in bleeding (Neville 1995). ACI (234R-06) has stated that bleeding is reduced as the content of silica fume is increased because very little free water is available to bleed.

Typically, air entraining admixture in a silica fume concrete must be increased by 125 to 150% over that of similar concrete with cement only (ACI 234R-06). This has been attributed to the high surface area of the particle (Neville 1995).

ACI (234R-06) indicates that there is no significant delay in setting time. However, they have shown that there is an increase in heat of hydration. Peak temperatures increase with higher contents of silica fume because of its interactions with C<sub>3</sub>S. Silica fume tends to accelerate the exothermic hydration of C<sub>3</sub>S; consequently, more CH is produced. In turn, this action starts the pozzolanic reaction with the silica fume, which further increases the concrete temperature. They have also suggested, however, that the total heat is somewhat decreased as the increase in silica fume dosage.

The effect of silica fume on the hardened properties is directly a function of the pore structure, cement paste-aggregate transition zone, and chemical composition (ACI 234R-06). As hydration continues, the pore structure becomes more homogenous and capillary pores sizes are reduced and become disconnected (Neville 1995). However, ACI (234R-06) has found that total porosity is largely unaffected by silica fume at all w/cm.

The cement paste-aggregate zone, or interfacial transition zone (ITZ), is composed of less C-S-H, has a higher localized w/cm and permeability, and contains large crystals of CH and ettringite. Silica fume greatly improves the ITZ by eliminating large pores and making the structure more homogeneous. This eliminates the growth of CH or transforming the already present CH to C-S-H by pozzolanic reaction. Furthermore, the rheological properties of a fresh concrete are improved by reducing internal bleed because the small size of the silica fume particles allow it to pack between cement particles and aggregate. (Mindess et al. (2003))

ACI (234R-06) has found that concretes made with silica fume exhibit higher compressive strengths at earlier ages, up to 28 days. They have also found that there is minimal contribution to compressive strength after 28 days. Neville (1995) indicates that the behavior of silica fume beyond the age of 3 months depends on the moisture conditions. In wet cured conditions, the silica fume concrete showed only a small increase in compressive strength for up to 3.5 years of age. Conversely, under dry conditions a reduction of strength, typically 12% below the peak at 3 months, was observed. These findings indicate the tendencies of a silica fume concrete to self-desiccate. Therefore, adequate curing is essential for full development of strength.

The trends of the development of compressive strength to flexural and splitting tensile strength of a concrete made with silica fume is similar to that of a cement only concrete (ACI 234R-06). In other words, as compressive strength increases, the tensile strength also increases, but with a decreasing ratio. They have found that a 20% silica fume had a compressive to flexural strength ratio that ranged from 0.13 to 0.15. They have also found splitting tensile strength at various ages to range from 5.8 to 8.2% of the compressive strength.

It has been shown that the use of silica fume reduces water permeability and chloride diffusion rates in concrete. ACI 234R-06 indicates that an 8% substitution in a 0.40 w/cm concrete resulted in a reduction in diffusion coefficient by a factor of seven. Furthermore, addition rates above 8% resulted in little additional improvement to resistance of chloride penetration. Reduced permeability is the primary mechanism in which silica fume increases the

resistance to sulfate attack by sodium sulfate (ACI 234R-06). However, an additional increase in sulfate resistance occurs from the pozzolanic reactions with silica fume as there is a large consumption of CH, the major component in sulfoaluminate corrosion (Mindess et al 2003).

### 2.3.7 SUMMARY

In summary, all of the SCM previously described improve mechanical and durability properties of portland cement concrete by virtue of their pozzolanic reactions and their ability to fill the portland cement paste pore structure to increase overall density. This increases the compressive strength and slows the diffusion of harmful ions through the concrete. Table 8 provides a reference table which covers the key aspects of each SCM.

Table 8 – Summary of SCM Effect on Concrete Properties

SCM	Source	Replacement <sup>b</sup> (% by weight)	Mean particle size ( $\mu\text{m}$ )	Effect on Concrete (compared to concrete with no SCM)		Diffusion Coefficient <sup>e</sup> ( $\times 10^{-12} \text{ m}^2/\text{s}$ )
				Fresh Properties	Hardened Properties	
fly ash	by-product of Coal-burning power plants	18-22	20-30 <sup>a</sup>	-improve workability -reduce water demand -delay set time	-reduce heat of hydration -strength gain delay	5.0
ultra fine fly ash	by-product of Coal-burning power plants	8-12	1-5 <sup>a</sup>	-reduce water demand	-improved early strength gain over fly ash	4.8
slag	by-product of iron refinement	25-70	varies	-improve workability -increase water demand -delay set time	-strength gain delay -reduction in heat of hydration -may increase early shrinkage	2.7
metakaolin	Kaolin clays	8-12	1.4 <sup>d</sup>	-increase water demand -reduce bleed -delay set time	-early strength gain	1.1
silica fume	by-product of silicon metal production	7-9	0.1-0.2 <sup>c</sup>	-increase water demand -reduce bleed -reduce segregation -increase in susceptibility to plastic shrinkage cracking	-early strength gain	2.1

<sup>a</sup>American Coal Ash Association (2003)

<sup>b</sup>FDOT Specification (2007)

<sup>c</sup>ACI 234R-06

<sup>d</sup>Manufacturer's information

<sup>e</sup>Vivas et al (2006).

### **3 MIXTURE DESIGN**

This chapter discusses the materials and proportions used in the concrete mixtures that were evaluated in this investigation. Preparation of the concrete mixtures, specimen fabrication, and curing conditions are also described.

#### **3.1 MATERIALS**

The materials used in the concrete mixtures are described in the following sections. These constituents can be divided into three categories: Basic Ingredients, SCM, and Chemical Admixtures.

##### **3.1.1 BASIC INGREDIENTS**

The water used in the concrete mixtures was obtained from the local city water supply. Silica sand from pit number 11-067 was used as fine aggregate in all concrete mixtures. The sand from this pit was tested and passed the gradation requirements of Section 902 of the 2004 Florida Department of Transportation Standard Specification for Road and Bridge Construction (FDOT Spec.). Additional testing of the sand determined a fineness modulus of 2.39 and a bulk specific gravity of 2.65, which were used in the mixture design to calculate yield. Specific test results on the fine aggregate are provided in Appendix A.

This sand was placed into cloth bags and dried in the oven until all moisture was removed. Prior to integration in the concrete mixtures, the sand was allowed to cool to the ambient temperature.

Crushed limestone from pit number MX-411 was used as the coarse aggregate in all concrete mixtures. The aggregate from this pit was tested and passed the gradation requirement of Section 901 in the FDOT Spec. for a  $\frac{3}{4}$ -in. maximum diameter aggregate. Additional testing of the limestone determined a bulk specific gravity of 3.61, which were used in the mixture design to calculate yield and adjust for moisture content. Specific test results on the fine aggregate are provided in Appendix A.

The coarse aggregate was used in its approximate saturated surface dry (SSD) condition. This SSD condition was obtained by filling woven polypropylene bags with coarse aggregate. The bags were then submerged in water for a minimum of 48 hours to fully saturate the aggregate. One day prior to mixing, the coarse aggregate bags were removed from the water and allowed to drain for approximately one hour before batching.

Type II portland cement manufactured by Holcim in the Theodore plant was used in each mixture. This cement complied with Section 921 of the 2004 FDOT Spec. Tests showed that the cement had an initial set time of 140 minutes, and a final set time of 215 minutes. This information is useful when determining the effects of the SCM and set retarding chemical admixture on a mixture. Additional test results are provided in Appendix A.

### 3.1.2 SUPPLEMENTARY CEMENTITIOUS MATERIALS

Evaluating highly reactive SCM was an integral part of this research. The following sections describe the individual admixtures used along with its source and role in the modification of fresh and hardened concrete properties. General information was obtained from Mindess (et al. 2003).

Fly ash is the waste product from the burning of pulverized coal in boiler furnaces used to generate electricity at power stations. It is commonly used as a cement replacement in concrete. In addition to the obvious environmental advantages, use of concrete containing fly ash is advantageous because of the cost, particle size and shape and mineral composition. The cost of fly ash is typically slightly less than half that of portland cement. The spherical shape of fly ash particles increases workability, which allows a lower water to cementitious material (w/cm) ratio to be used. In addition, the small particle size increases the packing density of the cementitious system. Thus, the permeability through interconnected voids is reduced, further improving durability. The mineral composition is also advantageous because of the high volume of reactive silica. This silica allows for a pozzolanic reaction to consume calcium hydroxide (CH) and creates more calcium silicate hydrates (C-S-H), which forms a denser paste structure.

A class F fly ash meeting the requirements of ASTM C 618, AASHTO M-321, and AASHTO M-295 was used in this investigation and was obtained from the Big Bend Power Station in Tampa, Florida. The fly ash also complied with Section 929-2 of the 2004 FDOT Spec. This class F fly ash satisfies the requirements of ASTM C-618 and AASHTO M-295. Specific tests results are provided in Appendix A.

Blast furnace slag is the residue wastes formed from the production or refinement of iron. Slag is removed from the molten metal and rapidly cooled. The raw slag is then dried and ground to a specific fineness so that it can be used as a cement replacement. Slag is advantageous for its chemical composition; it is rich in lime, silica, and alumina. Because of the high lime content, slag is a hydraulic admixture, meaning it will react with water to form a

cementitious compound. This compound adds to the strength of the mix, while also increasing durability by decreasing the interconnectivity of the voids. In addition, the high silica and alumina content promote pozzolanic reactions. The CH produced from cement hydration will be consumed and transformed into more cementitious compounds. These compounds are in the forms of C-S-H or C-A-H, depending on whether the reactive compound was silica or alumina. These new hydration products are denser and more homogenous than that produced by cement hydration alone.

CAMCEM, produced by Civil and Marine (Holdings) Ltd., is a Grade 100 ground granulated blast furnace slag used in this study. The slag complied with Section 929-5 of the 2004 FDOT Spec by meeting the requirements of ASTM C 989. Specific tests results are presented in Appendix A.

Ultra-fine fly ash is the same composition as regular fly ash. However, it has been sieved to greatly reduce the average particle size. The advantage of using an ultrafine fly ash over a standard fly ash is because the particle size is typically four times smaller; the small particles increase reactivity by increasing surface area, resulting in higher early strengths and lower permeability than a standard fly ash mixture of the same proportions. In addition, smaller particles have the ability to pack between the cement grains and aggregate creating a less permeable paste structure by reducing the interconnectivity of the voids.

The ultra-fine fly ash used in this investigation was Micron 3, a product of Boral Material Technologies. The typical mean diameter of Boral's Micron 3 is 3.0  $\mu\text{m}$ . As certified by Boral Material Technologies Inc., the distribution of particle size measured by a laser particle size analyzer indicated a minimum of 50% of particle sizes less than 3.25 microns and minimum of 90% of particle sizes less than 8.50 microns.

This class F fly ash satisfies the requirements of AASHTO M-321, ASTM C-618, and AASHTO M-295. The ultra-fine fly ash complied with Section 929-2 of the 2004 FDOT Spec. Specific test data are presented in Appendix A.

Metakaolin is manufactured by calcining clay at high temperatures. This results in a material that is largely composed of highly reactive amorphous aluminosilicates, which makes metakaolin advantageous for use as a cement replacement. Typically, the reactive silica and alumina content in metakaolin is over 85%. Through pozzolanic reactions, CH will react with both silica and alumina to form a cementitious hydration product. These can be in the form of C-S-H or C-A-H, depending on whether the reactive compound is silica or alumina. These new

hydration products are denser and more homogenous than that produced by cement hydration alone. In addition to the composition, the small particle size of metakaolin is advantageous. With a typical particle size of 1.4  $\mu\text{m}$ , particle packing will occur to create a less permeable paste structure by decreasing the interconnectivity of the voids.

The metakaolin used for this study was OPTIPOZZ, manufactured by Burgess. The requirements of ASTM C 618 Class N were met with a few modifications proposed by the FDOT Spec.:

- The sum of silica, iron, and alumina oxides was 87.9%.
- The loss on ignition was 0.8%.
- The percentage of available alkalis was negligible.
- The strength index at 7 days was 96%.
- Tests on the concrete containing metakaolin included ASTM C 39, ASTM C 157, ASTM C 1012, ASTM G 109, and FM 5-516.

Therefore, the metakaolin complied with Section 929-4 of the 2004 FDOT Spec. Specific test results are presented in Appendix A.

Silica fume is the byproduct of producing silicon metals or ferrosilicon alloys. It is commonly used as a cement replacement in concrete because of its size, shape, and chemical composition. The small size, typically 0.1 to 0.3 $\mu\text{m}$ , allows the silica fume particles to pack between cement grains. These particles will pack between cement grains, and decrease segregation and bleeding while reducing permeability by reducing the interconnectivity of the voids. In addition to the benefits related the shape and size of the particles, the chemical composition of silica fume is also advantageous. The extremely high reactive silica content, typically 85-98%, will allow for large volumes of CH to be converted into C-S-H. Also, because the silica content is so high, a secondary pozzolanic reaction will occur that converts tricalcium silicate (C3S) to a C-S-H product. These reactions will create a stronger, more homogenous paste matrix.

Force 10,000 D, produced by W. R. Grace & Co., was used as the silica fume in this investigation. It is a dry, densified microsilica powder made from silica fume. The silica fume is densified by air floatation in silos. The tumbling action induces progressive entanglement of particle to form dense clusters. These clusters allow for much easier transporting and handling, in contrast to the original form. Force 10,000 D complied with Section 929-3 of the 2004 FDOT

Spec by meeting the requirements of ASTM C 1240. Specific test data is presented in Appendix A.

### 3.1.3 CHEMICAL ADMIXTURES

Air entraining admixtures are composed of an aqueous solution of neutralized resin acids and rosin acids in which the molecules have ends that are hydrophilic and hydrophobic. In other words, one end of the molecule is attracted to water, while the other end is repelled by water. This behavior causes the molecules to attach to air bubbles within a fresh concrete mixture forming a tiny, stable bubble that is disconnected from other bubbles. The advantages of having a disconnected air void structure is because it will increase the resistance of a concrete to freezing and thawing cycles, improve the workability and cohesiveness of a fresh concrete mixture, and reduce segregation and bleeding (Mindess et al. 2003). Because Florida concrete are not exposed to freezing and thawing cycles, the addition of air entraining admixture in this investigation was to increase workability and decrease segregation.

The air entrainer used in this study was Daravair 1000, produced by W. R. Grace & Co. This admixture complied with Section 924 of the 2004 FDOT Spec by meeting the requirements of AASHTO M 154.

Set retarding admixtures are typically composed of a polymer based aqueous solution of lignosulfonate, amine, and compound carbohydrates. These carbohydrates extend the setting time of fresh concrete mixture by slowing down the rate of early hydration of  $C_3S$  and  $C_3A$ . A set retarding admixture was used in this investigation because of the large number of test specimen fabricated from each mixture. By increasing the setting time, all specimens were able to be properly consolidated before mixture began to harden.

WRDA 60, produced by W. R. Grace & Co., was the set retarding admixture used in this investigation. WRDA 60 complied with Section 924 of the 2004 FDOT Spec by meeting the requirements of AASHTO M 194.

Surface charges on particles within a fresh concrete will cause flocculation. A considerable amount of water is usually tied up in these agglomerations, leaving little available to reduce the viscosity of the paste. The addition of a superplasticizing admixture, which is typically composed of an aqueous solution of carboxylated polyether, will serve to break up the bonds found between particles. This releases the available water within the mixture, thereby

increasing workability. This increase in workability then allows for a decrease in water to cementitious material ratio. Consequently, the strength and durability of a mixture is improved.

The superplasticizer used in this study was ADVA 140, a product of W. R. Grace & Co. It complied with Section 924 of the 2004 FDOT Spec. by meeting the requirements of AASHTO M 194.

### 3.2 PROPORTIONS

Selection of the mixture proportions and other mixture design parameter for bridges in Florida is based on the local environment. The Structures Design Guidelines (July 2005) defines three exposure conditions:

- Slightly Aggressive
- Moderately Aggressive
- Extremely Aggressive

For substructure elements, such as piling, the environment classification is a function of the chloride content or pH level of the surrounding soil or water. Higher chloride content, lower pH, or both will result in a more aggressive environment and a more restrictive rating.

If prestressed concrete piles are used in an extremely aggressive environment that is due to elevated chlorides in a marine environment, then silica fume must be used in the concrete mixture. The object of this research was to evaluate the use of other highly reactive SCM on the fresh and hardened properties of concrete. These admixtures included slag, ultrafine fly ash, metakaolin, and fly ash.

Prestressed concrete piling must use Class V (Special) or Class VI concrete for any environment. Class V (Special) is the mixture design typically specified and has the following characteristics:

- maximum water to cement ratio of 0.35
- minimum total cementitious material content of a 752 lb/yd<sup>3</sup>
- air content range of 1 to 5%
- target slump of 3 in., which may be increased to 7 in. when a water reducing admixture is used.

When the piles are in a moderately or extremely aggressive environment, the use of fly ash, slag, or both is required. Fly ash cement replacement rate is 18% to 22%, while slag is 25% to 70% for moderately aggressive and 50% to 70% for extremely aggressive environments.

Larsen and Armaghani (1987) found that the most effective addition rate of fly ash was between 18% and 22%. They found the rate in excess of this range caused the additional mineral admixture to stop reacting and essentially become fillers. Furthermore, rates below this range caused no significant improvement in durability. Consequently, the FDOT Specifications (2007) adopted this range and now requires the use of fly ash in moderately aggressive environments.

The dosage rates in the current FDOT Specification (2007) for slag, metakaolin and ultrafine fly ash are based on the manufacturer's recommendations. The suggested addition rate for slag is 25% to 70% by weight for moderately aggressive environments, while metakaolin and ultrafine fly ash are 8 to 12%. At addition rates below the minimum, there were not significant improvements to mechanical properties and durability. Addition rates above the maximum will not react and become expensive fillers.

The effect of silica fume replacement rates on modulus of rupture and permeability were investigated by Tia et al. (1990). They found that the most effective replacement rate was in the range of 7% to 9% by weight. Replacement rates below the minimum did not significantly improve the permeability and had little affect on the modulus of rupture, while rates above the maximum did not show any improvement in test data. Consequently, the FDOT Specification (2007) has adopted this range for silica fume replacement levels.

Two control mixtures were designed. The first control mixture contained only portland cement as the binder. A second control mixture was designed to contain portland cement and fly ash at a cement replacement rate of 18% by weight. Therefore, the proportion of fly ash used in every mixture was selected to be 18%. The FDOT Specification (2007) minimum was selected because fly ash would be used in conjunction with other SCM.

To thoroughly investigate the effects of SCM, three mixtures containing different proportions of each admixture were designed. For example, three mixtures containing metakaolin at proportions of 8%, 10%, and 12% were designed. These percentages were selected based on the metakaolin guidelines in the FDOT Specification (2007). The minimum and maximum proportions were selected. In addition, a percentage that was midway between the maximum and minimum was selected to provide a broad distribution of data. The ultrafine fly ash mixtures were also designed in this manner; proportions of 10%, 12%, and 14% were

selected. Because the range of silica fume replacement rates in the FDOT Specification (2007) was narrow (7 to 9%), only mixtures containing the minimum and maximum proportions were designed. The range of replacement rates for slag in an extremely aggressive environment is 25 to 70% by weight. Because slag was being used in conjunction with fly ash, the maximum slag replacement rate would be too high to create a durable concrete because the proportion of cement would be too low. Neville (1995) found that for the highest medium term strength, the cement to cementitious material should be about 1:1. Therefore, smaller proportions of slag replacement in combination with 18% fly ash were selected to be investigated; slag proportions of 25%, 30%, and 35% were used. The cementitious material proportions for all mixtures are presented in Table 9 and Table 10.

Table 9 - Proportions of cementitious materials (a)

	<b>CTRL1</b>	<b>CTRL2</b>	<b>SLAG1</b>	<b>SLAG2</b>	<b>SLAG3</b>
Cement	100%	82%	57%	52%	47%
Fly Ash (FA)	---	18%	18%	18%	18%
Slag	---	---	25%	30%	35%
Metakaolin	---	---	---	---	---
Ultrafine (FA)	---	---	---	---	---
Silica Fume	---	---	---	---	---

Table 10 - Proportions of cementitious materials (b)

	<b>META1</b>	<b>META2</b>	<b>META3</b>	<b>UFA1</b>	<b>UFA2</b>	<b>UFA3</b>	<b>SF1</b>	<b>SF2</b>
Cement	74%	72%	70%	72%	70%	68%	75%	73%
Fly Ash (FA)	18%	18%	18%	18%	18%	18%	18%	18%
Slag	---	---	---	---	---	---	---	---
Metakaolin	8%	10%	12%	---	---	---	---	---
Ultrafine (FA)	---	---	---	10%	12%	14%	---	---
Silica Fume	---	---	---	---	---	---	7%	9%

The volume occupied by the cementitious materials, water, and air was subtracted from the total concrete volume to determine the required aggregate volume. Proportions of coarse aggregate were selected from Table 6.3.6 (Volume of Coarse Aggregate per Unit Volume of Concrete) in ACI 211.1-91. The fine aggregate content was determined by subtracting this coarse aggregate volume from the total aggregate volume. These proportions of fine and coarse

aggregate were determined to be 35% and 65%, respectively. The resulting mixture designs are shown in Table 11 and Table 12.

Several chemical admixtures were used to control the fresh properties of the concrete, including air entraining, set retarding, and high-range water reducer. Recommended addition rates for air entraining admixtures are not typically provided by the manufacturer because many factors affect the process of air entraining a concrete mixture. These factors included cement and mineral admixture, coarse and fine aggregate, mixer type, mixing time, and vibration. Therefore, laboratory experience was used to determine the addition rate, which was 0.4 oz. per 100 lb of cementitious materials.

The set retarder, WRDA 60, had a recommended dosage rate of 2.5 to 6 oz. per 100 lb of cementitious materials. In this investigation, 2.5 oz. was used for each mixture. The lower end of the range was used because only a short delay in setting time was needed to ensure that all specimens could be fabricated before the mixture stiffened.

To ensure consistency among the various mixes, the water content was held constant. It was deemed important, however, that the slump also remain consistent to ensure that the specimens were consolidated similarly. Consequently, slump was adjusted with a high-range water reducer, rather than with additional mixing water. The manufacturers recommended dosage rate for the superplasticizer, ADVA 140, is 6 to 20 oz. per 100 lb of cementitious materials. Because each mineral admixture affects the mixture differently, the quantity of superplasticizer needed to get the desired slump was different for each mixture. An initial estimation of 9 oz per 100 lb of cementitious materials was used for each mixture. Slump readings were taken immediately after mixing was completed. If the slump was below the target range, additional superplasticizer was added at the lab manager's discretion. Addition rates that were too large would cause segregation resulting in loss of strength and durability. This would be evident by large percentages of bleeding. However, the small variations in quantity of superplasticizer in each mixture of this investigation do not affect the durability or strength, but rather ensure consistent consolidation among specimens.

Table 11 – The resulting mixture designs (a) (lb/yd<sup>3</sup>)

<b>Material</b>	<b>CTRL1</b>	<b>CTRL2</b>	<b>SLAG1</b>	<b>SLAG2</b>	<b>SLAG3</b>
Cement	752	617	429	391	354
Fly Ash	0	135	135	135	135
Slag	0	0	188	226	263
Micron 3	0	0	0	0	0
Metakaolin	0	0	0	0	0
Silica Fume	0	0	0	0	0
Water	263	263	263	263	263
Fine Agg.	1055	1042	1035	1034	1032
Coarse Agg.	1078	1743	1736	1734	1734
Air Entrainer	3 oz.	3 oz.	3 oz.	3 oz.	4 oz.
Water Reducer	23 oz.				
Superplasticizer	68 oz.				
Additional	0 oz.	0 oz.	0 oz.	0 oz.	7 oz.
<b>Total</b>	<b>68 oz.</b>	<b>68 oz.</b>	<b>68 oz.</b>	<b>68 oz.</b>	<b>75 oz.</b>

Table 12 – The resulting mixture designs (b) (lb/yd<sup>3</sup>)

<b>Material</b>	<b>META1</b>	<b>META2</b>	<b>META3</b>	<b>UFA1</b>	<b>UFA2</b>	<b>UFA3</b>	<b>SF1</b>	<b>SF2</b>
Cement	557	542	527	542	527	512	564	549
Fly Ash	135	135	135	135	135	135	135	135
Slag	0	0	0	0	0	0	0	0
Micron 3	0	0	0	75	90	105	0	0
Metakaolin	60	75	90	0	0	0	0	0
Silica Fume	0	0	0	0	0	0	53	68
Water	263	263	263	263	263	263	263	263
Fine Agg.	1030	1027	1024	1037	1037	1035	1032	1029
Coarse Agg.	1731	1728	1726	1739	1737	1737	1734	1731
Air Entrainer	5 oz.	6 oz.	6 oz.	6 oz.	7 oz.	8 oz.	8 oz.	8 oz.
Water Reducer	23 oz.	23 oz.	23 oz.	23 oz.	23 oz.	23 oz.	23 oz.	23 oz.
Superplasticizer	68 oz.	68 oz.	68 oz.	68 oz.	68 oz.	68 oz.	68 oz.	68 oz.
Additional	20 oz.	30 oz.	41 oz.	0 oz.				
<b>Total</b>	<b>88 oz.</b>	<b>98 oz.</b>	<b>109 oz.</b>	<b>68 oz.</b>				

### 3.3 PREPARATION OF CONCRETE MIXTURES

In preparation for mixing, the coarse aggregate was placed in woven polypropylene bags which were submerged in water for a minimum of 48 hours to fully saturate the aggregate. One day prior to mixing, the coarse aggregate bags were removed from the water and allowed to drain for approximately one hour. The coarse aggregate was then batched and sealed for casting on the following day. This was done to keep the coarse aggregate in a saturated surface dry condition so that it would not affect the water requirements of a mixture by absorbing or releasing water during mixing. Moisture content was measured on representative samples taken from the batched material. Variations from saturated surface dry were accommodated during mixing by reducing or increasing the mixing water.

The fine aggregate was placed in cotton sand bags. The bags were then oven dried to remove any in-situ moisture. One day prior to casting, batch quantities were weighed and sealed in plastic 5-gallon buckets.

All SCM and cement were collected from their receptacle one day prior to casting. The materials were then weighed and sealed in plastic 5-gallon buckets.

The thirteen concrete mixtures were produced in the two cubic feet rotary drum mixer shown in Figure 1. A butter mixture, which is a small portion of a concrete mixture that contains no coarse aggregate, was used prior to mixing to completely cover the interior surface of the concrete mixer. This limits changes in paste content due to adherence to the interior mixing surfaces; butter mixtures improve the consistency of concrete mixtures.

The procedure for mixing complied with ASTM C 192. Initially, the coarse and fine aggregates were placed in the mixer with approximately half of the water and air entraining admixture. These constituents were then mixed for two minutes. Next, the cement, SCM, set retarding and superplasticizer admixtures, and remaining water were added to the mixer and mixed for three minutes. The mixture was then allowed to rest for three minutes. A slump test was then conducted to evaluate the mixture. If the slump was not within the desired range, additional superplasticizing chemical admixture was integrated into the fresh concrete and mixed for an additional three minutes.



Figure 1 - Rotary drum mixer

### 3.4 SPECIMEN FABRICATION

The desired testing scheme, discussed in chapter 4, required the fabrication of various concrete specimens. These included cylinders, beams, prisms, and ASTM G 109 specimens. Each specimen was fabricated in accordance with the requirements of ASTM C 192. The 6-in. diameter x 12-in. long cylinders were constructed in 3 lifts. Other specimens were placed in two lifts. Specimens were consolidated with a vibrating table. Vibration was applied until the surface of the concrete became smooth and large air bubbles ceased to break the surface. Specimen molds were then sealed to prevent evaporation. Twenty-four hours after fabrication, specimens were removed from their molds and placed in the curing environment called for by the applicable test methods.

### 3.5 CURING CONDITIONS

The curing condition of each specimen was dictated by their respective test method. These conditions included full submersion in aqueous solutions containing aggressive agents, dry cure in a controlled environment, wet cure in a controlled environment, and a wet cure in an elevated temperature water bath.

With the exception of the specimens tested according to ASTM G 109, ASTM C 157, ASTM C 512, ASTM C 1556, and ASTM C 1012, curing procedures of ASTM C 511 were followed. This standard calls for demolding after 24 hours and placement into a curing

environment that is controlled at  $73.4 \pm 3.0^{\circ}\text{F}$  and 100% humidity, so that free water is maintained on the surfaces at all times.

Specimens used for ASTM G 109 were cured for 28 days in accordance with ASTM C 511. Upon removal from the moist room, specimens were dry cured for two weeks in an environment controlled at a temperature of  $73 \pm 3^{\circ}\text{F}$  and a relative humidity of  $50 \pm 4\%$ . The epoxy barrier was then applied. Each specimen was then returned to the controlled dry curing environment for an additional two weeks. Next, the specimens were placed in their exposure conditions. ASTM C 157 calls for specimens to be placed in a curing environment that is maintained at  $73 \pm 3^{\circ}\text{F}$  and a relative humidity of  $50 \pm 4\%$  immediately after demolding. ASTM C 512 also required that specimen be moved into a controlled dry cure after a 7-day initial cure in 100% humidity room. For ASTM C 1556, a portion of the specimens followed an accelerated curing regime to simulate an older age. This was accomplished by placing the appropriate specimens in a water bath maintained at  $105 \pm 5^{\circ}\text{F}$  for 28 days. All specimens were then placed into their exposure solutions. Specimens used for ASTM C 1012 had no curing period prior to testing. These specimens were demolded at 24 hours and immediately placed into an exposure solution.

### **3.6 ADDITIONAL MIXTURES**

New specimens were created for the modulus of elasticity, Poisson's ratio, splitting tensile strength, and flexural strength tests due to errors in conducting the tests on the original mixtures.

## 4 LABORATORY TESTING

Evaluating the durability of concrete made with highly reactive pozzolans involved not only durability tests, but also plastic properties and mechanical properties. This chapter describes the test methods used to evaluate these important properties. To the extent possible, standard test methods were used. However, in some cases it was necessary to deviate from standard procedures or specimen configurations. These deviations are noted in the appropriate sections.

### 4.1 PLASTIC PROPERTIES TESTS

The plastic properties tests were conducted to check the consistencies between mixtures and evaluate the affects of the SCM on the properties of the fresh concrete. The following plastic properties were measured: density, slump, air content, bleed water, time of set, and temperature.

#### 4.1.1 DENSITY (ASTM C 138)

The unit weight plastic property test is often conducted because of its simplicity. Typically, unit weight is measured as part of the air content procedure. From these results, yield estimation can be calculated. The use of different SCM has little affect on density as it is more greatly affected by aggregate type and entrained air (Mouli and Khelafi 2006).

#### 4.1.2 SLUMP (ASTM C 143)

The slump test is a relatively simple field test that gives an estimate of concrete workability. This test is typically used to ensure a consistent workability and is sometimes used to determine if sufficient superplasticizer has been added to a mixture. The target slump of the design mixtures for the present research was 7 in. Slump readings were taken immediately after the concrete was mixed. If the slump was less than the target, high range water reducing admixture was added and slump was retested until the target slump was achieved. Because the recommended manufacture's dosages were not exceeded, it is expected that the physical characteristics of the hardened concrete remained relatively unaffected.

Fly ash reduces interparticle friction and increases slump due to the spherical shape of the particles (Neville 1995). Silica fume and ultrafine fly ash particles, however, because of their small size, have high surface areas and tend to increase the cohesiveness of the mixture (Mindess 2003). This results in a decrease in slump and a need for greater high range water reducer

dosages to maintain the target slump. Slag and metakaolin also decrease the slump because of their angular and plate like particles (Bai et al 2003).

#### 4.1.3 AIR CONTENT (ASTM C 173)

This test measures, by the volumetric method, the air contained in the mortar fraction of the concrete, without being affected by air contained within aggregate pores. This test method is unable to distinguish between entrapped and entrained air, as it only measures total air content. However, it does provide the means of evaluating the effects of an air entraining admixture when a mixture is properly consolidated to remove all entrapped air.

The addition of SCM alters the effect of air entraining admixtures. High carbon content of some SCM will adsorb the entrained air, rendering the chemical admixture less effective. However, the carbon levels of the mineral admixture used in this investigation are low enough such that air entrainment was likely unaffected. The high surface areas also alter the effectiveness of the air entraining admixture by requiring a larger dosage of air entrainment to reach the same air content (Neville 1995). Therefore, if the same dosage of air entrainment was used for mixtures containing SCM as was with the control, the air content will be lower.

Air entraining admixture was implemented to decrease the bleeding, as well as increase the workability and cohesiveness of the concrete mixtures. The measurements of air content were used to establish a correlation between bleeding and air content.

#### 4.1.4 BLEEDING OF CONCRETE (ASTM C 232)

This test measures the percentage of bleeding of a fresh concrete mixture. A metal beaker is filled with concrete and then consolidated. After troweling the surface level, the bleed water is collected and measured.

Bleeding is a form of segregation in which there is an upward movement of water after the concrete has been consolidated. This causes the upper layer of the concrete to have a high water-to-cement ratio resulting in increased porosity and lower durability in the cover concrete. Strength will also be reduced when large water pockets, caused by the upward movement of water during excessive bleeding, form under aggregate or reinforcing bars. Yet another adverse affect of bleeding is laitance. This occurs when a film of fine particles are carried to the surface by the bleed water. If the concrete is poured in lifts, this surface film will create a poor bond to the next lift. (Mindess et al., 2003)

Bleeding is reduced by using an air entraining admixture. The entrained air increases the cohesiveness of the particles, thus reducing bleeding segregation. Bleeding is also reduced by the use of SCM. Silica fume, ultrafine fly ash, and metakaolin have small particles that allow it to pack between cement grains, thus reducing the porosity; consequently, bleeding is reduced (Neville 1995). Research has shown, however, that slag may increase bleeding (Wainwright and Rey 2000).

#### 4.1.5 TIME OF SETTING (ASTM C 403)

The initial and final setting times of a freshly mixed concrete were determined by measuring the stress needed to penetrate the surface of a concrete. A stress of 500 lb/in<sup>2</sup> and 4000 lb/in<sup>2</sup> determined the initial and final setting, respectively.

Excessively long or short set times indicate possible problems with cement manufacturing, adverse chemical admixture reactions, or excess gypsum. Specific setting time patterns can indicate which problem may be the cause. Time of setting is also an important measurement to predict maximum mixing and transit times and to gauge the effectiveness of set-controlling admixtures.

The use of SCM affect the setting times of concrete mixture. Research has shown that all SCM used in this investigation lengthen the setting time (Brooks et al. 2000). Fly ash retards the early hydration of C<sub>3</sub>S (ACI 232.2R-03). Mixtures containing over 25% slag will see delays in setting time (ACI 233R-03). Conversely, metakaolin mixtures have shown shortening of set times (Zongjin and Ding 2003). ACI (234R-06) have suggested that silica fume does not significantly affect the setting times.

#### 4.1.6 TEMPERATURE (ASTM C 1064)

Temperature measurements were taken immediately from fresh concrete, and completed within 5 minutes after obtaining the sample. The temperature of fresh concrete mixes becomes a critical factor when placing in hot or cold environments. In hot weather concreting, problems can occur when concrete temperatures become too high. High temperatures can cause plastic shrinkage cracking, loss of workability and decreased setting times. In cold weather concreting, problems can arise if the fresh concrete temperatures becomes low enough to freeze early in its life. Therefore, a measurement of fresh concrete temperature can provide an estimate on how it will perform in extreme temperature environments.

Generally, low reactivity SCM as small cement replacements will result in lower mixture temperatures. Conversely, high reactivity admixtures will increase the fresh concrete temperature. The use of the low reactivity slag mineral admixture will result in a lower heat of hydration (Sioulas and Sanjayan 2000). On the other hand, metakaolin additions have been shown to increase the fresh concrete temperature (Frias et al 2000). Fly ash and silica fume will also reduce the temperature of a fresh concrete mixture (Langan et al 2002). However, this research has also shown that the combination of fly ash and silica fume retarded the initial hydration, resulting in lower temperatures.

## 4.2 MECHANICAL TESTS

Standard test methods were conducted to determine the mechanical characteristics of the concrete. These characteristics are frequently used in structural design to estimate a variety of other concrete properties. Physical behavior also can be predicted based on the results of these mechanical tests, such as deflection and prestressing losses.

### 4.2.1 COMPRESSIVE STRENGTH (ASTM C 39)

The addition of SCM has a significant effect on the compressive strength of concrete. The early strength will be reduced if a low reactivity admixture, such as fly ash and slag, are used in a mixture (ACI 232.2R-03 and ACI 233R-03). The increased fineness of ultrafine fly ash makes it more reactive than ordinary fly ash. Jones (et al 2006) has shown that there is still a reduction in early strength development of ultrafine fly ash mixtures when compared to the control. Conversely, early age strengths are typically higher than the control for high reactivity pozzolans such as metakaolin and silica fume (Qian 2001 and ACI 234R-06). Late age strengths of concretes containing these SCM will be higher than the control. This is attributed to the stronger, more homogenous paste matrix created by the pozzolanic reactions.

The compressive strength of three 6-in. diameter x 12-in. long cylinder were tested at ages of 3, 7, 28, 91, and 365 days. In lieu of capping, the ends of each cylinder were ground smooth using a DIAM-end Grinder manufactured by M&L Testing Equipment as shown in Figure 2.

All cylinders were cured in a moist condition at a temperature of  $73.4 \pm 3.0^{\circ}\text{F}$ , so that free water was maintained on the surface at all times. Each test was completed within an hour of removal from the curing room on a Test Mark load frame as shown in Figure 3 and were maintained wet. Cylinders were loaded continuously and without shock at 20 to 50 psi/sec.



Figure 2 - DIAM-end grinder



Figure 3 - Test Mark load frame

#### 4.2.2 FLEXURAL STRENGTH (ASTM C 78)

Because cracking is initiated in the tensile region of concrete beams, the durability behavior is governed by the tensile strength and extent of cracking that the beam will experience. Since the tensile strength of a concrete is largely a function of the aggregate to paste bond, flexural strength is sensitive to the strength and size of the interfacial transition zone (ITZ). SCM consume Calcium Hydroxide (CH) and reduce ettringite formation, creating a stronger concrete ITZ. Therefore, the use of SCM will typically improve the flexural strength of a

concrete over time. Early strength development is reduced in the admixture with low reactivity, such as fly ash and slag (ACI 232.2R-03 and ACI 233R-03). Conversely, the higher reactivity SCM, silica fume and metakaolin, will have higher modulus of rupture when compared to the control (ACI 334R-06 and Kim et al 2007). Research related to the effect of ultrafine fly ash on flexural strength was not found. However, it is expected that because the surface area is increased, the ultrafine fly ash mixtures will show a larger flexural strength at early ages when compared to the ordinary fly ash mixtures. At later ages, the SCM will provide an increase in flexural strength when compared to the control mixtures because of the improvement in the ITZ.

Specimens were cast into 4-in. x 4-in. x 14-in. long beams and tested at two ages—7 day and 28 day. All beams were moist cured at a temperature of  $73.4 \pm 3.0^\circ\text{F}$ , so that free water was maintained on the surface at all times. Each test was completed within an hour of removal from the curing room and were kept moist until testing. Beams were loaded continuously and without shock at a rate of 125 to 175 psi/min on an Instron load frame as shown in Figure 4 and Figure 5.

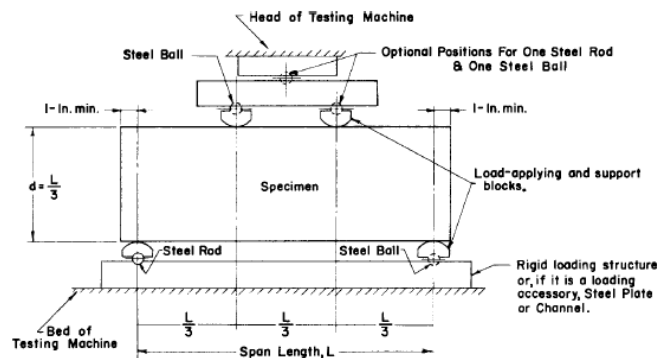


Figure 4 - Diagram of the third-point loading flexure testing apparatus



Figure 5 - Instron load frame testing flexural strength

#### 4.2.3 STATIC MODULUS OF ELASTICITY AND POISSON'S RATIO (ASTM C 469)

Research has shown (Nassif et al. 2005) that the addition of SCM will increase the modulus of elasticity at late ages. However, for high volume replacement of low reactive SCM such as fly ash and slag, early age modulus of elasticity may be reduced. The amount of decrease will depend on the type and quantity of admixture implemented.

Very little research has been conducted to find the effect of SCM on Poisson's ratio. The research that had been conducted shows no discernable change in Poisson's ratio with the addition of SCM (Mirza et al 2002).

The test procedure was performed in slight variation to ASTM C 469. The Standard calls for the specimen to be loaded to 40% of its ultimate strength. However, slight damage may be induced at this level. Bond cracks will exist in concrete at zero load due to differences in the elastic moduli between the hardened cement paste and the aggregates, different coefficients of thermal expansion, as well as different responses to moisture content. For stress levels up to 30% of the ultimate, little additional cracking is expected. Bond microcracking begins to increase at stresses above 30 to 40% of the compressive strength (Mindess et al., 2003). Consequently, each specimen was loaded to 25% of its rupture strength initially with the remainder of the procedure conducted in accordance with the Standard. Figure 6 shows the instrumentation and testing apparatus used to measure the Modulus of Elasticity and Poisson's Ratio.



Figure 6 - Modulus of elasticity and Poisson's ratio test setup on the TEST MARK system

Because of the low stress levels used to test for Modulus of Elasticity (MOE), the same 6-in. diameter x 12-in. long cylinders that were used for MOE could be used for compressive strength tests. An initial test of compressive strength was conducted on the first cylinder from each set of three. Each of the two remaining cylinders was loaded three times to measure the MOE. The initial load, which was primarily for seating the gages, was ignored. The two subsequent loadings were then used to calculate an average modulus of elasticity for that cylinder. An average was then taken of the results from the two cylinders. Testing was conducted at 3, 7, 28, 91, and 365 day ages.

Poisson's Ratio was also obtained when testing for MOE. The results from the second and third loading were averaged for each cylinder. The data from both cylinders were used to calculate an average Poisson's ratio for each mix. Testing was conducted at 3, 7, 28, 91, and 365 day ages.

#### 4.2.4 SPLITTING TENSILE STRENGTH (ASTM C 496)

Because the failure of concrete in tension is governed by microcracking, the ITZ will control the tensile strength of a concrete. (Mindess et al., 2003) The use of SCM will result in consumption of CH and reduction of ettringite formation, creating a stronger ITZ. As with flexural strength tests, the use of SCM in concrete used for splitting tensile strength tests will improve the tensile strength of a concrete as the pozzolanic reactions take place.

Specimens cast into 4-in. diameter x 8-in. long cylinders were tested at 3, 7, 28, 91, and 365 days of age. All cylinders were cured in a moist condition at a temperature of  $73.4 \pm 3.0^{\circ}\text{F}$ , so that free water was maintained on the surface at all times. Each test was completed within an hour of removal from the curing room on a Forney Load frame as shown in Figure 7.



Figure 7 - Splitting tensile strength test on Forney load frame

### 4.3 DURABILITY TESTS

The deterioration of concrete is the result of poor performance of the three major components: reinforcement, paste, and aggregate. This can be the result of either chemical or physical causes. The durability tests performed in this investigation involve the assessment of each concrete mixture's physical characteristics and response to chemical attack. The use of SCM will alter the concrete paste and paste structure by creating a stronger, more homogenous paste matrix, less permeable void space, and refined capillary pore structure—all of which result in an improvement to durability.

#### 4.3.1 LINEAR SHRINKAGE (ASTM C 157)

The linear shrinkage test assesses volumetric expansion or contraction of concrete due. Moisture loss through the concrete pore structure is the dominant factor in shrinkage (Mindess et al. 2003). Because of the typical reduction in capillary porosity, the use of SCM will reduce linear shrinkage by decreasing the porosity in a concrete. Research has shown that metakaolin mixtures exhibit a reduction in total linear shrinkage (Brooks and Megat Johari 2001). ACI has suggested that slag will reduce linear shrinkage (ACI 363R-03). Research conducted by Akkaya (et al. 2007) has shown that fly ash and ultrafine fly ash show little decrease in total shrinkage compared to the control. ACI (364R-06) states that silica fume also has little effect on total shrinkage.

ACI also states that silica fume and fly ash has no significant affect on linear shrinkage at small replacements levels (ACI 364R-06 and ACI 323.2R-03). Research on the effects of ultrafine fly ash on linear shrinkage was not found.

Linear shrinkage specimens were cast into 3-in. wide x 3-in. high x 11.25-in. long prism molds. Immediately after removal from the molds, the specimens were dry cured by placing them an environment controlled at a constant temperature of  $73 \pm 3$  °F and a constant relative humidity of  $50 \pm 4\%$ . Due to mechanical problems with the environmental control system, temperature and relative humidity were slightly varied from that specified in ASTM C 157. The actual temperature and relative humidity readings are presented in Appendix A. Comparator readings were taken on all specimens at an age of 4, 7, 14, and 28 days, and after 8, 16, 32, and 64 weeks.

#### 4.3.2 VOLUME OF VOIDS (ASTM C 642)

This method was used to measure the percentage of voids within hardened concrete. If exposed to a corrosive environment, these voids allow the transport of harmful ions. Samples were cut from 2 in. below the finished surface of a molded 4-in. diameter x 8-in. long concrete sample. Tests were conducted on each mixture at 28 days of age.

#### 4.3.3 SULFATE EXPANSION (ASTM C 1012)

Length change measurements permit the relative assessment of the sulfate resistance of concrete or mortar subjected to total immersion in a sulfate solution. The sulfate ions in the solution combine with gypsum and CH to create an expansive reaction. This reaction, however, can be limited by the use of SCM. There are two means that SCM inhibit sulfate expansion: a refinement of the capillary porosity and a reduction in CH. ACI (232.2R-03; 233R-03; 234R-06) suggests that fly ash, slag, and silica fume increase a concrete's resistance to sulfate attack. Research has shown that metakaolin also improves the resistance to sulfate attack (Khatib and Wild 1998). Little research has been conducted on the effect of ultrafine fly ash on sulfate attack. It is expected, however, that ultrafine fly ash will perform better than fly ash concretes, because the smaller particle size will further reduce permeability.

Specimens for the present research were cast into 3-in. wide x 3-in. high x 11.25-in. long and 1-in. wide x 1-inch deep x 11.25-in. long molds for concrete and mortar, respectively. Mortar was sampled from the fresh concrete mix; fresh concrete was passed through a 3/8-in. sieve to remove the coarse aggregate. All specimens were immersed into a 5% SO<sub>4</sub> solution at 24 hours after casting, immediately after their removal from the molds. The water temperature of the sealed tanks containing the sulfate solution was maintained at 73.5 ± 3.5°F. Readings were taken at 1, 2, 3, 4, 8, 13, and 15 weeks of exposure.

#### 4.3.4 ABSORPTION (ASTM C 642)

There are four transport mechanisms that allow the penetration of deleterious chemicals into concrete. These mechanisms are permeability, diffusivity, evaporative transport, and absorptivity. In an unsaturated concrete, absorption will play a significant role in chemical transport. Absorption is controlled, in large part, by the connectivity of the capillary pore system. Solution is drawn by capillary suction allowing harmful chemicals, such as chlorides and sulfates, to enter the concrete. This test method gives a means of assessing the capillary pores structure by measuring the absorptivity of an unsaturated concrete. The use of SCM will

refine the capillary pore structure through pozzolanic reaction. Consequently, the absorptivity of a concrete will be reduced.

Specimens for the present research were prepared using a 4-in. diameter x 8-in. long cylinder molds. Each cylinder was cured in a moist condition at a temperature of  $73.4 \pm 3.0^{\circ}\text{F}$ , so that free water was maintained on the surface at all times. From each of these cylinders a 2-in. thick slice was cut from 6 in. below the finished surface. This test was conducted on each mixture at 28 days of age.

#### 4.3.5 CORROSION OF EMBEDDED STEEL REINFORCEMENT (ASTM G 109)

Corrosion is a particularly problematic phenomenon in reinforced concrete structures exposed to chloride ions. Because it is an expansive reaction, corrosion of steel reinforcement leads to the cracking and spalling of the adjacent concrete. This will then lead to a direct, unobstructed path for additional elements to corrode the underlying steel reinforcement. This method provides the means of assessing a concrete's ability to inhibit the corrosion of embedded steel reinforcement. The use of mineral admixture will delay or even prevent the corrosion of the embedded steel reinforcement by improving the resistance of the surrounding concrete to the penetration of chloride ions. The SCM refine capillary porosity, reduce permeability, and improve the ITZ. Each of these effects will reduce the ingress of chloride ions.

Each specimen was fabricated using a mold containing three #4 deformed steel reinforcing bars and a titanium reference electrode as shown in Figure 8. At an age of 24 hours, each specimen was demolded and allowed to cure in a moist condition at a temperature of  $73.4 \pm 3.0^{\circ}\text{F}$ , so that free water was maintained on the surface at all times until they were 28-days of age. At this time, each specimen was placed in an environmental chamber maintained at 50% relative humidity for a period of two weeks. Following this conditioning, a 6-in. x 3-in. x 3-in. plastic dam was adhered to the top of each specimen. All sides were then sealed, with the exception of the bottom and the inside of the dammed area, using Sikadur 32 High Mod epoxy. Figure 9 shows the ASTM G109 specimen after the dam and epoxy seal was constructed.

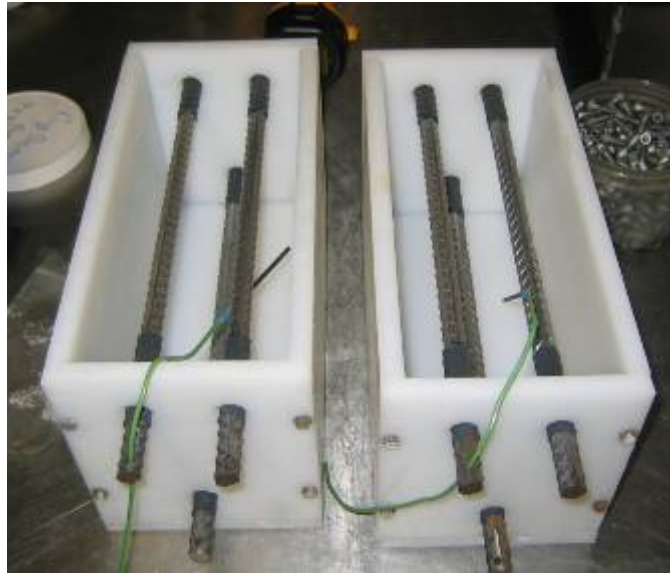


Figure 8 - ASTM G109 specimen molds containing the reinforcing bars and reference electrode



Figure 9 - ASTM G109 specimen after the epoxy has been applied

Samples were then placed in the environmental chamber until they were of 56 days of age. At this time, a non-standard testing procedure was followed. ASTM G 109 states that samples should be ponded with a 3% NaCl, and stored at  $73 \pm 5.0^{\circ}\text{F}$  and a relative humidity of  $50 \pm 5\%$ . To accelerate corrosion, a 15% NaCl solution was used with the specimens exposed to  $90 \pm 5^{\circ}\text{F}$ . The specimens were connected to automated monitored device that measured current and potential once daily (Figure 10). Each specimen was subjected to a cycled regime of the 15% NaCl solution; the cycles were maintained at two weeks of sealed continuous ponding,

followed by two weeks of drying. An electrical diagram of the test setup is presented in Figure 11.



Figure 10 - Environmental room containing the automated monitoring device and corrosion specimens.

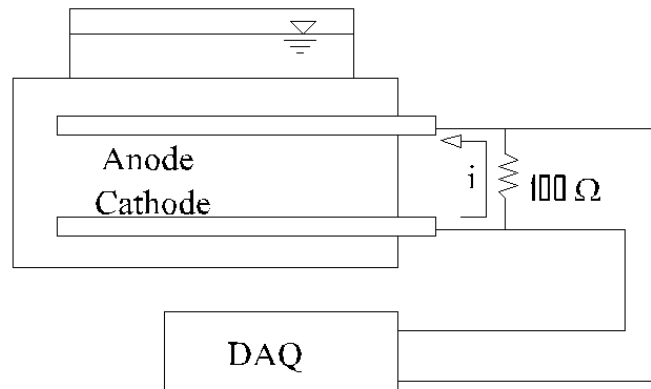


Figure 11 - Electrical diagram of corrosion specimens

#### 4.3.6 BACKGROUND CHLORIDE LEVEL (FM 5-516)

This method is used to determine the background levels of chloride in a concrete mixture. The results were used in calculations to determine the absolute level of chloride intrusion for ASTM C1556. The use of SCM has no effect on this test, as their compositions do not contain significant levels of chlorides.

A concrete and paste sample was taken from the fresh concrete and allowed to hydrate for 3 days. Next, the hydrated concrete and paste was pulverized so that samples could be taken

for chloride analysis. A chemical titration was performed to find the initial chloride content of each mix.

#### 4.3.7 SURFACE RESISTIVITY (FM 5-578)

This non-destructive test measures the electrical resistivity across the face of a saturated concrete specimen to provide an indication of its permeability. The electrical resistivity of saturated concrete depends primarily upon the capillary pore size, pore system complexity, and interconnectivity of the pore system. As the pore system decreases in volume and becomes less interconnected, the measured surface resistance increases indicating that chlorides will diffuse more slowly through the concrete. The use of SCM contributes to the decrease in surface resistivity by decreasing the pore volume and interconnectivity.

All specimens were water-saturated 4-in. diameter x 8-in. long molded cylinders. These samples were cured in a moist room containing no saturated lime water, as this decreases the resistivity of the concrete. A Surface Resistivity meter with a Wenner linear four-probe array was implemented as shown in Figure 12. Surface resistivity was found in accordance with FM 5-578 for concrete cylinders at 3, 7, 28, 91, and 365 days of age.

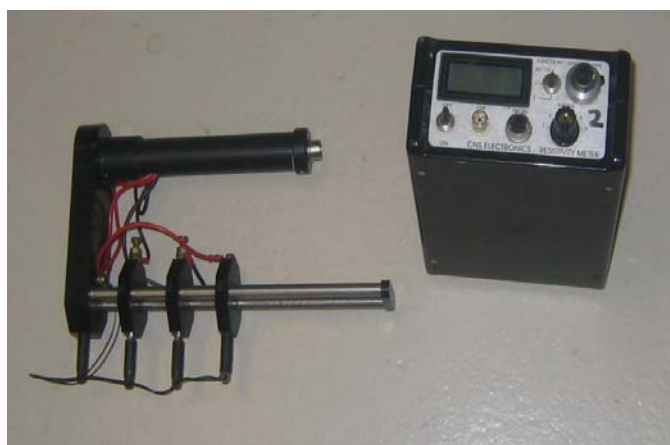


Figure 12 - Wenner linear four-probe array and display

#### 4.3.8 RAPID MIGRATION TEST (NTBUILD 492)

This procedure was used to determine the chloride migration coefficient in concrete from non-steady-state migration experiments. A lower migration coefficient measured with the Rapid Migration Test (RMT) indicates that the concrete will have reduced chloride diffusion rates.

Samples for this research were cut from 4 in. below the finished surface of molded 4-in. diameter x 8-in. long concrete cylinders. Cylinders were cured in a moist condition at a

temperature of  $73.4 \pm 3.0^{\circ}\text{F}$ , so that free water was maintained on the surface at all times. Tests were conducted at 28, 56, and 91 days of age. At the appropriate test date, specimens were removed from the curing room and preconditioned by desiccating for three hours. Next, while maintaining vacuum, the desiccation chamber was filled with a saturated  $\text{Ca}(\text{OH})_2$  and held under vacuum for an additional hour. The specimens were kept in the solution for  $18 \pm 2$  hours. Each specimen was then placed in the test setup as shown in Figure 13. The power supply was preset to 60 volts and the initial current through each specimen was recorded. The test voltage was then adjusted based on the initial current reading (see Table 13) and left running for 18 hours. A data logger system similar to the RCP equipment read temperature of the anolyte solution, charge passed, and current every 5 minutes.

After the monitoring process of 18 hours was completed, the RMT set-up was disassembled and the concrete samples were removed. The specimens were rinsed with tap water and the excess solution was wiped off the surfaces.

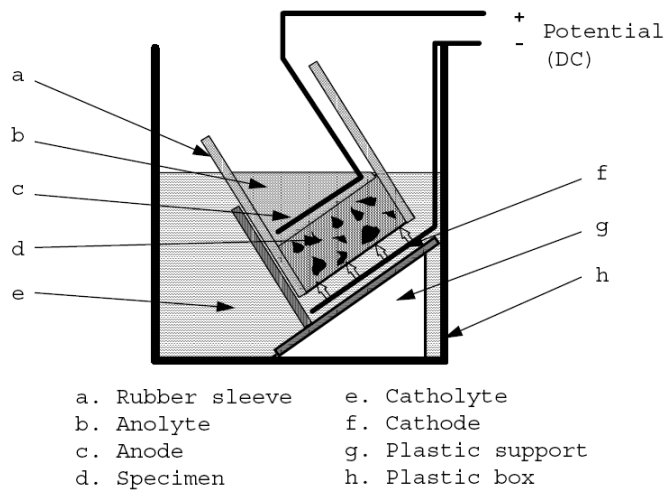


Figure 13 - RMT test setup

Table 13 - Test voltage and duration for NTBuild 492

Initial Current @ 30V [mA]	Applied Voltage [Volts]	Test Duration [hr]	Expected Penetration [mm]	V*t [V-hr]
< 5	60	96	< 23	5,760
5-10	60	48	12-20	2,880
10-15	60	24	10-15	1,440
15-20	50	24	12-16	1,200
20-30	40	24	12-18	960
30-40	35	24	15-21	840
40-60	30	24	18-27	720
60-90	25	24	22-33	600
90-120	20	24	26-35	480
120-240	15	24	26-54	360
240-400	10	24	36-77	240
400-600	10	24	36-77	240
> 600	10	6	> 19	60

Immediately following the test, each specimen was removed and split longitudinally. A silver nitrate solution was then sprayed on exposed surface to highlight the chloride penetration. Measurements to the nearest 0.1 mm were then made using a digital caliper. From these measurements the migration coefficient was calculated from the following equation:

$$D_{nssm} = \frac{0.0239(273+T)L}{(U-1)t} \left[ x_d - 0.0238 \sqrt{\frac{(273+T)Lx_d}{U-2}} \right] \quad \text{Equation 1}$$

where  $D_{nssm}$  is the migration coefficient,  $\times 10^{-12} \text{ m}^2/\text{s}$ ;  $U$  is the absolute value of the applied voltage,  $V$ ;  $T$  is the average value of the initial and final temperature in the anolyte solution,  $^{\circ}\text{C}$ ;  $L$  is the thickness of the specimen,  $\text{mm}$ ;  $x_d$  is the average value of the penetration depths,  $\text{mm}$ ;  $t$  is the test duration,  $\text{hr}$ .

#### 4.3.9 WATER PERMEABILITY (UF METHOD)

A concrete structure can be severely compromised through direct intrusion of deleterious chemicals, such as chloride and sulfate. Therefore, the concrete's ability to resist sulfate or chloride ion penetration is an essential factor in the performance of a durable concrete. It is for this reason that permeability becomes an important characteristic of a concrete. The

implementation of SCM will create a less permeable concrete. The concrete rheology and hardened structure will be altered by the pozzolans. Better consolidation and less bleeding can be achieved. This creates a concrete with less capillaries and interconnected pores. The mature concrete is also affected; through pozzolanic reaction, a denser and less permeable C-S-H product is produced.

In previous research (Soongswang et al., 1989) a testing method was developed to directly measure the water permeability of a concrete sample. Permeability specimens were created for this method from molded 4-in. diameter x 8-in. long molded concrete cylinders. All cylinders were cured in a moist condition at a temperature of  $73.4 \pm 3.0^{\circ}\text{F}$ , so that free water was maintained on the surface at all times. From each of these cylinders a 2-in. thick slice was cut from 3 in. below the finished surface. Around each slice, a 2-in. wide impermeable epoxy (Sikadur 32 High-Mod ) ring was cast and allowed to cure for 24 hours. This epoxy ring serves to bond with the sides of the concrete so that a one-dimensional flow will be achieved during the permeability test. Sikadur 32 High-Mod epoxy was utilized because it has a higher strength and a similar coefficient of thermal expansion as the concrete used in this investigation. The permeability testing specimens was then installed into the acrylic fixture as shown in Figure 14.

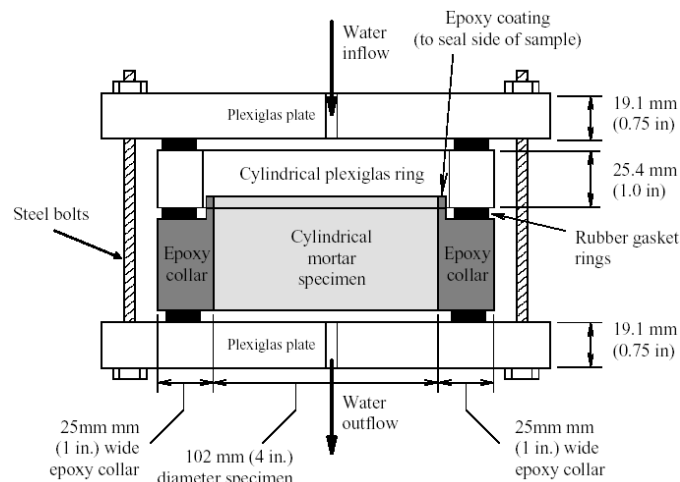


Figure 14 - Cross-section of water permeability specimen fixture

The specimen and fixture was then attached to the permeability testing apparatus as shown in Figure 15. A constant 100 psi water pressure was applied to each specimen. After steady state had been achieved, the specimen was then removed from the apparatus.

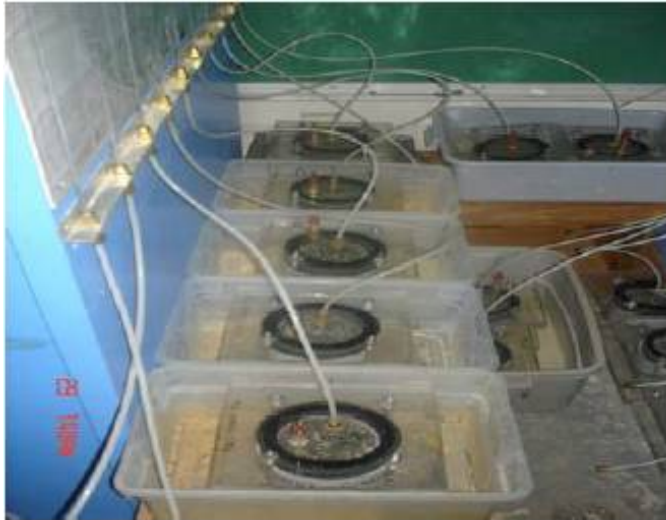


Figure 15 - Water permeability test setup

## 5 RESULTS AND DISCUSSION

This chapter describes and discusses the results obtained through experimental analysis. Inconsistencies in test data prompted the re-creation of test specimens for MOE, Poisson's ratio, and flexural strength tests. These changes are presented in the mechanical test section below.

### 5.1 PLASTIC PROPERTIES TESTS

The results from the plastic properties tests are presented in Table 14. Each value represents either a single test result or an average of individual tests, depending on the test method. Unit weight, for example, was taken during mixing and represents a single test. The values differed by no more than 2% from the extreme measured values.

Table 14 - Plastic properties

Mixture	Density (lb/ft <sup>3</sup> )	Slump (in)	Air (%)	Bleed (%)	Initial Set (min)	Final Set (min)	Temp. (°F)	Air Temp. (°F)
CTRL1	145	5.75	2.0	0.00	300	395	81	75
CTRL2	145	6.00	1.5	0.10	330	400	84	75
SLAG1	144	6.50	1.1	0.19	340	430	81	75
SLAG2	144	6.00	1.0	0.17	355	460	81	75
SLAG3	146	6.50	0.6	0.27	300	445	80	75
META1	144	6.25	1.4	0.00	375	435	84	75
META2	144	7.25	1.5	0.00	390	470	80	75
META3	144	6.00	1.4	0.00	N/A	N/A	80	75
UFA1	146	5.75	0.6	0.55	375	465	78	75
UFA2	145	6.75	1.8	0.00	385	485	78	75
UFA3	144	8.00	1.6	0.00	400	480	78	75
SF1	143	6.25	2.3	0.00	370	445	76	75
SF2	143	6.00	2.3	0.00	385	465	76	75

Density was measured and found to vary by 2% for all mixtures. This indicates that there were no large variations in entrapped air or aggregate volume among mixtures.

Slump measurements were between 5.75 to 8 in., indicating reasonably consistent plastic properties. Due to natural variability of concrete workability, a consistent concrete slump from mixture to mixture is difficult to obtain. For most mixtures, however, the slump values were within  $\pm 1$  inch of the 7-in. target value. This allowed for consistent consolidation among mixtures, thus minimizing variation in test results due to inconsistent specimen fabrication.

Air content was found to range from 0.6% to 2.3%, which was below the target air content of 3%. The measured values, however, were within the acceptable range of 1 to 5% except for SLAG3 and UFA1, which had an air content of 0.6%. These lower air contents appeared to result in an increase in bleeding when comparing the results for SLAG3 and UFA1 of 0.27% and 0.55%, respectively. CTRL2, SLAG1, and SLAG2, however, also showed some bleeding, but without an extremely low air content.

Setting times on the cement paste indicated that initial set was at 140 minutes and final set at 215 minutes. The concrete mixtures in this investigation had initial set times that ranged from 300 to 400 minutes; final set times ranged from 395 to 485 minutes. These set times were greater than that of the paste by 114% to 185% and 84% to 126% for initial and final setting times, respectively. For CTRL1, the setting time increased by 114% for initial set and 84% for final set over the cement tests. This indicates that the addition of the retarder was successful in delaying the setting times. CTRL2 (18% fly ash) also showed extended setting times when compared to CTRL1 (cement only), revealing that the replacement of cement with fly ash retards the setting times. In addition, all other mixtures show an increase in setting times over CTRL2, indicating that the larger quantity of SCM further delays the setting times. The literature has suggested that metakaolin shortens the setting times, while silica fume has no affect (Zongjin and Ding 2003; ACI 234R-06). However, when looking at the mixtures with the same proportions of SCM, such as META1 (18% fly ash and 8% metakaolin) and SF1 (18% fly ash and 7% silica fume), little difference in setting times are noticed. This suggests that setting time is more greatly affected by the decreases in proportions of cement, rather than the addition of a particular admixture.

Fresh concrete temperatures ranged from 76 to 84°F, while the air temperature remained constant at 75°F. This temperature range is small; therefore, with this level of replacement, there was little affect on the fresh concrete temperature from the addition of SCM.

## **5.2 MECHANICAL TESTS**

The mechanical test results for compressive strength, flexural strength, modulus of elasticity (MOE), Poisson's ratio, and splitting tensile strength are presented below. Trends and relationships have been noted in the results of each test.

### 5.2.1 COMPRESSIVE STRENGTH (ASTM C 39)

Figure 16 shows the strength gain curve for all the mixtures. Early compressive strength of concrete made with slower reacting SCM, such as slag and fly ash, was less than that of the concretes made with portland cement alone, as seen in the lower values of early strength in the plot. In contrast, mixtures made with silica fume and metakaolin exhibited a higher strength than with portland cement alone. At later ages, however, the low reactivity SCM continued to react and by 365 days, the compressive strength had converged to values of approximately 10.5 ksi. The lower compressive strength of SLAG3 was likely the result of errors in mixing that will be discussed subsequently.

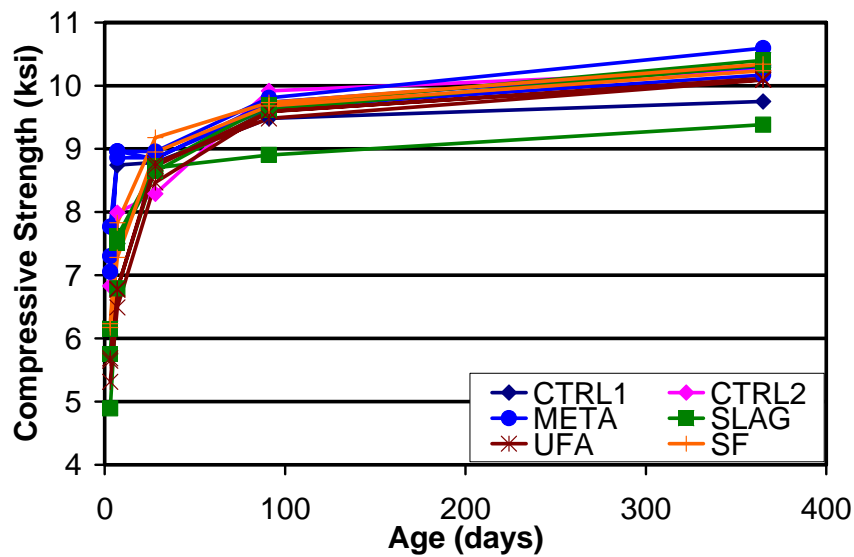


Figure 16 - Compressive strength of all mixtures

Although the strength gain curve is not linear, it is useful to examine the rate of strength gain by considering the slopes of the lines between the 91 and 365 day strengths. These slopes presented in Table 15 show the average 365 day compressive strength for each mixture. The compressive strengths are also normalized to the CTRL1 strength to show the improvement and relative value. Disregarding SLAG3, the compressive strengths vary from CTRL2 by no more than 3%, indicating very consistent values at late ages. The slopes of CTRL1 and CTRL2, however, are nearly parallel, indicating that their rates of hydration are comparable even though CTRL2 contains fly ash.

Table 15 - Average compressive strength at 365 days, normalized 365 day compressive strength to CTRL2, and 91 to 365 day slope

Mixture	365 day Compressive Strength (ksi)	Normalized Compressive Strength	91 to 365 day Slope (ksi*10 <sup>5</sup> /day)
CRTL1	9.75	0.95	9.8
CTRL2	10.25	1.00	11.9
SLAG1	10.40	1.02	26.0
SLAG2	10.33	1.01	25.8
SLAG3	9.38	0.92	17.5
META1	10.17	0.99	19.1
META2	10.31	1.01	20.7
META3	10.59	1.03	28.8
UFA1	10.09	0.99	18.3
UFA2	10.09	0.98	22.3
UFA3	10.11	0.99	19.2
SF1	10.24	1.00	20.4
SF2	10.34	1.01	22.1

Furthermore, the slopes of the slag mixtures are parallel and are steeper than that of the control mixtures, indicating a higher rate of hydration. Similarly, the metakaolin, ultrafine fly ash, and silica fume mixtures show steeper slopes than the control mixtures. Therefore, it is likely that these mixtures will produce higher compressive strength than the controls at later ages. However, because the strength gain curves are non-linear, only trends can be noted and accurate predictions of later compressive strengths cannot be made.

At various ages, the compressive strength of a concrete plays a key role in the selection of a mixture. For example, in prestressed concrete, early compressive strength is needed to allow for the transfer of prestress and allow the concrete member to be removed from the prestressing bed. Conversely, higher compressive strength at later ages is needed for piling to prevent damage during driving. Therefore, a more refined analysis of the early and late compressive strengths of each mixture is discussed.

Figure 17 shows the early age strength development of the concrete mixtures containing ground granulated blast furnace slag compared to the two control mixtures. Figure 18 presents the late age strength development. The control mixture, CTRL1 (cement only), had a higher early strength than CTRL2 (18% fly ash), which is typical of low early strength developing mixtures containing low reactive SCM.

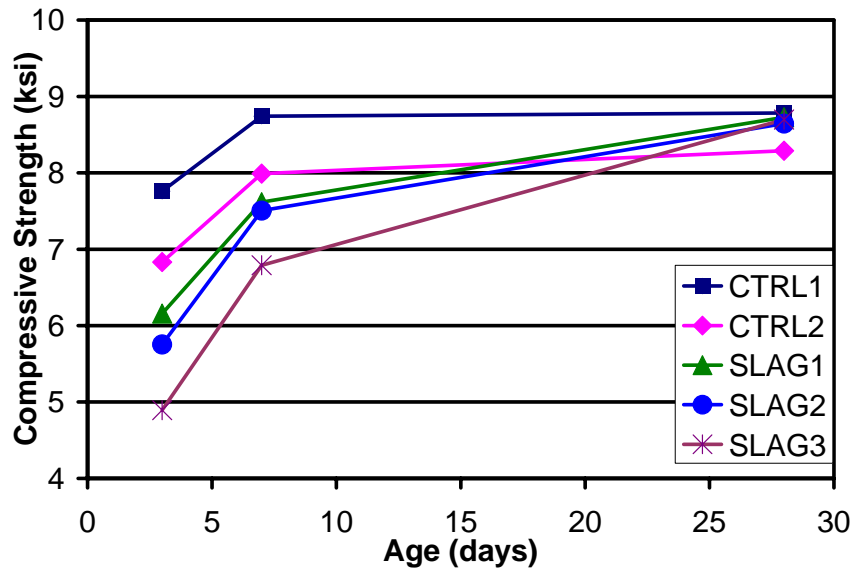


Figure 17 - Average early strength of slag mixtures

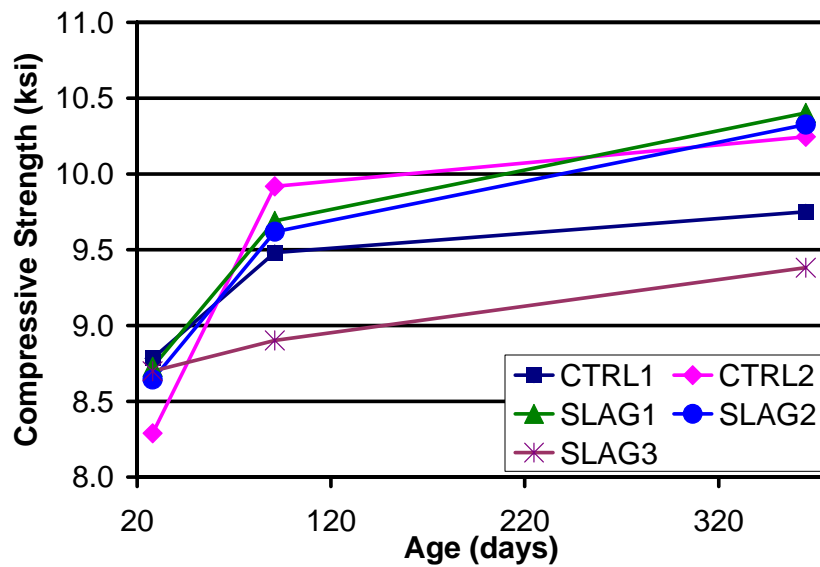


Figure 18 - Average late strength of slag mixtures

The data show that the average compressive strength of each slag mixture at 3 days and 7 days age is below that of the two control mixtures, which is a result of the further delay caused by the replacement of portland cement with slag. Generally, slag has low reactivity at early ages and therefore will not contribute to early strength development. Indeed, it is not until around an age of 91 days when the slag mixtures begin to have a higher compressive strength than CTRL1.

At 365 days, the compressive strength of both SLAG1 and SLAG2 show a strength well above that of CTRL1, and slightly higher than CTRL2.

The data from Figure 17 and Figure 18 show that SLAG3 exhibits lower strength than SLAG1 and SLAG2. As mentioned before, the higher SCM content in SLAG3 was expected to develop higher compressive strengths than SLAG1 and SLAG2. However, this did not happen. From Table 14, it is clear that SLAG3 shows a high bleed percentage when compared to other mixtures. This would suggest that there were problems with mixing. If the proportions were incorrect, this may lead to poorer performance than would be expected. Indeed, this trend of poor performance of SLAG3 is noted throughout subsequent test procedures.

Figure 17 also shows that at early ages, the average compressive strength decreases as SCM content is increased. In contrast, this trend seems to be reversed as the age increases. The data show that at 91 days, all slag mixtures are very close to having the same compressive strength. As mentioned before, ground granulated blast furnace slag generally has low reactivity at early ages and will begin to develop a dense C-S-H matrix as hydration continues. Therefore, the mixtures containing higher proportions of slag will exhibit a low early strength. At later ages, however, the slag will begin to react and eventually develop a higher strength concrete in the mixtures containing higher volumes of slag.

Figure 19 shows the early age strength development of the mixtures containing metakaolin compared to the two control mixtures. Figure 20 presents the late age strength development. Because of its high reactivity, the metakaolin mixtures show a high early strength when compared to the control mixtures. As expected, all metakaolin mixtures have an average compressive strength above that of CTRL2 for 3 day, 7 day and 28 day ages. The strength of the metakaolin mixtures then begin to overtake that of CTRL1 at an age of apparently 7 days. At an age of 91 days, however, CTRL2 has developed a higher strength than CTRL1 and all mixtures containing metakaolin. This is explained by the denser C-S-H matrix developed in slower hydration of the fly ash itself in CTRL2. By 365 days, however, the compressive strength of META1 and META2 are nearly equal to that of CTRL2. META3 shows that highest strength.

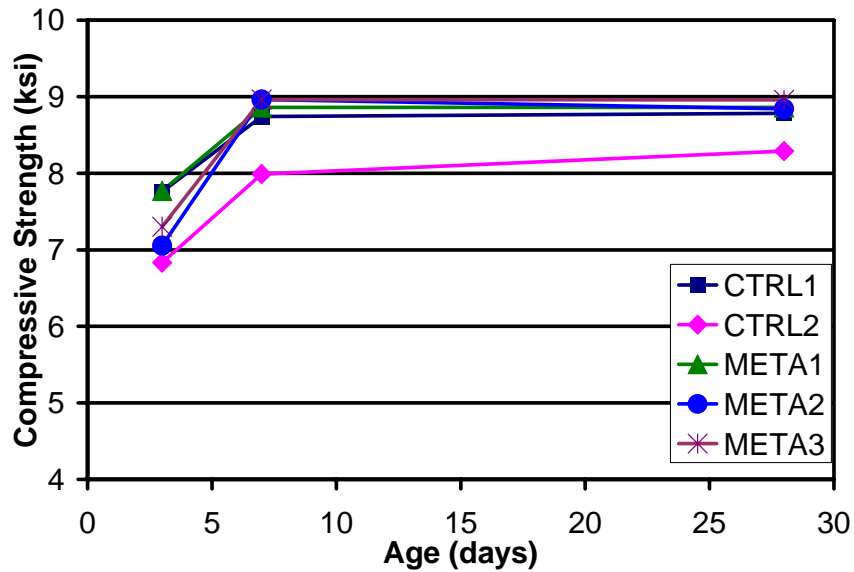


Figure 19 – Average early strength of metakaolin mixtures

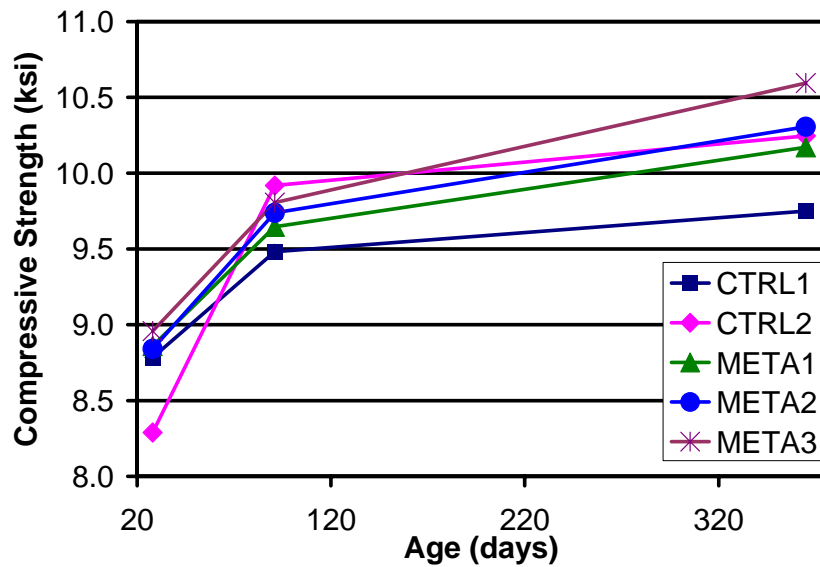


Figure 20 - Average late strength of metakaolin mixtures

As the proportion of metakaolin increases, the data show a higher average compressive strength at later ages. The higher content of SCM results in a larger amount of available silicate oxide (S) to react with calcium hydroxide (CH) to produce a denser matrix of C-S-H compounds.

Figure 21 shows the early age strength development of the mixtures containing ultrafine fly ash compared to the two control mixtures. Figure 22 presents the late age strength development. At 3 day and 7 day ages, all mixtures containing ultrafine fly ash have a lower average compressive strength than both CTRL1 and CTRL2. At 28 day age, all three ultrafine

fly ash mixtures have a higher strength than CTRL2, while CTRL1 remains at nearly the same strength. As the strength begins to develop, CTRL2 compressive strength becomes the highest. This again is due to the dense C-S-H matrix formed by the slow hydration rate of fly ash. At 91 days, CTRL2 continues to develop strength, while the ultrafine fly ash mixtures and CTRL1 have nearly the same compressive strength. However, by 365 days, the compressive strength of the ultrafine fly ash mixtures is only slightly lower than CTRL2. The strength of CTRL1 is still considerably lower than the other mixtures.

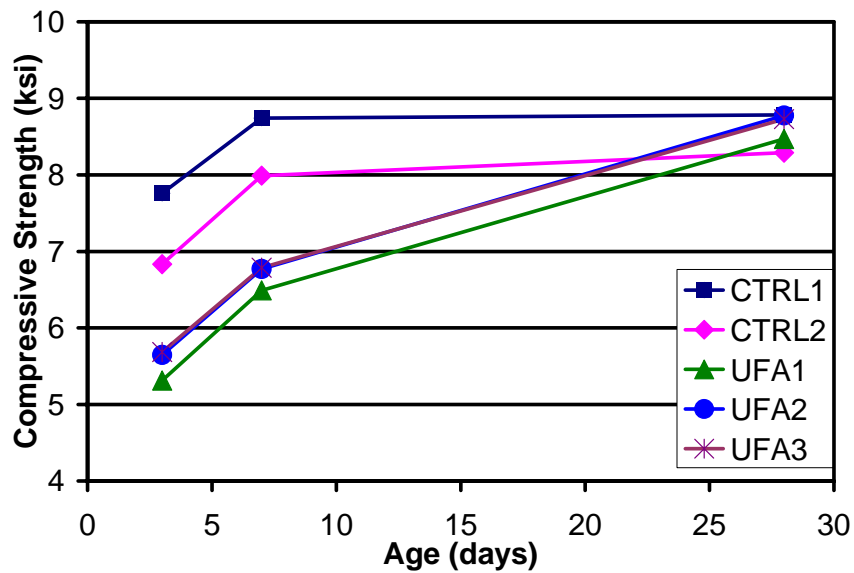


Figure 21 - Average early compressive strength of ultra-fine fly ash mixtures

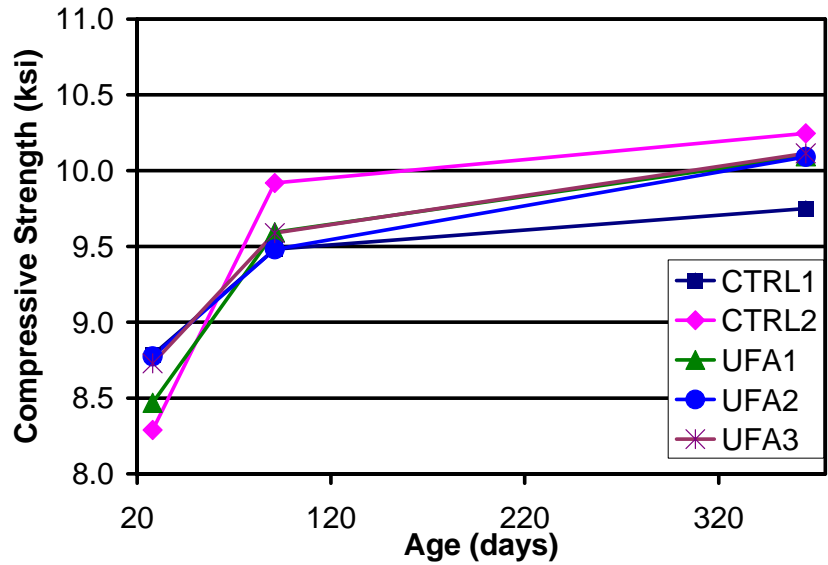


Figure 22 - Average late compressive strength of ultra-fine fly ash mixtures

It is apparent that the compressive strength increases as the dosage of ultrafine fly ash is increased. Due to the increase in S as SCM is increased, a large quantity of CH is consumed. Thus, a denser matrix of C-S-H will form as proportions of ultrafine fly ash are increased.

Figure 23 shows the early age strength development of the mixtures containing silica fume compared to the two control mixtures. Figure 24 presents the late age strength development. Because of its high reactivity, the silica fume mixtures show a comparable early strength to the control mixtures. At 3 day and 7 day tests, the strength of the silica fume is nearly the same as CTRL2 and only slightly less than CTRL1. At 28 days of age, the silica fume mixtures have gained strength and surpassed the average compressive strength of both CTRL1 and CTRL2. At 91 days, the silica fume mixtures have continued to gain strength and remain higher than CTRL1. The compressive strength of CTRL2, however, has increased considerably and now is the highest. By 365 days, both silica fume mixtures show a large increase in strength, and are now nearly equal to that of CTRL2.

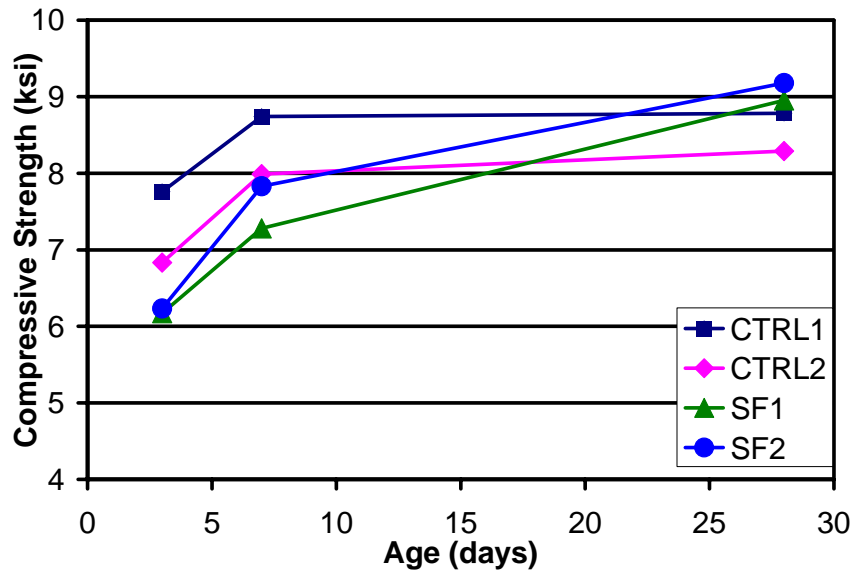


Figure 23 – Compressive strength of silica fume mixtures

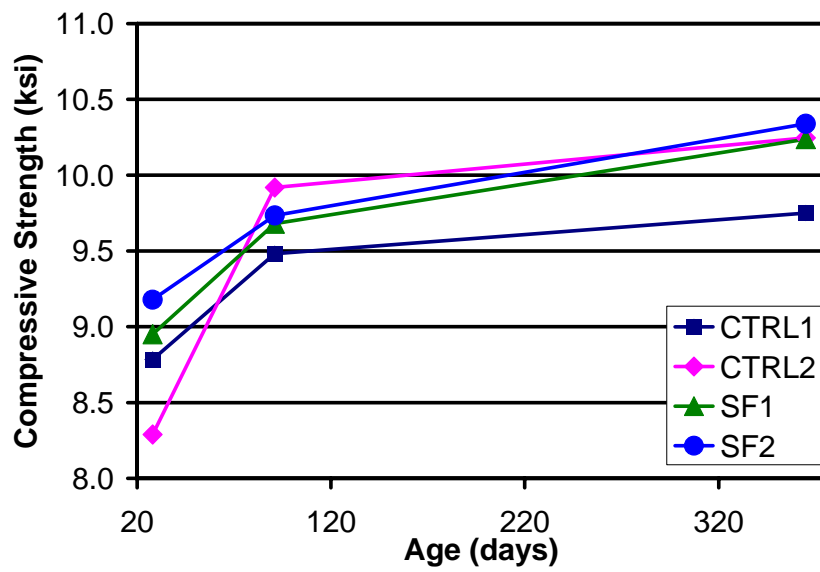


Figure 24 - Compressive strength of silica fume mixtures

From Figure 23, it is apparent that the mixture with the higher proportion of silica fume, SF2, has a higher strength at all ages when compared to SF1. This is explained by the larger quantity of reactive silica, S, gained by increasing the proportion of the SCM. Again, a stronger, denser C-S-H matrix is formed, thus increasing the compressive strength.

Manufacturing of prestressed concrete piles depends primarily on the early strength development of the concrete mixture. Prestress cannot be transferred until a minimum

compressive strength is achieved. Consequently, production is slowed and profits are reduced while the member remains in the forms. It is likely that the manufactures would prefer a high early strength mixture. Typically, prestressed forces are transferred when the concrete has a compressive strength in the range of 3,500 to 4,500 psi. At 3 days, all mixtures in this investigation exceeded this range. Therefore, in relation to early removal from prestressing forms, the SCM did not improve the mixture over the controls.

The compressive strength also becomes important during pile driving because the forces associated with driving damage may damage the piles. At stresses above 30% of the compressive strength, microcracking begins to develop; at about 70%, the cracks begin to propagate through the paste (Mindess et al. 2003). Cracking that develops will reduced the durability by providing a direct path for deleterious chemicals to enter the concrete. Therefore, a higher compressive strength will reduce the amount of damage caused by the pile driving process. Typically at around 28 days, the piles are removed from storage and driven. At this age, CTRL2 showed the lowest compressive strength. The slag, metakaolin, and ultrafine fly ash mixtures had nearly the same compressive strength as CTRL1. The silica fume mixtures, however, did show a slight improvement in compressive strength over CTRL1. Therefore, it appears that the silica fume mixtures would provide the best resistance to damage caused by driving at this age.

### 5.2.2 FLEXURAL STRENGTH (ASTM C 78)

The number of flexural strength specimens cast in the first mixture allowed testing at 7 and 28 day ages. A second mixture was done so that tests could be conducted at 7, 28, and 365 days and to correct potential laboratory errors noted in the first set of tests. The data presented in this section are the results from both the first and second set of mixtures.

The early modulus of rupture (MOR) of concrete made with low reactivity SCM is usually less than that of portland cement alone. The slower reaction time results in a delay of strength gain, which varies with the type of SCM. From Figure 25, the ultrafine fly ash and slag mixtures showed the lowest strength at early age. In contrast, concrete made with a highly reactive SCM will gain strength faster, as seen with the metakaolin and silica fume mixtures. At 365 days, the silica fume and slag mixtures showed the highest MOR.

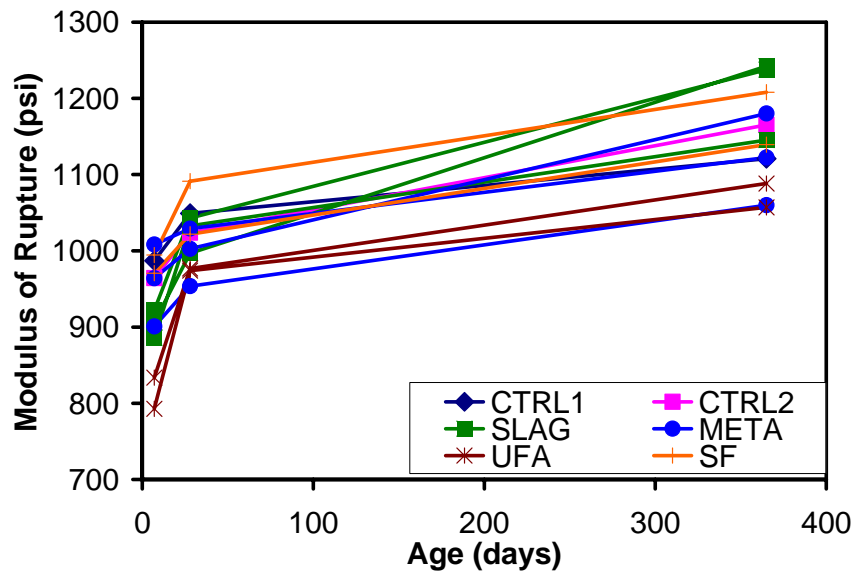


Figure 25 - Modulus of rupture of all mixtures

Table 16 shows the individual MOR values along with the average and COV at each age. If there were significant differences in performance between the various mixes, then the COV would be expected to be high. The COV for the 7-day data is 7.0% and is even lower (3.5%) at 28-days. This indicates that the SCM do not significantly affect the tensile strength of the concrete either at early or late ages.

The MOR is an important parameter used to calculate the cracking strength of reinforced and prestressed concrete members. ACI (363R-92) has found that for both lightweight and normal weight high-strength concrete, the MOR falls in the range of  $7.5\sqrt{f'_c}$  to  $12\sqrt{f'_c}$  in psi. The following formula is recommended as a prediction of the tensile strength of concrete as measured by the MOR from the compressive strength:

$$\text{Modulus of Rupture} = 11.7 * \sqrt{f'_c} \text{ (psi)} \quad \text{Equation 10}$$

where  $f'_c$  is the compressive strength (psi). Table 16 shows the MOR and compressive strength data for all mixtures, along with a calculated coefficient based on the  $\sqrt{f'_c}$ . The average coefficient was calculated for each of the three test ages of 7, 28, and 365 days.

The coefficients range from 9.6 to 12.8, with an average of 10.5, 10.8, and 11.4 for 7, 28, and 365 days, respectively. The actual coefficients are slightly lower than what is predicted in

the ACI equation. This may be a reflection of the type of aggregate used in the tests that were conducted to determine the coefficient of the ACI equation.

Table 16 - Modulus of rupture, compressive strength, and coefficient

Mixture	7 days			28 days			365 days		
	$f_r$ (psi)	$f_c$ (psi)	$f_r/\sqrt{f_c}$	$f_r$ (psi)	$f_c$ (psi)	$f_r/\sqrt{f_c}$	$f_r$ (psi)	$f_c$ (psi)	$f_r/\sqrt{f_c}$
CTRL1	987	8,741	10.6	1049	8,784	11.2	1,121	9,750	11.4
CTRL2	964	7,990	10.8	1024	8,289	11.2	1,165	10,246	11.5
SLAG1	886	7,616	10.2	1033	8,728	11.1	1,145	10,403	11.2
SLAG2	922	7,506	10.6	1043	8,644	11.2	1,238	10,326	12.2
SLAG3	906	6,791	11.0	997	8,699	10.7	1,242	9,382	12.8
META1	901	8,860	9.6	954	8,860	10.1	1,060	10,171	10.5
META2	1,008	8,962	10.7	1029	8,841	10.9	1,122	10,306	11.1
META3	964	8,962	10.2	1003	8,959	10.6	1,180	10,594	11.5
UFA1	793	6,490	9.8	974	8,469	10.6	1,057	10,094	10.5
UFA2	834	6,770	10.1	977	8,775	10.4	1,088	10,090	10.8
UFA3	853	6,787	10.4	984	8,729	10.5	1,132	10,114	11.3
SF1	971	7,281	11.4	1022	8,951	10.8	1,139	10,024	11.4
SF2	994	7,831	11.2	1091	9,178	11.4	1,208	10,272	11.9
Average	922		10.5	1010		10.8	1,150		11.4
COV	7.0%		4.0%	3.5%		3.4%	5.0%		5.4%

### 5.2.3 MODULUS OF ELASTICITY AND POISSON'S RATIO (ASTM C 469)

A second set of mixtures were prepared from which modulus of elasticity (MOE) specimens were fabricated. Detailed results from tests on both mixtures are included in Appendix A.

At 7 days the metakaolin mixtures showed a higher MOE than the controls (Figure 26). Subsequent ages showed nearly equal MOE to controls. Although silica fume is also a highly reactive pozzolan, its interactions with fly ash decrease MOE at 7 and 28 days. By 365 days, however, the silica fume mixtures showed the highest MOE of all mixtures. Generally, every other mixture showed lower MOE than the controls because of their low reactivity.

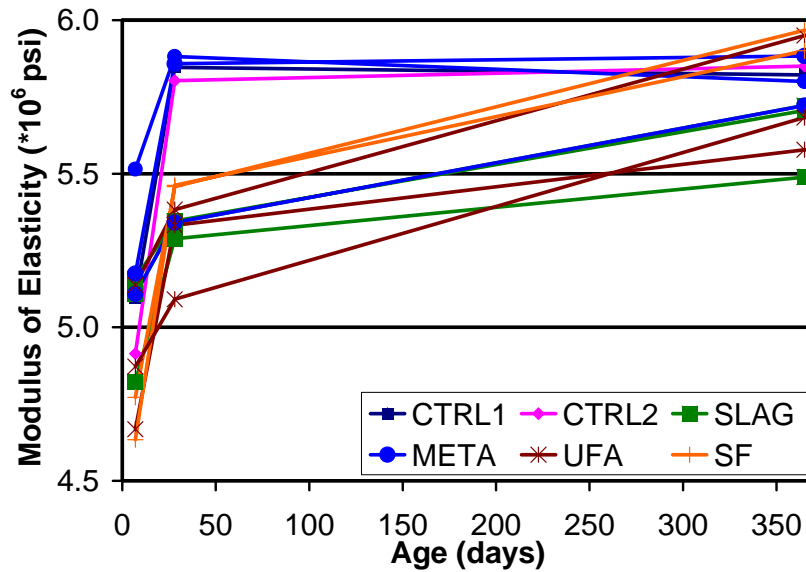


Figure 26 - Average modulus of elasticity of all mixtures

Figure 27 shows the change in MOE in the slag mixtures. At 7 days of age, SLAG1 and CTRL2 had a lower MOE than CTRL1; SLAG2 and SLAG3 were nearly the same as CTRL1. At 28 days, both control mixtures had shown a large increase in MOE to place them well above each slag mixture. Each slag mixture had shown small gains. Both CTRL2 and CTRL1 had shown almost no increase between 28 and 365 days of age, while the MOE in each slag mixture increased over this period.

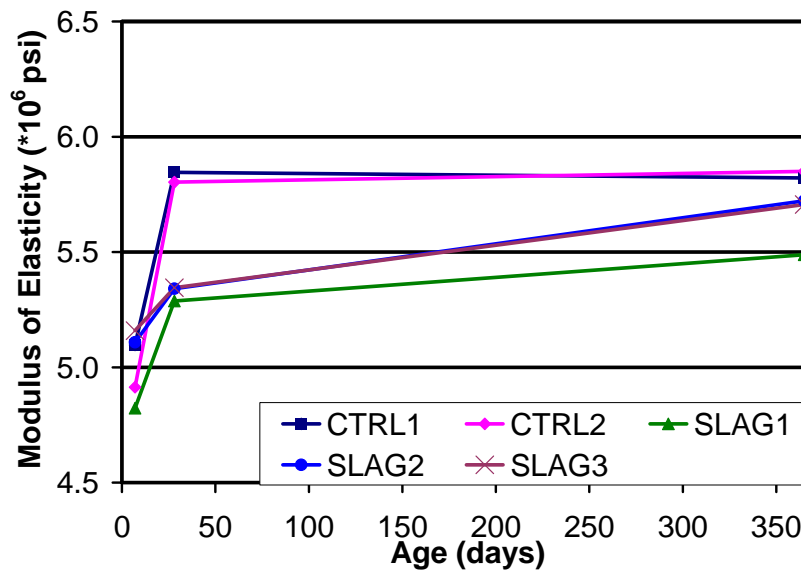


Figure 27 - Average modulus of elasticity of slag mixtures

The slow gain in MOE for the slag mixtures is attributed to the low reactivity of slag. At early ages, the breakdown of the silica within the slag is minimal. As cement hydrates, the release of hydroxyl ions increases, allowing the slag to be activated. As these mixtures hydrate, the porosity of the paste decreases. This effect is seen in Figure 27 by the slow increase in the MOE over time. In addition to the low reactivity of slag, the MOE gain of the mixtures is somewhat retarded at early ages from the interactions of fly ash with the decreased presence of alkalis. The hydration of the fly ash requires a high alkalinity in the pore solution. However, slag hydration reduces the alkalinity. Therefore, the hydration of slag within mixtures reduces the reactivity of the fly ash. This is also seen from the dramatic increase in MOE in CTRL2 over the slag mixtures—which contain the same percentage of fly ash.

The MOE for metakaolin mixtures is presented in Figure 28. At 7 days, each mixture containing metakaolin has a higher MOE compared to the control mixtures. The higher early MOE of the metakaolin mixtures is attributed to the high reactivity of the SCM. At early ages, the metakaolin mixtures have high strength development and low porosity. Therefore, when comparing the moduli to the controls, the metakaolin mixtures perform well at 7 days. The MOE at 28 days for all mixtures is nearly the equal. There is very little difference in MOE at 365 day age.

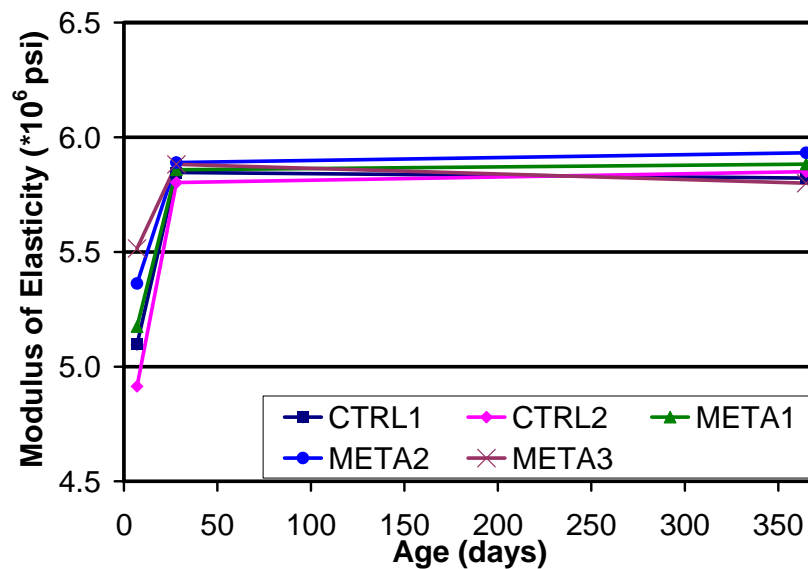


Figure 28 - Average modulus of elasticity of metakaolin mixtures

Figure 29 shows the MOE of ultrafine fly ash mixtures. The 7 day MOE of the ultrafine fly ash mixtures and CTRL2 were below that of CTRL1, with the exception of UFA1. At 28

days, there had been only little improvement in the MOE of the ultrafine fly ash mixtures. However, both control mixtures had a considerable gain in MOE and were nearly the equal. The results at 365 days show that there had been almost no increase for the control mixtures, while each ultrafine fly ash mixture had shown a large improvement in MOE.

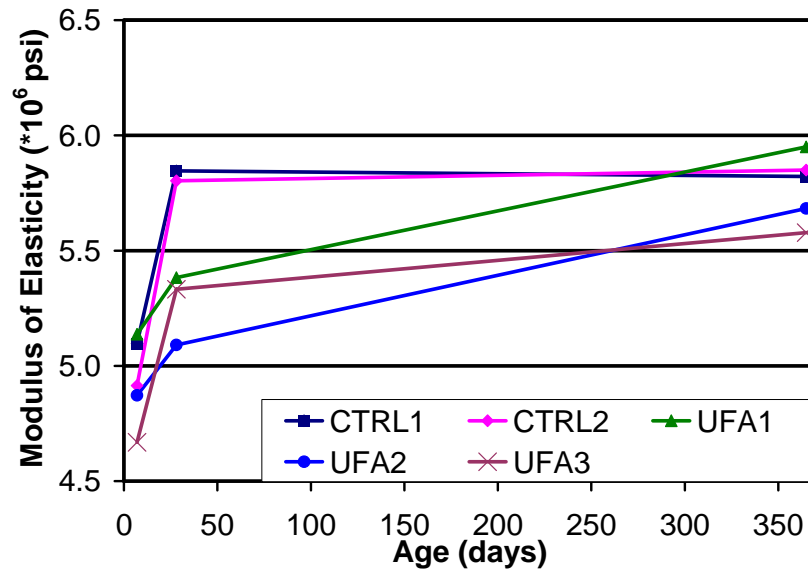


Figure 29 - Average modulus of elasticity of ultra-fine fly ash mixtures

The results from 28 days further illustrate the previous statement; the higher proportions of total fly ash have reduced the hydration compared to the control mixtures. However, by 365 days, the ultrafine fly ash mixtures have continued to hydrate to form a denser, less permeable concrete when compared to the control mixtures. This is seen in the large increase of the ultrafine fly ash mixtures in MOE between the ages 28 and 365 days, while the control mixtures have shown almost no increase.

The MOE for silica fume mixtures is presented in Figure 30. The MOE results at 7 days for the silica fume mixtures are below that on the control mixtures. By 28 days, the silica fume and control mixtures have all had nearly the same increase in MOE. The results at 365 days show that the control mixtures have not had any increase in MOE. The silica fume mixtures have continued to increase; however, and were greater than that of the control mixtures.

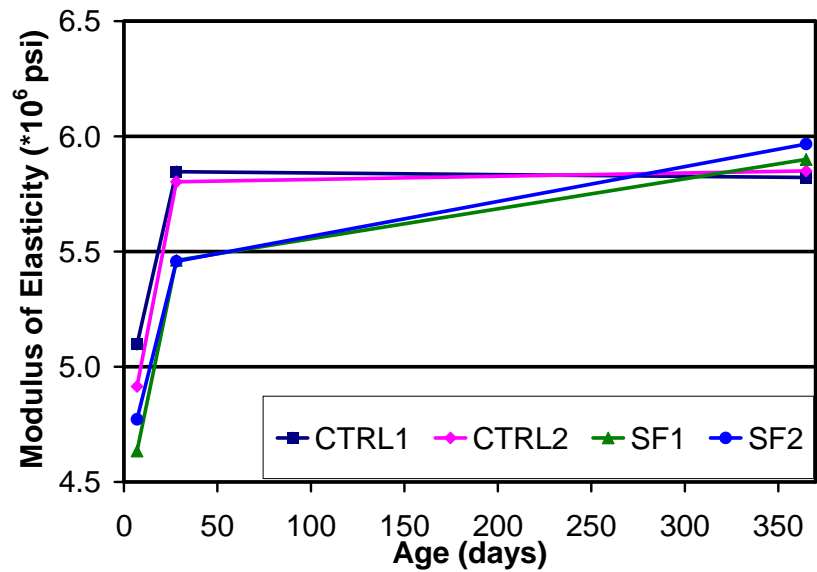


Figure 30 - Average modulus of elasticity of silica fume mixtures

It appears that the addition of silica fume in combination with fly ash lowers the MOE at 7 and 28 day ages. The reduction in MOE is attributed to the decreased reactivity of fly ash with silica fume. The alkalinity of the pore water is reduced with the pozzolanic reaction of silica fume, which causes the fly ash to remain inactive until the alkalinity is high enough to cause activation. This effect is seen at 7 and 28 day ages. By 365 days, the MOE of the silica fume mixtures has surpassed the control mixtures. This shows that the silica fume and fly ash has had enough time to continue hydration.

ACI (318R-02) has defined the concrete MOE for densities between 90 and 155 lb/ft<sup>3</sup> as:

$$E_c = 33w_c 1.5 * \sqrt{f'_c} \quad \text{Equation 11}$$

where  $E_c$  is the secant modulus,  $w_c$  is the density of the concrete in pcf, and  $f'_c$  is the compressive strength in psi. Consequently, factors that affect strength also influence MOE. The most dominant factor is porosity as modulus will decrease markedly with the increase in porosity (Mindess et al. 2003). Therefore, the mixtures containing SCM should have higher MOE because of associated decreases in porosity through pozzolanic reaction.

No clear trend's appear in the Poisson's ratio, either with age or across mixtures (Table 17).

Table 17 - Poisson's ratio

Mix	7—day	28—day	365—day
CTRL1	0.26	0.28	0.27
CTRL2	0.18	0.28	0.18
SLAG1	0.26	0.26	0.20
SLAG2	0.28	0.26	0.31
SLAG3	0.25	0.26	0.30
META1	0.27	0.29	0.23
META2	0.26	0.26	0.21
META3	0.25	0.26	0.21
UFA1	0.24	0.24	0.26
UFA2	0.24	0.26	0.37
UFA3	0.24	0.25	0.22
SF1	0.23	0.26	0.28
SF2	0.25	0.26	0.22
Average	0.25	0.26	0.25

#### 5.2.4 SPLITTING TENSILE STRENGTH OF CYLINDRICAL CONCRETE (ASTM C 496)

The data show high variability for all testing ages. Although care was taken to limit errors from affecting the results, the fact remains that the level of variability within the sample set is large enough to influence the trend. These errors are largely attributed to the specimen shape; many were not perfectly cylindrical through its entire length. Due to deformations in cylinder molds, the finished surface was oval shaped in many cylinders. This would allow a non-uniform load to be applied during the test, thus affecting the apparent tensile strength of the specimen. It is because of this high variability that no conclusions were drawn from these data.

### 5.3 DURABILITY TESTS

The results obtained from tests of linear shrinkage, volume of voids, change in length due to sulfate exposure, absorption, surface resistivity, rapid migration tests, and water permeability are discussed below. Trends and relationships in the results have been noted in the discussion for each test.

#### 5.3.1 LINEAR SHRINKAGE (ASTM C 157)

The average percent length change for a concrete age of 32 weeks is presented in Table 18. The two control mixtures, CTRL1 and CTRL2, have the highest levels of length change when compare to all other mixtures. This shrinkage is attributed mostly to the interconnectivity of the specimen porosity. CTRL 1 experiences the largest shrinkage because it contains no

SCM. Its paste most likely contains a higher volume C-S-H porosity and larger capillary pores. CTRL2 shows a less shrinkage when compared to CTRL 1 due to the addition of fly ash. The fly ash has reacted with CH to form a denser C-S-H matrix as well as decreased the amount and size of capillary pores (Neville 1995).

Table 18 - Average percent length change, COV, and normalized (to CTRL1) shrinkage values at 32 weeks of age

<b>Mix</b>	<b>Shrinkage (%)</b>	<b>COV</b>	<b>Normalized Shrinkage</b>
CTRL1	0.0360	12.1	1.00
CTRL2	0.0330	6.1	0.92
SLAG1	0.0307	13.2	0.85
SLAG2	0.0247	27.0	0.69
SLAG3	0.0270	6.4	0.75
META1	0.0243	8.6	0.68
META2	0.0210	20.2	0.58
META3	0.0227	3.1	0.63
UFA1	0.0330	4.6	0.92
UFA2	0.0207	43.4	0.57
UFA3	0.0193	36.7	0.54
SF1	0.0287	17.6	0.80
SF2	0.0253	6.0	0.70

Generally, as the proportion of SCM is increased, the average shrinkage is decreased. The increased SCM provides a larger quantity of reactive silica that allows more CH to react, and thus forming a denser C-S-H matrix. The increased proportion of SCM also reduces the quantity and size of capillary pores.

The ultrafine fly ash mixtures had the least shrinkage compared to the control mixtures. However, UFA1 shows a high level of shrinkage; in fact, this mixture shows the same change in length as CTRL2. The most likely cause is from a high volume of large capillary pores; this mixture exhibited the highest level of bleeding, as shown in Table 14. The metakaolin mixtures also performed well, followed by the silica fume and slag mixtures.

The importance of shrinkage in structures is related to cracking. The cracking tendency of a concrete is function of not only shrinkage but also the tensile strength and restraint from shrinkage deformation. If the stress created from the shrinkage in a restrained concrete exceeds the tensile strength of the concrete, cracking will occur. The limiting tensile strain ranges between  $100 \times 10^{-6}$  and  $200 \times 10^{-6}$  (Neville 1995). The linear shrinkage of all the mixtures

ranged from 0.019% to 0.036%, suggesting that each mixture will begin to develop shrinkage cracking in a restrained system. However, the extent of shrinkage cracking will differ between mixtures. CTRL1 showed the highest level of linear shrinkage, while UFA3 showed the lowest, followed by UFA2 and META2. With each group of SCM, shrinkage decreased as the proportion increased. As a whole, the ultrafine fly ash mixtures showed the best performance.

### 5.3.2 VOLUME OF VOIDS AND ABSORPTION (ASTM C 642)

The volume of permeable pore space, voids, range from 13.1 to 15.5%, while the average percent absorption ranges from 5.9 to 7.1% (Table 19). META3 has the maximum absorption and void content, while SLAG2 exhibits the lowest. However, the data are nearly equal for all mixtures. Therefore, neither voids nor absorption appears to be affected by the use of SCM. This is contradicted by research by Parande (et al. 2006) and Gonen and Yazicioglu (2006) in which the use of metakaolin, fly ash, and silica fume each resulted in a decrease in voids and absorption. This research, however, was conducted on mixtures with water to cementitious material ratios (w/cm) of 0.45 and 0.50, which were higher than what was used in this investigation. The higher w/cm produces a larger quantity and size of capillary pores (Mindess et al. 2003). Neville (1995) has found that at a w/cm below 0.38, capillary pores will no longer be present and voids will be small and disconnected within the hydrated cement paste. In this investigation, a w/cm of 0.35 was used. Therefore, there were no capillary pores available for the hydration products to fill, which is the reason why the use of SCM had no effect on the volume of voids and absorption characteristics of the concrete.

Table 19 - Average percent void and absorption, COV, and normalized (to CTRL1) void and absorption values at 32 weeks of age

Mixture	Voids			Absorption		
	(%)	COV	Normalized	(%)	COV	Normalized
CTRL1	13.9	4.1	1.00	6.31	4.9	1.00
CTRL2	13.8	2.6	0.99	6.30	2.5	1.00
SLAG1	13.6	2.4	0.98	6.20	1.3	0.98
SLAG2	13.1	2.3	0.94	5.92	1.7	0.94
SLAG3	14.5	1.7	1.05	6.66	1.9	1.05
META1	15.0	2.4	1.08	6.92	1.8	1.10
META2	15.0	3.7	1.08	6.89	1.9	1.09
META3	15.5	4.1	1.12	7.14	2.0	1.13
UFA1	14.2	2.3	1.03	6.52	2.0	1.03
UFA2	13.9	2.6	1.00	6.34	1.4	1.00
UFA3	14.3	1.4	1.03	6.56	1.9	1.04
SF1	13.6	2.1	0.98	6.31	1.8	1.00
SF2	13.3	2.9	0.96	6.18	2.8	0.98

### 5.3.3 SULFATE EXPANSION (ASTM C 1012)

Figure 31 depicts a plot of normalized values of average sulfate expansion for the concrete specimens. Each mixture was normalized to CTRL1 to provide a means of assessing the effects of the SCM of the sulfate resistance of the concrete. Generally, as the proportion of SCM is increased, the average expansion is decreased. This is attributed to an increase in reactive silica, S, as the SCM are increased. As a result, more CH is consumed and thus lowering the gypsum corrosion.

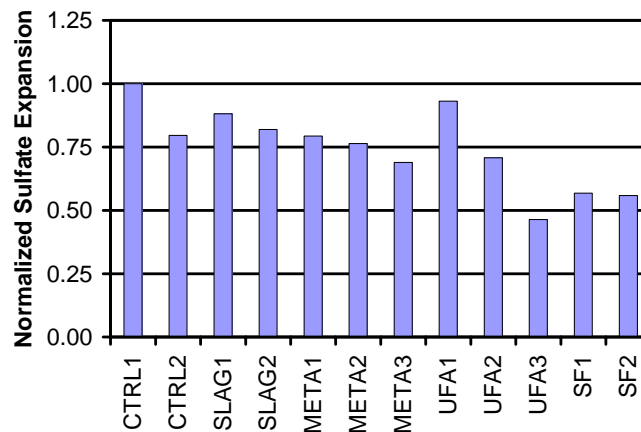


Figure 31 - Normalized values of sulfate expansion (concrete specimens)

SLAG3 was excluded from Figure 31 because its high expansive behavior that is most likely attributed to its higher permeability. The bleed water measurements presented in Table 14 for this mixture, show a high value when compared to other mixtures. This would indicate that SLAG3 had slight problems with segregation. This in turn increases the size and quantity of capillary pores, thus increasing the permeability. Therefore the more permeable concretes will allow a large ingress of sulfate, and eventually a higher average expansion.

Figure 32 presents the normalized values of the average sulfate expansion each mixture for mortar specimens that were sieved after mixing to remove the coarse aggregate. The data for each mortar specimen was also normalized to CTRL1 so that a relative comparison can be made for each mixture. The first and most important indication is that SCM reduce sulfate expansion of the paste. As the proportion of SCM is increased, the sulfate expansion is decreased. The increased proportions of SCM increase the total available reactive silica within the mixture. This in turns allows for more CH to be consumed, thus lowering the gypsum corrosion.

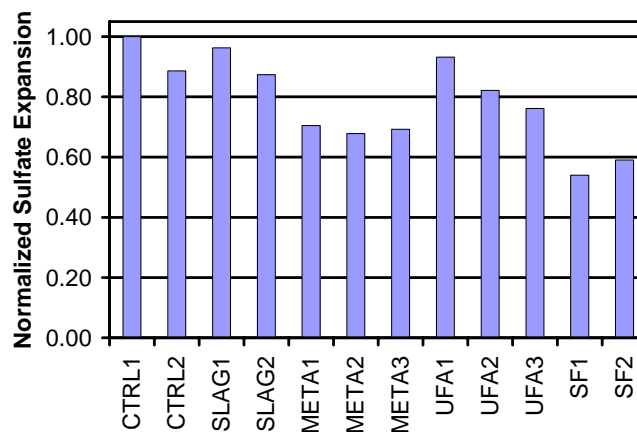


Figure 32 - Normalized values of sulfate expansion (mortar specimens)

External sulfate attack is typified by expansion of concrete, leading to cracking and spalling. Skalany (et al. 2002) has found research that suggests several expansion limits as a failure criterion for mortar and concrete samples exposed to an external sulfate attack. A 0.1% expansion was proposed as the maximum acceptable criterion for failure for a moderate sulfate resistant concrete, while a 0.05% expansion was the limit for a high sulfate resistant concrete when tests were performed according to ASTM C 1012. According to these limits, each mixture

could be classified as highly sulfate resistant as their expansion was well below the 0.05% limit (Table 20).

Table 20 - Total concrete and mortar expansion (%)

<b>Mixture</b>	<b>Concrete Expansion</b>	<b>Mortar Expansion</b>
CTRL1	20.9	12.0
CTRL2	18.1	11.7
SLAG1	15.9	10.7
SLAG2	24.3	6.3
SLAG3	10.6	18.3
META1	18.2	6.7
META2	30.8	20.7
META3	15.7	4.7
UFA1	27.0	4.1
UFA2	49.8	13.0
UFA3	35.6	10.8
SF1	16.9	8.9
SF2	29.4	17.7

The percent expansions in the concrete prisms are about half as much as the mortar prisms (Figure 33). This is because the coarse aggregate is not susceptible to sulfate attack and therefore is not expansive. In both the concrete and mortar prisms, CTRL1 showed the highest levels of sulfate expansion. As a whole, the silica fume and metakaolin mixtures performed the best. However, these improvements may not significantly extend the life of the concrete as each concrete is well below the 0.5% expansion limit proposed by Skalny (et al. 2002). Extended sulfate attack tests are needed to determine the attributes of each mixture at later ages.

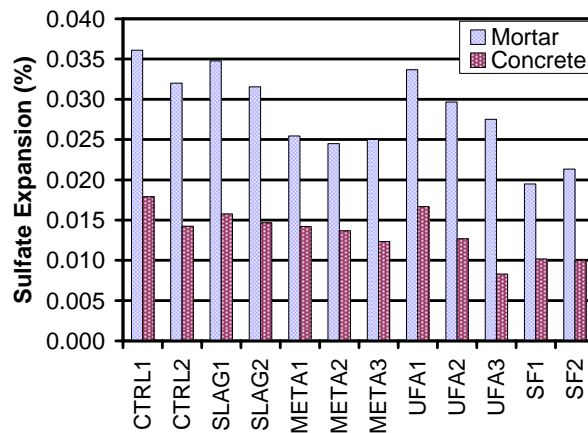


Figure 33 - Comparison of mortar and concrete sulfate expansion specimens

### 5.3.4 CORROSION OF EMBEDDED STEEL REINFORCEMENT (ASTM G 109)

A plot of current vs. ages for UFA3 is shown in Figure 34. It is apparent that there is no change in current throughout the test duration. This is typical of all mixtures in this investigation. Therefore, at the present time, corrosion has yet to initiate in the specimens for the corrosion of embedded steel reinforcement tests. Plots of all mixtures are shown in Appendix A.

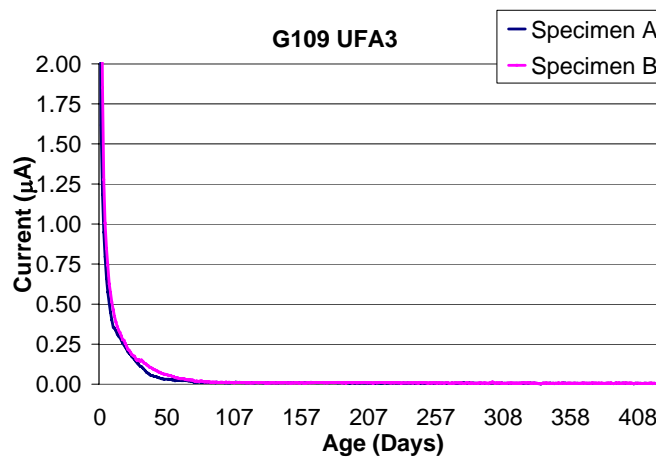


Figure 34 - Corrosion of embedded steel reinforcement

### 5.3.5 SURFACE RESISTIVITY (FM5-578)

Whiting and Mohammed (2003) have found that the conductivity of a concrete is related to its permeability and diffusivity of ions through the concrete. Consequently, the electrical resistance can be used as an estimation of chloride ion penetrability (Hooton et al. 2001). Research conducted by Chini (et al. 2003) relating the surface resistivity measurements to Rapid Chloride Penetration tests produced a reference table to aid the interpretation of the surface

resistivity results, which was later adopted by FM 5-578. The table categorizes the chloride ion penetrability of a concrete from surface resistivity measurements.

Figure 35 compares the surface resistivity (SR) of the control and slag mixtures. At the early ages of the control and slag mixtures of 3 and 7 days, there was not much of a difference in the SR values of all slag mixtures from the control mixtures. However, beyond these early ages, there were noticeable increases in the slag mixture's resistivity. At the 28 day age, the slag mixtures had increased by roughly 150%, while the controls had only increased by about 50% (Table 21). At the 91 day age, all slag mixtures had continued to increase, but at a slower rate. CTRL2 had shown a large increase (128%) to about double the surface resistivity in CTRL1. The SR reading of CTRL1 had only increase by 20%. At 365 day age, the SR of all slag mixtures had continued to increase. The resistivity of CTRL2 has also continued to increase but at a faster rate than the slag mixtures. By this age, the surface resistance of CTRL2 is nearly equal to that of the slag mixtures. CTRL1 has shown only a minimal increase (8%) in surface resistance.

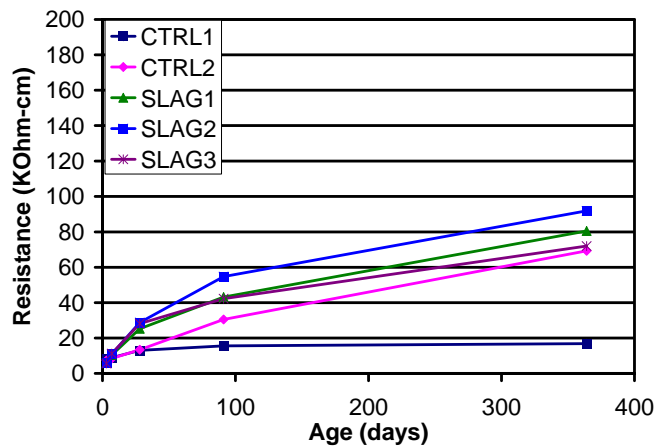


Figure 35 - Average surface resistance of slag concrete mixtures

Table 21 - Increase in surface resistivity between test ages (%)

Mixture	Age (days)			
	3 to 7	7 to 28	28 to 91	91 to 365
CRTL1	8	46	20	8
CRTL2	15	58	128	127
SLAG1	70	142	71	86
SLAG2	91	164	90	68
SLAG3	101	150	50	70
META1	247	100	31	82
META2	309	80	54	89
META3	261	163	27	78
UFA1	34	250	200	126
UFA2	24	271	200	133
UFA3	27	332	200	109
SF1	107	461	79	43
SF2	154	501	89	14

As the proportion of SCM is increased, larger volumes of reactive silica are available to chemically combine with CH to form more C-S-H. Consequently, a denser, less permeable concrete is produced. However, SLAG3 had the largest volume of SCM, but was the worst performing slag mixture. This was most likely attributed to mixing problems. The bleed water measurements presented in Table 14 for this mixture, show a high value when compared to all others. This would indicate that SLAG3 had slight problems with segregation. This in turn increased the size and quantity of capillary pores, thus increasing the permeability. However, SLAG3 still performed better than both control mixtures at all ages.

From Table 21, it is clear that CTRL2 (18% fly ash) showed the largest increases in SR at 91 and 365 days; the earlier dates showed only small gains. This shows the slower reactivity of the fly ash SCM. Beyond 28 days the fly ash reaction accelerates and improves the SR properties of the mixture. The slag mixture, on the other hand, showed larger increases in the earlier ages than fly ash; the largest gains were seen between 7 and 28 days, with a steady increase in SR throughout the testing regime. This indicates that the slag is more reactive and will contribute more to the early properties of the concrete than fly ash.

Figure 36 shows a plot of the average surface resistance of the metakaolin concrete mixtures compared with the control mixtures. At 3 days of age, there was no noticeable difference between the metakaolin mixtures and the control mixtures. However, because of the

high reactivity of metakaolin, the 7 day measurements showed a large increase (241% to 309%) in SR. At 28 days of age, the SR of the metakaolin mixtures had increased by 80% to 163% and now was about 3 to 4 times that of the control mixtures. By 91 day of age, the metakaolin mixtures had continued to show an increase in SR. At 365 days of age, the SR of all metakaolin mixtures had increased by about 80% and had a SR much higher than CTRL1 and about 3 times that of CTRL2.

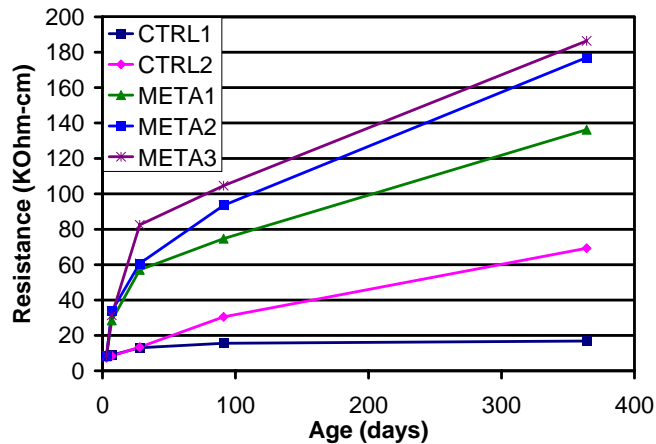


Figure 36 - Average surface resistance of metakaolin concrete mixtures

The largest gains in SR in the metakaolin mixtures were seen in the early ages. Each metakaolin mixtures showed an increase of roughly 275% and a 125% increase at 3 days and 7 days, respectively. This illustrates the very high reactivity of metakaolin. Indeed, the metakaolin showed the largest gain in SR between 3 and 7 days of all the mixtures in this investigation.

The SR of ultrafine fly ash concrete mixtures are compared with the control mixtures in Figure 37. At early ages, 3 day and 7 day, the ultrafine fly ash mixtures show nearly equal resistance when compared to the control mixtures. However, by 28 days, the ultrafine fly ash mixtures showed large increases in SR ranging from 250% to 332%. At 91 days of age, the ultrafine fly ash mixtures continued to have substantially increases (200%) in SR; they were nearly 4 times that of the control mixtures. At 365 days of age, the resistance of the ultrafine fly ash mixtures had increased by roughly 125%. The SR in the ultrafine fly ash mixtures were nearly 10 times greater than CTRL1.

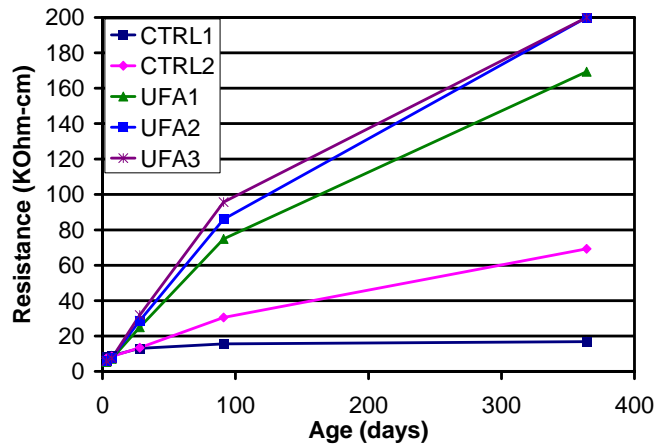


Figure 37 - Average surface resistance of ultra-fine fly ash concrete mixtures

The ultrafine fly ash mixtures showed the largest increases in SR beyond 7 days. The largest gains were seen between 7 and 28 days. The subsequent testing dates also showed significant gains of 200% and roughly 125% at 91 days and 365 days, respectively. The later age SR gains show the low reactivity of the fly ash. However, when comparing the data from CTRL2 to the ultrafine fly ash mixtures, it can be seen that the SR increase at an earlier age than CTRL2. This is attributed to the increased fineness of the ultrafine fly ash.

The SR of silica fume mixtures are compared with the control mixtures in Figure 38. At 3 day ages, silica fume mixtures and control mixtures have nearly equal SR. At 7 days of age, the silica fume mixtures begin to show a greater increase in SR (107% and 154%) than the control mixtures (8 and 15%). At 28 day of age, the mixtures containing silica fume show a dramatic increase in SR (461% and 501%). The silica fume mixtures have a SR of nearly 5 or 6 times greater than the control mixtures. At 91 days of age, all silica fume mixtures showed an increase in SR of about 85%.

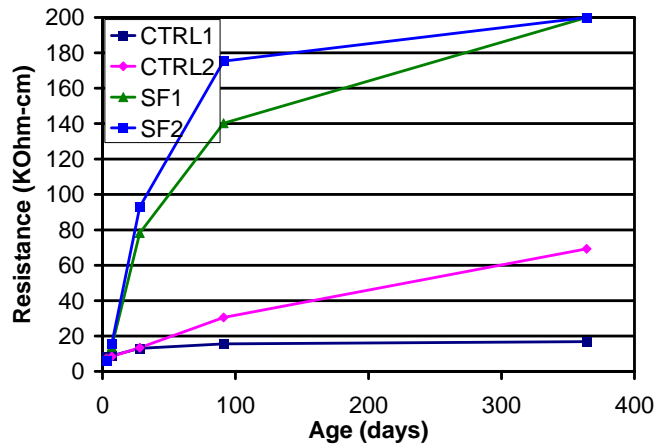


Figure 38 - Average surface resistance of silica fume concrete mixtures

The silica fume mixtures showed the largest increases in SR at the early ages. The largest increases in SR was between 7 and 28 days. In fact, these mixtures showed the largest gains at this age of all mixtures in this investigation. This illustrates the high reactivity of the silica fume. When comparing the metakaolin mixtures with the silica fume, each showed high early reactivity. However, the metakaolin appears to improve the SR at a slightly earlier age than the silica fume. This suggests that the metakaolin is slightly more reactive than silica fume. However, later, the silica fume increase the SR much higher than the metakaolin mixtures, which is likely attributed to the higher reactive silica content in the silica fume.

The research by Chini (et al. 2003) produced a reference table that was developed from their test data to aid the interpretation of the SR result. The table correlated SR with categories of chloride ion penetrability, which was established by Whiting (1981) based on the amount of coulombs passed from the rapid chloride penetration (RCP) test results. The categories of high, moderate, low, very low, and negligible penetrability were related to the depth of chloride penetration after a 90 day ponding test. Table 22 represents a summary of the chloride ion penetrability categories, chloride ion penetration depths, coulombs passed, and SR.

Table 22 - Summary of penetrability category, penetration depth, coulombs passed and surface resistivity

<b>Penetrability Category</b>	<b>Penetration Depth (mm)</b>	<b>Coulombs Passed (Coulombs)</b>	<b>Surface Resistivity (kΩ-cm)</b>
High	> 1.3	> 4,000	< 12
Moderate	0.8 – 1.3	2,000 - 4,000	12 - 21
Low	0.55 – 0.8	1,000 - 2,000	21 - 37
Very Low	0.35 – 0.55	100 - 1,000	37 - 254
Negligible	< 0.35	< 100	> 254

Typically, concrete with RCP results of less than 1000 coulombs is specified by the engineer or owner for concrete elements under extremely aggressive environments (Pfeifer, McDonald and Krauss 1994). From Table 22, this corresponds to a *Very Low* and *Negligible* category. Because the RCP results are based on 90 day ponding tests on specimen that were cured for 28 days, SR at 28 days will be evaluated for each mixture in this investigation.

At 28 days, only the metakaolin and silica fume mixtures were in the *Very Low* category, corresponding to a RCP value less than 1000 coulombs (Table 23). Therefore, based on the 1000 coulomb limit, only the metakaolin and silica fume mixtures would meet the limit for use in an extremely aggressive environment. The use of some SCM creates a slower hydration process, which results in mixtures that may have acceptable SR at later ages. It is not clear if this short delay (relative to the life of the structure) would adversely affect the overall resistance of the concrete to chloride penetration.

Table 23 - Surface resistivity (kΩ-cm)

<b>Mix</b>	<b>3 day</b>	<b>7 day</b>	<b>28 day</b>	<b>91 day</b>	<b>364 day</b>
CRTL1	8	9	13	16	17
CRTL2	7	8	13	30	69
SLAG1	6	10	25	<b>43</b>	<b>80</b>
SLAG2	6	11	29	<b>55</b>	<b>92</b>
SLAG3	6	11	28	<b>42</b>	<b>72</b>
META1	8	29	<b>57</b>	<b>75</b>	<b>136</b>
META2	8	34	<b>61</b>	<b>94</b>	<b>177</b>
META3	9	31	<b>82</b>	<b>105</b>	<b>186</b>
UFA1	5	7	25	<b>75</b>	<b>169</b>
UFA2	6	8	29	<b>86</b>	<b>*200</b>
UFA3	6	7	32	<b>96</b>	<b>*200</b>
SF1	7	14	<b>78</b>	<b>140</b>	<b>*200</b>
SF2	6	15	<b>93</b>	<b>175</b>	<b>*200</b>

### 5.3.6 RAPID MIGRATION TEST (NTBUILD 492)

The rapid migration test (RMT) is an electrical test that relies on estimating the concrete permeability based upon the electrical conductivity properties of a concrete. The RMT calls for an applied potential to force chloride ion to migrate through the concrete. After the test is complete, penetration depths are measured. Because the penetrability of the concrete is based on the interconnectivity of voids, the use of SCM will reduced the depth of chloride ion penetration by creating a denser, less permeable paste structure through pozzolanic reactions.

Figure 39 shows the average Non-Steady-State Migration Coefficient of slag mixtures plotted against the control mixtures. From this plot it is clear that at 28 days, all slag mixtures showed lower migration coefficients than the control mixtures. At this age, the slag within the concrete had started to hydrate. The reactive silica contained within the slag particles is beginning to convert CH to C-S-H, which produces a denser concrete than that of the control mixtures. Thus, the migration coefficients are decreased.

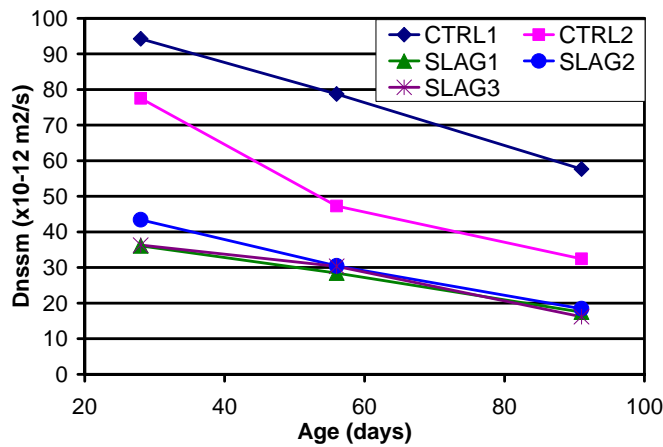


Figure 39 - Average migration coefficient of slag mixtures

At 56 days, CTRL2 shows a 49% decrease in migration coefficient, while CTRL1 only showed a 16% decrease (Table 24). The slag mixtures showed less of a decrease in migration coefficients when compared to CTRL2, however, each slag mixture has a lower absolute migration coefficients at this age. At 91 days, both control mixtures showed a decrease in migration coefficient of about 30%. Each slag mixture showed a larger decrease (39% to 49%) in migration coefficient than the control mixtures. The migration coefficient in CTRL2 was about half that of CTRL1, while each slag mixture was approximately 25% of CTRL1.

Table 24 - Decrease in migration coefficient (%)

Mixture	Age (days)	
	28-56	56-91
CTRL1	16	27
CTRL2	39	31
SLAG1	21	39
SLAG2	30	39
SLAG3	16	47
META1	25	49
META2	2	46
META3	32	32
UFA1	34	74
UFA2	49	37
UFA3	39	63
SF1	13	69
SF2	52	42

Figure 40 shows the average Non-Steady-State Migration Coefficient of metakaolin mixtures plotted against the control mixtures. At all ages, each metakaolin mixture showed a lower migration coefficient when compared to the control mixtures. At 28 days, the migration coefficients in the metakaolin mixtures were roughly 25% of that of CTRL1. At ages of 56 and 91 days, the metakaolin mixtures showed a continual decrease in migration coefficients, ranging from 2% to 32% and 32% to 49%, respectively. The migration coefficient for the metakaolin mixtures were again approximately 25% of CTRL1 at 56 days, and 17% at 91 days.

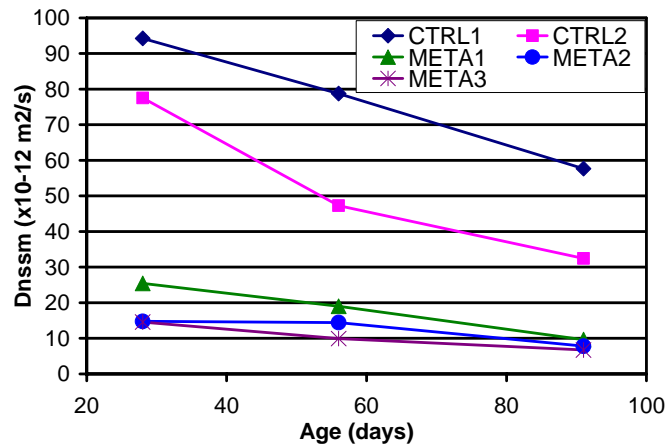


Figure 40 -Average migration coefficient of metakaolin mixtures

Figure 41 shows the average Non-Steady-State Migration Coefficient of ultrafine fly ash mixtures plotted against the control mixtures. At all ages, each ultrafine fly ash mixtures showed a lower migration coefficient when compared to the control mixtures. At 28 days, the migration coefficients in the ultrafine fly ash mixtures were roughly 1/2 of that of CTRL1. At ages of 56 and 91 days, the ultrafine fly ash mixtures showed a continual decrease in migration coefficients, ranging from 34% to 49% and 37% to 74%, respectively. The migration coefficient for the ultrafine fly ash mixtures were approximately 1/4 of CTRL1 at 56 days, and 1/6 at 91 days.

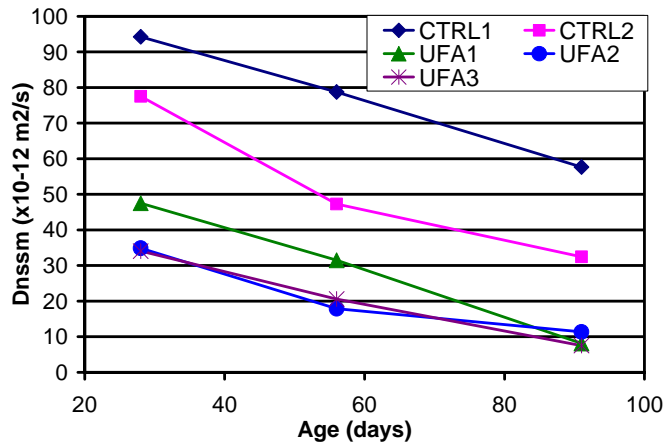


Figure 41 - Average migration coefficient of ultra-fine fly ash mixtures

Figure 42 shows the average Non-Steady-State Migration Coefficient of silica fume mixtures plotted against the control mixtures. At all ages, each mixture showed a lower migration coefficient when compared to the control mixtures. Indeed, both silica fume mixtures show the lowest migration coefficients of all mixtures at all ages. At 28 days, the migration coefficients in the silica fume mixtures were nearly a 10% of that of CTRL1. At ages of 56 and 91 days, the silica fume mixtures showed a continual decrease in migration coefficients, ranging from 13% to 52% and 42% to 69%, respectively. The migration coefficient for the silica fume mixtures were again approximately 13% of CTRL1 at 56 days, and 10% at 91 days.

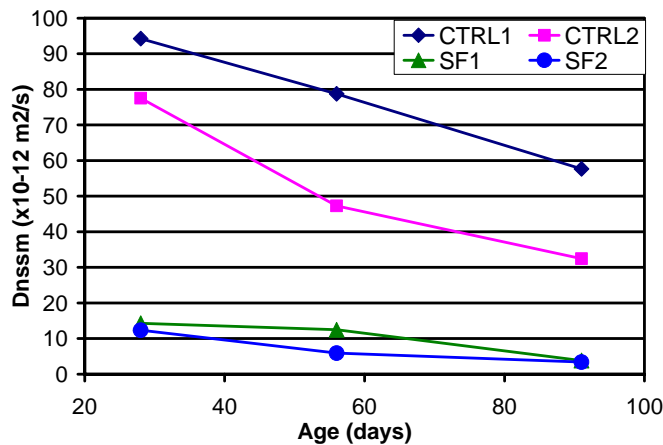


Figure 42 - Average migration coefficient of silica fume mixtures

Acceptance criteria for RMT results have not been established. However, Stanish (et al 2005) has developed a relation between the result of RMT and RCP (Table 25).

Table 25 - RMT and RCP relationship

<b>RMT value (mm/V*hr.)</b>	<b>RCP Value (Coulomb)</b>
0.034	3000
0.024	2000
0.012	800

Typically, concrete mixtures that allow less than 1000 coulombs of charge to pass is specified by the engineer or owner for concrete elements in extremely aggressive environments (Pfeifer, McDonald and Krauss 1994). Through a linear interpolation of the data in Table 25, a RMT value of 0.014 mm/V\*hr. was found to correlate to an RCP value of 1000 coulombs. Based upon the maximum 1000 coulomb limit, an assessment of acceptable mixtures can now be made in Table 26. The mixtures that exceed the limit are illustrated in bold typeface. The data leading to the 1000 coulomb limit was based on 90-day ponding tests that were cured for 28 days. Therefore, 28 day RMT values will be discussed.

The metakaolin and silica fume mixtures have RMT values lower than 0.014 at 29-days. All other mixtures except CTRL1 had RMT values that met the limit by 91-days. This supports the findings from SR tests for both the short term (28-day) and long-term (91-day) test ages.

Table 26 - RMT values (mm/V\*hr)

<b>Mixture</b>	<b>28</b>	<b>56</b>	<b>91</b>
CTRL1	0.029	0.029	0.021
CTRL2	0.025	0.020	<b>0.014</b>
SLAG1	0.016	<b>0.014</b>	<b>0.010</b>
SLAG2	0.016	0.015	<b>0.009</b>
SLAG3	0.017	0.017	<b>0.010</b>
META1	<b>0.013</b>	<b>0.011</b>	<b>0.007</b>
META2	<b>0.008</b>	<b>0.009</b>	<b>0.006</b>
META3	<b>0.009</b>	<b>0.007</b>	<b>0.005</b>
UFA1	0.019	<b>0.014</b>	<b>0.006</b>
UFA2	0.015	<b>0.010</b>	<b>0.008</b>
UFA3	0.017	<b>0.012</b>	<b>0.005</b>
SF1	<b>0.009</b>	<b>0.007</b>	<b>0.006</b>
SF2	<b>0.008</b>	<b>0.005</b>	<b>0.004</b>

### 5.3.7 WATER PERMEABILITY (UF METHOD)

The results gathered from the water permeability test are scattered and inconclusive (Table 27). The most likely cause of variation in coefficients of permeability is caused by poor bond between the concrete specimen and the epoxy barrier.

Table 27 - Coefficient of permeability (28-day)

<b>Mixtures</b>	<b>K<sub>p</sub> (ft/hr)</b>
CRTL1	8.89E-10
CTRL2	8.97E-10
SLAG1	9.81E-10
SLAG2	3.77E-10
SLAG3	4.97E-10
META1	4.45E-10
META2	7.06E-10
META3	1.06E-09
UFA1	5.45E-10
UFA2	8.03E-10
UFA3	1.01E-09
SF1	6.28E-10
SF2	4.34E-10

## 6 SELECTION OF MIXTURE DESIGNS FOR PILES

This chapter describes this method and the rationale for choosing the mixtures to be implemented in the piles for the Key Royale bridge replacement project. The relative cost, mechanical properties, and durability of a concrete are all important factors in bridge construction. Each of these factors was analyzed to determine the mixtures with the most favorable attributes.

Because of the approaching deadline for pile construction, final mixture designs were needed before later age testing could be completed. Consequently, ninety-one day data for the first series of specimens and 28 day data for the second series were available for use in selecting the mixture designs.

### 6.1 SELECTION APPROACH

To rank the mixture designs, a decision matrix was generated using the data collected from both mechanical and durability tests. In addition, relative costs were included. Each set of results were assigned weighting factors to adjust for their relative importance. These results were then normalized to the CTRL1 mixture (cement only) and summed to result in a single score for that mix. For consistency, each of the normalized values was adjusted so that the more favorable results were less than 1.0. Scores were ranked to aid in selection of the best mixture design for each class of SCM. The following sections describe each of the three major selection criteria along with the rationale for the weighting factors.

### 6.2 SELECTION CRITERION I – COST

Although perhaps not the most important factor, material cost often plays a significant role in bridge design and construction. Because of this, cost was a major selection criterion in the decision matrix.

Water, coarse aggregate and fine aggregate quantities are relatively constant among the possible mixtures; consequently, only the relative costs of the cement and SCM were included. Market costs (\$/ton) were collected for cement, fly ash, slag, metakaolin, ultrafine fly ash, and silica fume from the appropriate manufacturers (Table 28). The relative costs are the ratio of the SCM to that of the cement

Table 28 - Material costs

<b>Component</b>	<b>Cost (\$/Ton)</b>	<b>Relative Cost</b>
Cement	95	1.000
Fly Ash	42	0.442
Slag	90	0.947
Metakaolin	480	5.053
Ultrafine Fly Ash	1000	10.526
Silica Fume	600	6.316

### 6.3 SELECTION CRITERION II – MECHANICAL PROPERTIES

The mechanical tests included in the decision matrix were compressive strength, flexural strength, modulus of elasticity, and shrinkage (Table 29). Because the data were highly variable, the splitting tensile strength tests were not included in the analysis. Results from Poisson's ratio were also excluded because they were inconclusive.

Table 29 - Normalized mechanical test results

<b>Mixture</b>	<b>Compressive Strength</b>	<b>Flexural Strength</b>	<b>Modulus of Elasticity</b>	<b>Shrinkage</b>
CRTL1	1.000	1.000	1.000	1.000
CTRL2	0.956	1.092	0.993	0.917
SLAG1	0.978	1.049	0.905	0.852
SLAG2	0.986	1.043	0.914	0.685
SLAG3	1.065	1.132	0.914	0.750
META1	0.983	1.086	0.951	0.676
META2	0.974	1.056	1.008	0.583
META3	0.967	1.041	1.006	0.630
UFA1	0.988	1.084	0.921	0.917
UFA2	1.000	1.081	0.871	0.574
UFA3	0.989	1.091	0.912	0.537
SF1	0.979	1.108	0.934	0.796
SF2	0.974	0.987	0.926	0.704

Time constraints for the approaching construction deadlines for the field portion of the investigation did not allow for 365 day age data. Therefore, 91 day age data for compressive strength were analyzed. Complete testing data from the linear shrinkage tests were available.

Because of the mechanical errors in the testing setup for modulus of elasticity, additional mixtures were produced to retest these specimens. At the time the mixtures were selected, only 28 day modulus of elasticity data were available to be used in the mixture determination process.

Similarly, flexural strength specimens were recreated and tested. Twenty-eight day data were available for analysis.

#### 6.4 SELECTION CRITERION III – DURABILITY

The durability tests included in the decision matrix were surface resistivity, rapid migration test, volume of voids, absorption, and sulfate expansion of mortar specimens (Table 30). Because of time constraints, results from the corrosion of embedded steel reinforcement, ASTM G109, were not available to be used in the decision matrix. Water permeability results were also not included because it was determined that the data were erroneous due to leaks in the bond between the concrete and epoxy.

Table 30 - Normalized durability test results

Mixture	Surface Resistivity	RMT	Voids	Absorption	Sulfate Expansion
CRTL1	1.000	1.000	1.000	1.000	1.000
CTRL2	0.511	0.563	0.993	0.997	0.886
SLAG1	0.360	0.303	0.977	0.982	0.963
SLAG2	0.285	0.320	0.941	0.938	0.874
SLAG3	0.369	0.281	1.046	1.054	0.977
META1	0.208	0.167	1.082	1.096	0.666
META2	0.167	0.136	1.078	1.092	0.609
META3	0.149	0.117	1.119	1.131	0.715
UFA1	0.208	0.141	1.026	1.033	0.932
UFA2	0.181	0.262	0.999	1.005	0.729
UFA3	0.163	0.130	1.029	1.038	0.786
SF1	0.111	0.143	0.980	1.000	0.540
SF2	0.089	0.092	0.960	0.978	0.591

#### 6.5 IMPORTANCE FACTORS

An average normalized test result was calculated for each of the three major categories, cost, mechanical properties, and durability. One consequence of this approach was that each test method result was weighted equally within each category. Therefore, each category was also assigned an importance factor. Because the focus of this investigation was on the durability aspect of concrete mixtures, the durability test category was assigned an importance factor of 50%. The mechanical test category was assigned a factor of 40%, while cost was assigned a

value of 10%. The final score for each mixture design was calculated using the following equation:

$$\text{Score} = 0.10(\text{Cost}) + 0.40(\text{Mechanical Properties}) + 0.50(\text{Durability}) \quad \text{Equation 12}$$

Because each value was normalized so that the more favorable result was represented by a number less than 1.0, the mixture with the lowest score then indicated the mixture design with the most favorable attributes. Therefore, from each class of SCM, the mixture design with the lowest score was selected. Table 31 summarizes the normalized results for the selection criterion for each mixture with the final score.

From these data, CTRL1 and CTRL2 were selected to be the control mixtures for the field investigation. SLAG2, META2, UFA2 and SF2 were selected because of they had the lowest final score within each class of SCM. For clarity, SLAG2 contained 30% slag, META2 contained 10% metakaolin, UFA2 contained 12% ultrafine fly ash, and SF2 contained 9% silica fume.

Table 31 - Summary of normalized results and equation values

<b>Mixture</b>	<b>Cost</b>	<b>Mechanical Tests</b>	<b>Durability Tests</b>	<b>Equation Value</b>
CRTL1	1.000	1.000	1.000	1.000
CTRL2	0.900	0.989	0.790	0.881
SLAG1	0.886	0.946	0.717	0.826
SLAG2	0.884	0.907	0.672	0.787
SLAG3	0.881	0.965	0.745	0.847
META1	1.224	0.924	0.644	0.814
META2	1.305	0.905	0.616	0.801
META3	1.386	0.911	0.646	0.826
UFA1	1.852	0.977	0.668	0.910
UFA2	2.043	0.881	0.635	0.874
UFA3	2.233	0.882	0.629	0.891
SF1	1.272	0.955	0.555	0.786
SF2	1.378	0.898	0.542	0.768

## 7 CONCLUSIONS AND RECOMMENDATIONS

In order to provide sufficient laboratory test data in which the Florida Department of Transportation (FDOT) can utilize in assessing the implementation of alternative SCM in Florida Concretes, various plastic, mechanical, and durability testes were conducted. Thirteen mixtures were investigated that contained fly ash in conjunction with varying proportions of slag, metakaolin, ultrafine fly ash, and silica fume. Plastic property tests were conducted on temperature, air content, slump, bleeding, and setting times. The mechanical test procedures included compressive strength, flexural strength, splitting tensile strength, modulus of elasticity, and Poisson's ratio. Several durability related tests were performed; these tests included, surface resistivity, rapid migration test, volume of voids, absorption, water permeability, shrinkage, sulfate expansion, and corrosion of embedded steel reinforcement. Additionally, this research provided the FDOT with a recommendation of the most effective mixtures containing various pozzolans for the utilization in the piling of the Key Royale bridge replacement project.

Conclusions are as follows:

- It was found that the plastic properties, volume of voids, and absorption were not significantly affected by the use of any of the SCM. Set times were increased slightly in some cases, which were likely a result of the relative reduction in portland cement content.
- In the compressive strength tests, the metakaolin mixtures performed the best at ages of less than 28 days. At 28 days, each mixture exhibited nearly equal compressive strength in which the silica fume mixtures showed the highest. At later ages, all mixtures displayed larger strength than the control mixture. However, at 365 days each mixture containing SCM were nearly equal.
- Tensile strength of the various concrete mixtures as measured by the modulus of rupture (MOR) tests showed insignificant variation as a result of the SCM used.
- The metakaolin mixture showed the best results for modulus of elasticity (MOE), as they were nearly equal to the control at all ages. The silica fume mixtures displayed the lowest MOE at 7 days, and the highest at 365 days.
- Poisson's ratio appeared to be unaffected by the use of SCM, as the average ratio was about 0.25 for all ages.

- The use of SCM improved the resistance to shrinkage; each mixtures exhibited lower linear shrinkage than the control. The 14% ultrafine fly ash mixture showed the lowest amount of shrinkage, followed by the 12% ultrafine fly ash, then 10% metakaolin.
- In the sulfate attack experiments, it was found that the expansion, when compared to the control, was less than 0.5% for mortar and 0.05% for concrete specimens. Generally, the silica fume mixtures showed the lowest amount of expansion, followed by the metakaolin mixtures. However, the 14% ultrafine fly ash mixture showed the largest decrease (54%) in expansion from the control in the concrete specimens.
- The surface resistivity was significantly affected by the use of SCM. At ages beyond 3 days, each mixture showed higher surface resistivity than the control mixture. The slag mixtures showed the lowest surface resistivity, with the exception of the control mixtures. The silica fume mixtures showed the largest surface resistivity, followed by the ultrafine fly ash, then metakaolin.
- The chloride ion penetration was tested using the Rapid Migration Test Method. At each age, all mixtures showed an improvement in migration coefficients when compared to the control. The silica fume showed the best performance, followed closely by metakaolin. The ultrafine showed the least improvement of all the SCM at 28 days; however by 91 days, the slag mixtures showed the least improvement. A relation to the 1000 coulomb limit was also made for RMT results. Again, only the metakaolin and silica fume mixtures were the only acceptable mixtures to be used in an extremely aggressive environment at 28 days. However, at 91 days, all mixtures (excluding CTRL1) were found within the limit.
- Based on results from the decision matrix, the most efficient proportions of SCM to be used in conjunction with 18% fly ash were: 30% slag, 10% metakaolin, 12% ultrafine fly ash, and 9% silica fume.

## 8 REFERENCES

- ACI Committee 232, "Use of Fly Ash in Concrete (ACI 232.2R-03)," American Concrete Institute, Farmington Hills, MI, 41 pp.
- ACI Committee 233, "Slag Cement in Concrete and Mortar (ACI 233R-03)," American Concrete Institute, Farmington Hills, MI, 18 pp.
- ACI Committee 234, "Guide for the Use of Silica Fume in Concrete (ACI 234R-06)," American Concrete Institute, Farmington Hills, MI, 63 pp.
- Akkaya, Y., Ouyang, C., Shah, S., "Effect of Supplementary Cementitious Materials on Shrinkage and Crack Development in Concrete," *Cement & Concrete Composites*, 2007, V. 29, pp. 117-123.
- American Coal Ash Association, "Fly Ash Facts for Highway Engineers," Federal Highway Administration Report FHWA-IF-03-019, June 13, 2003, 76 pp.
- ASTM C 39 "Compressive Strength of Cylindrical Concrete Specimens." ASTM International, West Conshohocken, PA, 2001, 7 pp.
- ASTM C 78 "Flexural Strength of Concrete (Using Simple Beam with Third-Point Loading)." ASTM International, West Conshohocken, PA, 2002, 3 pp.
- ASTM C 138 "Density (Unit-Weight), Yield, and Air Content (Gravimetric) of Concrete." ASTM International, West Conshohocken, PA, 2001, 4 pp.
- ASTM C 143 "Slump of Hydraulic-Cement Concrete." ASTM International, West Conshohocken, PA, 2000, 4 pp.
- ASTM C 512 "Creep of Concrete in Compression." ASTM International, West Conshohocken, PA, 1999, 4 pp.
- ASTM C 173 "Air Content of Freshly Mixed Concrete by the Volumetric Method." ASTM International, West Conshohocken, PA, 2001, 8 pp.
- ASTM C 232 "Bleeding of Concrete." ASTM International, West Conshohocken, PA, 2004, 5 pp.
- ASTM C 403 "Time of Setting of Concrete Mixtures by Penetration Resistance." ASTM International, West Conshohocken, PA, 1999, 7 pp.
- ASTM C 469 "Static Modulus of Elasticity and Poisson's Ratio of Concrete in Compression." ASTM International, West Conshohocken, PA, 2000, 5 pp.

- ASTM C 496 “Splitting Tensile Strength of Cylindrical Concrete.” ASTM International, West Conshohocken, PA, 1996, 5 pp.
- ASTM C 157 “Length Change of Hardened Hydraulic-Cement Mortar and Concrete.” ASTM International, West Conshohocken, PA, 2002, 7 pp.
- ASTM C 642 “Density, Absorption, and Voids in Hardened Concrete.” ASTM International, West Conshohocken, PA, 1997, 3 pp.
- ASTM C 1012 “Length Change of Hardened Hydraulic-Cement Mortars Exposed to a Sulfate Solution.” ASTM International, West Conshohocken, PA, 2004, 6 pp.
- ASTM C 1064 “Temperature of Freshly Mixed Portland Cement Concrete.” ASTM International, West Conshohocken, PA, 2001, 3 pp.
- ASTM C 1585 “Measurement of Rate of Absorption of Water by Hydraulic-Cement Concretes.” ASTM International, West Conshohocken, PA, 2004, 6 pp.
- ASTM G 109 “Determining the Effects of Chemical Admixtures on the Corrosion of Embedded Steel Reinforcement in Concrete Exposed to Chloride Environments.” ASTM International, West Conshohocken, PA, 1999, 9 pp.
- Badogiannis, E., Kakali, G., Dimopoulou, G., Chaniotakis, E., Tsivilis, S., “Metakaolin as a Main Cement Constituent. Exploitation of Poor Greek Kaolins,” *Cement and Concrete Composites*, v. 27, 2005, pp. 197-203.
- Bai, J., Wild, S., Ware, J. A., Saber, B. B., “The Use of Neural Networks to Predict Workability of Concrete Incorporating Metakaolin and Fly Ash,” *Advances in Engineering Software*, v. 34, 2003, pp. 663-669.
- Boral Material Technologies, “Boral Micron 3, A Highly Reactive Pozzolan,” 2003.
- Brooks, J. J., Megat Johari, “The Effects of Metakaolin on Creep and Shrinkage of Concrete,” *Cement & Concrete Composites*, 2001, v. 23, pp. 495-502.
- Brooks, J. J., Megat Johari, M. A., Mazloom, M., “The Effects of Admixtures on the Setting Time of High-Strength Concrete,” *Cement & Concrete Composites*, 2000, v. 22, pp. 293-301.
- Chini, A.R., Muszynski, L.C., Hicks, J., “Determination of Acceptance Permeability Characteristics for Performance-Related Specifications for Portland Cement Concrete,” Florida Department of Transportation, 2003, Final Report No. BC 354-41.
- FDOT “Florida Department of Transportation Standard Specification for Road and Bridge Construction,” Florida Department of Transportation, 2007.

- FDOT “Florida Department of Transportation Structures Design Guidelines.” Florida Department of Transportation, July 2004.
- FM 5-516 “Florida Test Method for Determining Low-Levels of Chloride in Concrete and Raw Materials,” Florida Department of Transportation, revised June 14, 2005.
- FM 5-578 “Florida Test Method for Concrete Resistivity as an Electrical Indicator of Permeability,” Florida Department of Transportation, January 27, 2004.
- Frias, M., Sanchez de Rojas, M. I., Cabrara, J., “The Effect that the Pozzolanic Reaction of Metakaolin has on the Heat Evolution on Metakaolin-Cement Mortars,” *Cement and Concrete Research*, 2000, v. 30, pp.209-216.
- Gonen, T., Yazicioglu, S., “The Influence of Mineral Admixtures on the Short and Long-Term Performance of Concrete,” *Building and Environment*, v. 42, no. 8, 2006, pp. 3080-3085.
- Vivas, E., Boyd, A., and Hamilton III, H. R., “Permeability of Concrete – Comparison of Conductivity and Diffusion Methods,” Florida Department of Transportation, Final Report No. BC 354-41, 2006, 227 pp.
- Hooton, R.D., Thomas, M.D.A., Stanish, K., “Prediction of Chloride Penetration in Concrete.” Final Report No. FHWA/RD-00/142, Federal Highway Administration, 2001, 421 pp.
- Jones, M. R., McCarthy, A., Booth, A. P. P. G., “Characteristics of the Ultrafine Component of Fly Ash,” *Fuel*, 2006, v. 85, pp. 2250-2259.
- Khatib, J. M., and Wild, S., “Sulfate Resistance of Metakaolin Mortar,” *Cement and Concrete Research*, 1998, v. 28, pp. 83-92.
- Kim, H., Lee, S., Moon, H., “Strength Properties and Durability Aspects of High Strength Concrete Using Korean Metakaolin,” *Construction and Building Materials*, 2007, v. 21, pp. 1229-1237.
- Langan, B. W., Weng, K., Ward, M.A., “The Effect of Silica Fume and Fly Ash on Heat of Hydration of Portland Cement,” *Cement and Concrete Research*, 2002, v. 32, pp. 1045-1051.
- Larsen, T. J., Armaghani, J. M., “Quality Concrete with Fly Ash,” Florida Department of Transportation, 1987.
- Mirza, J., Mirza M. S., Roy, V., Saleh, K., “Basic Rheological and Mechanical Properties of High-Volume Fly Ash Grouts,” *Construction and Building Materials*, 2002, V. 16, pp. 353-363.

- Mindess, S., Young, J. F., and Darwin, D. *Concrete*, Second Edition, Pearson Education, Inc., Upper Saddle River, New Jersey, 2003, 644 pp.
- Mouli, M., Khelafi, H., "Performance Characteristics of Lightweight Aggregate Concrete Containing Natural Pozzolans," *Building and Environment*, 2008, v. 43, pp.31-36.
- Nassif, H. H., Najm, H., Suksawang, N., "Effect of pozzolanic materials and curing methods on the elastic modulus of HPC," *Cement and Concrete Composites*, 2005, v. 27, pp. 661-670.
- Neville, A. M., *Properties of Concrete*, Prentice Hall, New Jersey(1995) 884 pp.
- NT BUILD 492 "Concrete, Mortar and Cement-Based Repair Materials: Chloride Migration Coefficient from Non-Steady-State Migration Experiments," Nordtest method, 1999.
- Parande, A. K., Babu, B. R., Karthik, M. A., Kumar, D., Palaniswamy, N., "Study on Strength and Corrosion Performance for Steel Embedded in Metakaolin Blended Concrete and Mortar," *Construction and Building Materials*, 2006)
- Pfeifer, D.W., McDonald, D.B., Krauss, P.D., "The rapid chloride permeability test and its correlation to the 90-day chloride ponding test." *PCI Journal*, 1994, 41(4), pp. 82–95.
- Qian, X., Li, Z., "The Relationship between Stress and Strain for High-performance Concrete with Metakaolin," *Cement and Concrete Research*, 2001, V. 31, pp. 1607-1611.
- Saraswathy, V., Song, H., "Electrochemical Studies on the Corrosion Performance of Steel Embedded in Activated Fly Ash Blended Concrete," *Electrochimica Acta*, 2006, V. 51, pp. 4601-4611.
- Skalny, J., Marchand, J., and Odler, I.. *Sulfate Attack on Concrete*, Spon Press, New York, New York(2002).
- Sioulas, B., Sanjayan, J. G., "Hydration Temperatures in Large High-strength Concrete Columns Incorporating Slag," *Cement and Concrete Research*, 2000, V. 30, pp. 1791-1799.
- Soongswang, P., Tia, M., Bloomquist, D., Meletiou, C., and Sessions, L., "Efficient Test Setup for Determining the Water-Permeability of Concrete," *Transportation Research Record*, 1988, V. 1204, pp. 77-82.
- Stanish, K., Hooton, R.D., Thomas, M.D.A., "The Rapid Migration Test for HPC," *HPC Bridge Views*, Jan.-Feb. 2005, V. 37, pp. 2.
- Streicher, P.E., Alexander, M.G., "A Chloride Conduction Test for Concrete." *Cement and Concrete Research*, 1995, V. 25, pp. 1284-1294.

- Tang, L., Nilsson, L., “Rapid Determination of the Chloride Diffusivity in Concrete by Applying an Electrical Field.” *ACI Materials Journal*, 1992, V. 89, pp. 49-53.
- Tang, L. (1996). “Chloride Transport in Concrete – Measurement and Prediction,” PhD Dissertation, Chalmers University of Technology, 1996.
- Tia, M., Bloomquist, D., Yang, M. C. K., Soongwang, P., Meletiou, C. A., Amornsivilai, P., Dobson, E., Richardson, D., “Field and Laboratory Study of Modulus of Rupture and Permeability of Structural Concrete in Florida,” Florida Department of Transportation Technical Report, 1990.
- Vu, D. D. *Strength Properties of Metakaolin-blended Paste, Mortar, and Concrete*, Delft University Press, 2002, 154 pp.
- Wainwright, P. J., Rey, N., “The Influence of Ground Granulated Blastfurnace Slag (GGBFS) Additions and Time Delay on the Bleeding of Concrete,” *Cement & Concrete Composites*, 2000, v. 22, pp. 253-257.
- Whiting, D., and Mohamad, N., “Electrical Resistivity of Concrete-A Literature Review.” Portland Cement Association, 2003, R&D Serial No. 2457.
- Zongjin, L., Ding, Z., “Property Improvement of Portland Cement by Incorporating with Metakaolin and Slag,” *Cement and Concrete Research*, 2003, v. 33, pp. 579-584.

## **PART 2 – DETECTING CHLORIDE CONCENTRATION USING MICROSCOPY**

By Tanya Nash

## 1 INTRODUCTION

The current test methods to determine the level of chlorides (ASTM C1152/C1152M-90, AASHTO T260-97, and FM5-516) within a concrete sample all have the same problem. The concentration value is the result of pulverized slices at different depths of a sample. This includes the paste, aggregate and sand, which tend to dilute the chloride quantities that have migrated into the paste.

This portion of the report addresses the use of microscopy to determine chloride content. Previous studies have shown to have much promise in using microscopy to determine chloride levels in concretes [Rodrigues, 2001, Denes, 1987 , Thaulow, 1993 and Sutter 2003]. Using techniques such as the scanning electron microscope can give the chloride concentration at a point without the averaging effect of the aggregate. This will aid in better understanding the path that chlorides take through the concrete and the actual chloride concentrations needed to initiate corrosion.

## 2 INSTRUMENT THEORY AND BACKGROUND

### 2.1 SCANNING ELECTRON MICROSCOPE

The scanning electron microscope (SEM) is a microscope that uses an electron beam instead of light to produce a high resolution image of a sample's surface with great magnifications. One major advantage of the SEM over a conventional light microscope is its ability to examine the composition of a sample. This includes elements, compounds and their relative amounts to each other.

The SEM is divided into two major components, the column (electron gun, lenses, and detectors) and the control console (column controls, monitor and the image processing). Figure 43 shows the basic set-up of the column, which houses the electron beam and many sets of coils and lenses to help guide the electrons to the surface of the sample. The signal off the sample is then picked up by a number of different detectors surrounding the end of the column. The electron gun consists of a charged piece of metal that creates a stream of electrons called the filament; in our case the filament is tungsten [Goldstein, et. al, 2003]. The electrons are emitted off the tungsten in all directions, but with the help of a charged potential around the tip of the filament, the electrons accelerates down the column. A set of condensing lenses continue to guide the electrons down the column in a beam form. The beam is rastered, or moved, in a rectangular fashion across the sample surface by a set of scanning coils. Before passing through the objective lens where the beam gets focused, the shape of the beam is controlled by sets of magnetic coils. To help maintain the electron in a beam form, the column is kept under a high vacuum. This minimizes any interaction with other gas particles that may alter their path down the column or toward the detectors.

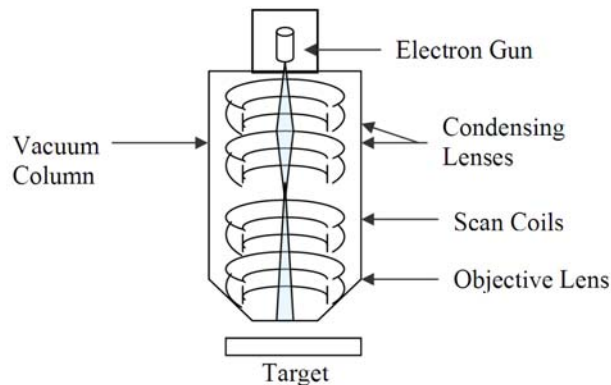


Figure 43 - Basic set-up of a Scanning Electron Microscope column

The beam finally hits the sample surface and irradiates the molecules inside. These interactions are detected by different types of detectors and amplifiers which then send signals to the control console. This entire process is summarized in Figure 44.

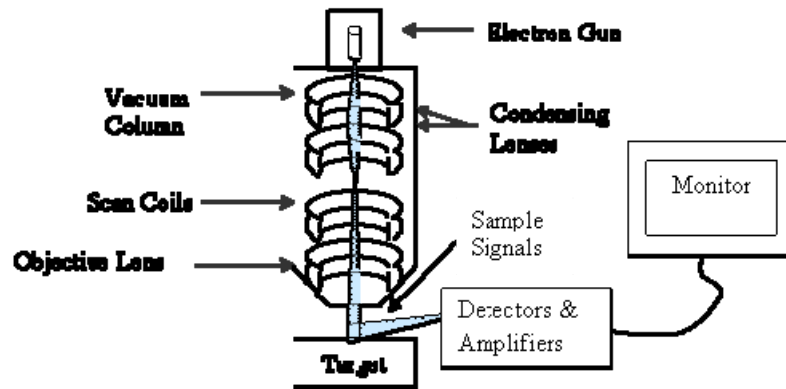


Figure 44 - Summary of the SEM column set-up from the electron gun to the image on the monitor.

The electrons exit the gun in a diamond shape which creates a tear-drop interaction volume within the samples, as shown by Figure 45. The interaction volume depicts the type of signals that are created as the electrons penetrate the sample. The secondary and backscattered electrons are used for imaging the sample, whereas the characteristic and continuum x-rays are used for compositional identification.

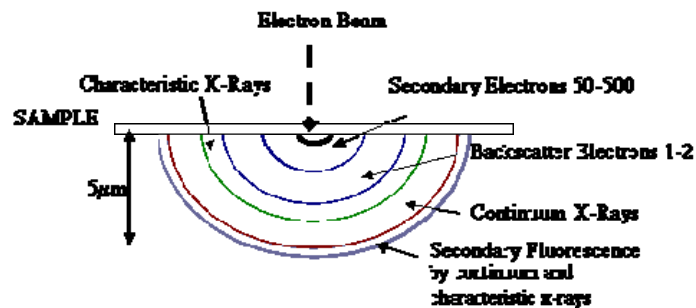


Figure 45 - A sample hit by an electron beam in a SEM, forms a typical interaction volume consisting of secondary electrons, backscattered electrons, characteristic (peak forming) and continuum (background) x-rays and secondary fluorescence.

As x-rays or photons hit the sample, they are either absorbed or scattered. When the energy is absorbed by an atom, an electron from the inner shell is ejected, which leaves vacant

areas in the shell. Now the atom is excited and tries to return to a stable condition by filling that vacant spot with other electrons from its outer shell, as seen in Figure 46. The process of filling a vacant spot on an inner shell produces characteristic X-rays as shown by the interaction volume in Figure 45; in other words, the atom fluoresces.

Each atom and shell has a distinct binding energy related to the electron of the atom. Since each element has unique binding energies, they produce a unique set of X-rays for identification. These X-rays are captured by a detector and then processed into energy values by an amplifier.

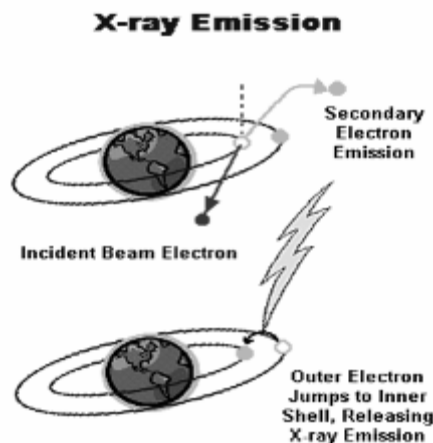


Figure 46 - Electron from an inner shell of an atom being knocked out of place and then being replaced by an electron from an outer shell; emitting a characteristic x-ray

The control console component of the SEM consists of the beam controls, the monitor and the image processing components to the system. Here the beam is turned on and off and the coils are increased or decreased in strength to create the best image on the monitor. The image created is not like a photograph. The signals received by the detectors are a variation of intensities of electron energy. These intensities are then mapped on the monitor to create an image. Therefore, the image that one sees is more of a map of intensities rather than a snapshot and since electrons have one energy value, the image is in a grayscale.

### 2.1.1 VARIABLE PRESSURE AND ENVIRONMENTAL SEM

The conventional SEM, which was described above, has some disadvantages. The sample under analysis must be clean, dry (usually desiccated), well polished and electronically conductive. If the sample is not conductive, then a thin coat of carbon is placed on the top of the

sample. This type of sample preparation is time consuming and potentially damaging to some samples.

The variable pressure and environmental SEM allow samples to be analyzed in a natural or ‘wet’ state. While the column of the SEM remains under a high vacuum ( $10^{-6}$  torr) the chamber is controlled by a different vacuum system and allowed to vary. The primary difference between a variable pressure SEM (VP-SEM) and an environmental SEM (ESEM) is the pressure capabilities. The VP-SEM can achieve a vacuum up to 270 Pascal (~2 torr) within the chamber, where as the ESEM has a specialized pumping and aperture system which allows the chamber pressures to reach over 600 Pascal (4.6 torr).

Allowing the pressure to change within the chamber allows the sample to outgas and dissipate charging (collected energy in the sample from the beam) through interaction with the chamber gas particles; typically this gas is air. The lowered pressure allows for a more natural state analysis, but also comes with its own problems. Even though the gas particles allow for a more humid state sample, it also effects how the sample is compositionally analyzed. The gas particles interacting with the sample signals create a skirt or cause the beam to spread. Figure 47 shows more detail on events that occur with the skirting effect. Overall, since it is more difficult to determine the area of analysis, it is more difficult to use a lower vacuum state for compositional analysis.

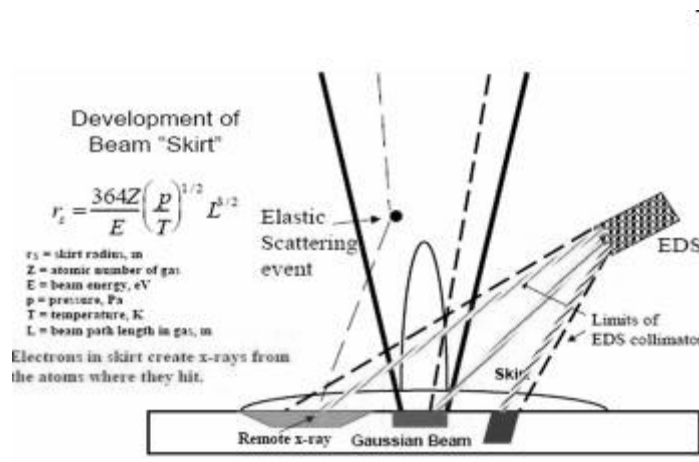


Figure 47 - Interaction of beam and backscattered electrons with gas atoms: Gas scattering removes electrons from beam into “skirt”

## 2.2 X-RAY MICROSCOPE

The x-ray microscope is based on the idea of using a CCD camera or film to detect x-rays passing through a sample rather than the reflection of light off the surface to create an image like a conventional light microscope. The resolution of this type of microscope has been known to be comparable to that of an electron microscope with the major advantage of being able to image things in their natural state and with a greater thickness under vacuum or atmospheric pressure. Figure 48 shows the components and set-up of the x-ray microscope. Above the guide tube lays a filament which produces electrons just like the electron gun of the SEM, which then hit an x-ray target. Since the primary beam on this microscope consists of x-rays, it can also be used to characterize the elements within the sample in a similar process to the SEM.

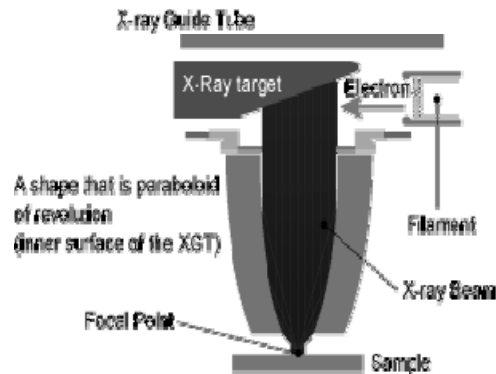


Figure 48 - Components of the x-ray microscope. *Image courtesy of Horiba.com.*

## 2.3 COMPOSITIONAL IDENTIFICATION

### 2.3.1 QUALITATIVE ANALYSIS

Energy dispersive spectroscopy (EDS) is the detection of the release of the distinct binding energies when an electron is bumped out of its shell by an electron from the beam of a SEM as described above. The resulting spectrum is one similar to Figure 49 where each peak is related to the presence of each element and shown on a scale of counts per second (cps). The low level background comes from the continuum x-rays which are non-distinct to any one element.

X-ray fluorescence (XRF) produces the same type of spectrum, but detects the fluorescent event that occurs when a vacant spot is filled after an elemental electron is knocked out of place by an x-ray beam. This process is how the x-ray microscope analyzes composition of a sample.

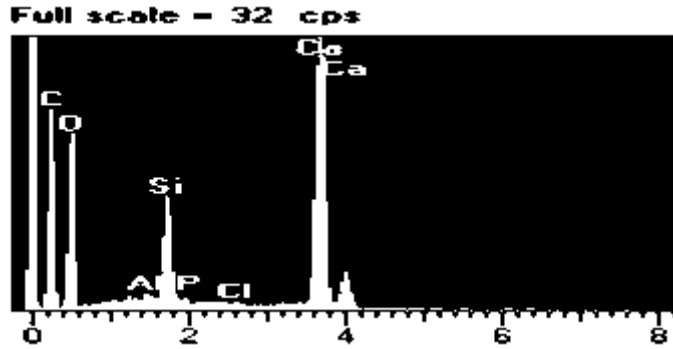


Figure 49 - Typical spectrum displaying characteristic energies for specific elements

Wavelength Dispersive Spectrometry (WDS) is one more process available for identification of elements within a sample. This process has a higher resolution and good for identification of trace elements. WDS is used to separate x-rays for specific elements by using a crystal with a known spacing (related to the element of interest) between the sample and the detector. This crystal will produce monochromatic x-rays and reject all other wavelengths. The WDS system can be applied to a SEM and other microscopy systems such as the electron probe microanalysis (EPMA) system.

All together each one of these processes allows one to qualitatively compare the elemental presence or perhaps relative ratios of elements in different samples or locations within a sample.

### 2.3.2 QUANTITATIVE ANALYSIS

The advantage to using the compositional identification processes is that they are also capable of quantifying the amounts different elements or compounds within a sample. In order to quantify a spectra, the background (continuum x-rays) should be removed from the spectrum. This ensures that the measured intensities consist only of the characteristic x-rays. If you are using a standard, the intensity ratios should be processed. Next the matrix corrections need to be obtained for the correction values.

There are three major matrix effects: atomic number (Z), x-ray absorption (A), and x-ray fluorescence (F), where Equation 2 shows the relationship each holds to the intensity or concentration of the specimen, i and standard, (i). This equation is applied to each element and the combined ZAF effect determines the total correction matrix.

$$C_i/C_{(i)} = I_i/I_{(i)} [ZAF]_i = [ZAF]_i k_i \quad \text{Equation 2}$$

In general, the Z determines the amount of x-ray intensity that is generated within the sample. The Z factor relies on the amount of backscattering events and the rate of energy loss due to inelastic scattering; the higher the Z, the more chances of interaction and backscattering, but less energy loss. The absorption factor is usually the biggest factor considered for compositional microanalysis. The x-rays have to travel a certain path in order to reach the detector – the shorter the path length the less absorption that occurs. The x-rays can either be absorbed within the sample or escape untouched as characteristic x-rays. As the x-rays get deeper in the sample, the more likely a fraction of them are to be lost by absorption. Lastly, the fluorescence factor, which is the least important factor in the correction, is measured. For this to occur, the sample must have atoms with critical excitation energy less than the energy of the characteristic x-ray being absorbed. Figure 50 is an example of an EDS quantification output using ZAF correction factors. Once these correction factors are found, the weight percent of each element is determined.

EDAX ZAF Quantification					
Element	Wt %	K-Ratio	Z	A	F
NaK	1.71	0.0064	1.0065	0.3695	1.0021
MgK	0.49	0.0025	1.0305	0.4957	1.0042
AlK	1.8	0.0114	1.0026	0.6292	1.0074
SiK	8.13	0.0609	1.0341	0.7192	1.0065
P K	0.1	0.0007	0.9965	0.7051	1.0108
S K	1.34	0.011	1.019	0.7906	1.0182
ClK	1.7	0.0143	0.9731	0.8416	1.0288
K K	0.29	0.0028	0.9757	0.9153	1.0807
CaK	3.57	0.3151	0.997	0.9409	1.0008
MnK	0.09	0.0008	0.8864	0.9283	1
FeK	1.82	0.0155	0.9019	0.9462	1
Total	51.033				

Figure 50 - Example of EDS quantification using ZAF correction factors

The weight percentage of each element is found by using Equation 3. This formula is used regardless if a standard is used or not. If a standard is used, the intensity of the pure

element (Equation 4) is actually measured, whereas if a standard is not used, the intensity of the pure element is calculated from a formula.

$$Wt\% = \frac{k - ratio}{Z \cdot A \cdot F} \times 100\% \quad \text{Equation 3}$$

$$k - ratio = \frac{IntensityElementSample}{IntensityPureSample} \quad \text{Equation 4}$$

The limitations of EDS and XRF detection in a bulk material is about 0.1 wt% (1000 ppm) whereas WDS can detect an element with the resolution of about 0.01% (100 ppm). Therefore, the determining factor of which instrument and analysis system to use may be a function of the quantification resolution.

### 3 PILOT STUDY

#### 3.1 MATERIAL AND SAMPLE PREPARATION

The pilot study began with the creation of 12 cement mixtures using autoclave molds (1 in x 1 in x 11.25 in), which had varying amounts of NaCl dissolved in the mixture water as shown in Table 32. After initial set, each bar was stored in a sealed plastic bag at 30±3° C for 28 days. The bars were not cured in water to ensure that the chlorides remained in the sample.

Table 32 - Mixture designs for autoclave bars used in blind study each totaling to 500g

Mixture	Cl (wt %)	NaCl (g)	Cement (g)	Water (g)
J	0.0000	0.0000	250.000	250.000
K	0.0010	0.0082	249.996	249.996
C	0.0025	0.0206	249.990	249.990
F	0.0050	0.0412	249.979	249.979
H	0.0100	0.0824	249.959	249.959
A	0.0200	0.1649	249.918	249.918
I	0.0400	0.3297	249.835	249.835
E	0.0800	0.6594	249.670	249.670
B	0.1600	1.3188	249.341	249.341
L	0.3200	2.6377	248.681	248.681
D	0.6400	5.2753	247.362	247.362
G	1.2800	10.5506	244.725	244.725

Each bar was removed from their bags and divided into four sections. The section with the label indicating the chloride content remained with FDOT personnel. The remaining sections went to the FDOT chemistry lab for XRF testing, PSI for titration by mean of FM 5-516 and UF for evaluation through energy dispersive spectroscopy (EDS).

##### 3.1.1 SEM/EDS SAMPLE PREPARATION

Three cross-sections were taken from the center of each autoclave section using an Allied Tech Cut 4 trim saw cooled by a glycol-based cutting fluid. All pieces were allowed to air dry, allowing the cutting fluid to evaporate before continuing with the grinding and polishing process.

The grinding was done by a dry process on an 8 in. Buehler Metaserv 2000 grinding/polishing wheel with 320 and 600 grit papers. The samples were manually ground for approximately 2 minutes for each paper at 250 rpm. The surface of the sample was blown clean with compressed air after each stage to remove any grit left on the surface. Half-way through the preparation process it there was a suspicion as whether or not the fluids involved in the polishing

process were washing the chlorides out of the samples. Therefore, samples H-L were stopped after the grinding stage of preparation and analyzed, whereas samples A-G continued with polishing process.

Six and one-micron oil-based diamond suspensions on nylon cloths were used to polish the surfaces of samples A-G. Each surface was manually polished for approximately 4 minutes with each suspension. The samples were cleaned with compressed air and allowed to dry for a minimum of 24 hours.

### 3.1.2 TITRATION AND XRF SAMPLE PREPARATION

Preparation for titration according to FM5-516 began with crushing the sample such that the particles were no larger than 0.5 in. in diameter. 400 grams of the crushed sample was then transferred to a 110°C oven to dry for 2-4 hours. Once dry, the sample was pulverized until it could pass a 50 mesh (0.020-in.) sieve.

Preparing a sample for XRF began with grinding the sample to pass through 150 micron sieve after all the metallic iron has been removed with a magnet. A 1 gram sample was then mixed with 9 grams of ignited lithium tetraborate and 1 gram of ignited lanthanum oxide. The dry powder was placed in a 50 ml mould and then in a furnace at 1100°C for 10 minutes. Circular beads 35-40 mm in diameter were made, the flat base of which was used for x-ray analysis after cooling.

## 3.2 EXPERIMENTAL

### 3.2.1 VP-SEM TESTING

Before any of the samples could be analyzed, a 2 mm barrier was marked around the edge with a carbon pen, which is visible in the SEM. The top edge of the bar was also marked by the carbon pen to have a reference point of how the bars were poured. The edges are avoided in analysis to negate any type of carbonation effects that might have occurred. A 4x3 grid, as shown in Figure 51, consisting of 6-7 mm between each row and 3-4 mm between each column was decided upon as a representative number of points to analyze for each sample slice. Therefore, the chloride percentage was based on an average of 36 chloride readings per mixture (12 readings/sample, 3 samples/mix).

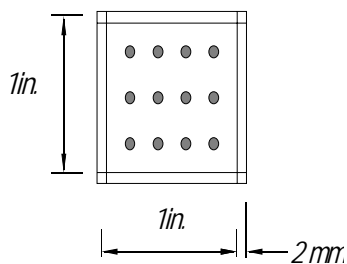


Figure 51 - Cross-section of autoclave bar. A 2mm border was marked to avoid carbonation effects and for a reference to find each location by stage reading.

The SEM and EDS settings were as follows:

- Accelerating Voltage: 20keV
- Magnification: 100 x
- Pressures: 20 and 60 Pa
- Working Distance: 15mm
- Dead Time: 30%
- Scan Time: 20 Live Seconds
- Element List: C, O, Na, Mg, Al, Si, S, Cl, K, Ca, Fe
- Quant: standardless ZAF correction

Once the samples were placed in the SEM with the correct orientation, the top left corner of the 2 mm barrier was located. All analysis points from this point forward were found using the location coordinates of the SEM stage. Once the point of interest was found, a magnification of 100x was used during EDS analysis.

Two pressures, 60Pa and 20Pa, were used for EDS to help limit the effects of skirting while in low vacuum mode. The spectrums from the different pressures were normalized to minimize the ‘skirting’ peak effects. The peaks that were identified as elements of interest are listed above. The quantification was run with standardless ZAF correction factors. The weight percent of each element was recorded and averaged for each mix. See Appendix D for more detail on the elemental data.

### 3.2.2 TITRATION TESTING

FM5-516 procedure for testing is as follows:

- Triplicate solutions
  - Add 3 grams of the pulverized material + 5 ml of deionized water → 100 ml beaker
  - Swirl to break up any clumps
- Acid Boil
  - Slowly fill each beaker with 35 ml of 1:12 nitric acid solution
  - Place on a medium heat hot plate with a watch glass until they boil
  - Boil for 2-4 minutes
- Filter
  - Filtered through Whatman No. 41 filter paper into 100 ml flask
  - Rinse residue on the filters 2-3 times with 30 ml of hot deionized water
  - Cool to room temperature
  - Fill to the mark with deionized water
- Blank
  - Add 100 ml of deionized water + 1.0 ml of low-level ISA → 250 ml beaker
  - Place on magnetic stirrer with a clean stir bar in beaker
  - Rinse electrodes with deionized water and immerse into solution
  - Stir at low to medium speed
  - Add 1.0 ml of 0.01 N AgNO<sub>3</sub> titrant to solution
  - Make four 0.5 ml additions of titrant – recording potential and volume after each increment
  - Remove Electrodes and rinse with deionized water
  - Enter data into chloride software making sure it falls into appropriate range
- Titration
  - Empty contents of one 100 ml flask from the filtering process into a 250 ml beaker

- Place on magnetic stirrer with clean stir bar
- Rise electrode with deionized water and immerse into solution – stir low to medium speed
- Proceed if potential exceeds 200 mV
- Add 0.01 N AgNO<sub>3</sub> titrant in 0.5 ml increments until scaling potential (determined by software with the blank data) is just exceeded → Record total volume of titrant and potential
- Make four more 0.5 ml additions of titrant and record the potential
- Remove and rinse electrodes
- Enter data into program and repeat with other two flasks
- Calculations
  - Performed by software

### 3.3 RESULTS AND DISCUSSION

The results of the pilot study for all methods involved – chemical titration (PSI), SEM with EDS (UF) and XRF (FDOT) are summarized in Table 33 and Figure 52.

Figure 52a shows a graphical view of the overall variation between the testing methods and the intended chloride content. The results, as shown by Figure 52a, indicate that the chloride contents obtained by PSI most closely matched the design chloride content. The trend seen with the higher chloride contents were consistent with the design, but still not within the acceptable error range of 1ppm. However, when the lower range values were compared as shown in Figure 52b, it was shown that the FDOT chemistry lab results obtained via the XRF were the most consistent until the high range values came into play. None of the tests proved to be precise enough to substantiate the use chloride profiling for research purposes.

After obtaining more information about proper mixing procedures from NIST, it was discovered that the mixing process performed for the pilot study was not adequate to ensure a uniform distribution of chlorides throughout the mix. Therefore, a high shear mixer was suggested for the next round of mixes. Meanwhile, UF continued to search for the proper procedures for sample prep, EDS analysis and other techniques available for chloride profiling.

Table 33 - Pilot study results reported in wt% of Cl-

Mixture	Design	XRF (FDOT)	FM5-516 (PSI)	EDS (UF)
J	0.0000	0.0050	0.0529	0.0982
K	0.0010	0.0140	0.0164	0.0733
C	0.0025	0.0260	0.0213	0.0550
F	0.0050	0.0090	0.0309	0.0797
H	0.0100	0.0080	0.0676	0.0894
A	0.0200	0.0200	0.0325	0.1078
I	0.0400	0.0200	0.0700	0.0844
E	0.0800	0.0960	0.1343	0.0994
B	0.1600	0.1050	0.2063	0.2506
L	0.3200	0.2960	0.4302	0.4261
D	0.6400	0.6260	0.7481	0.6200
G	1.2800	0.6340	1.3999	0.6975

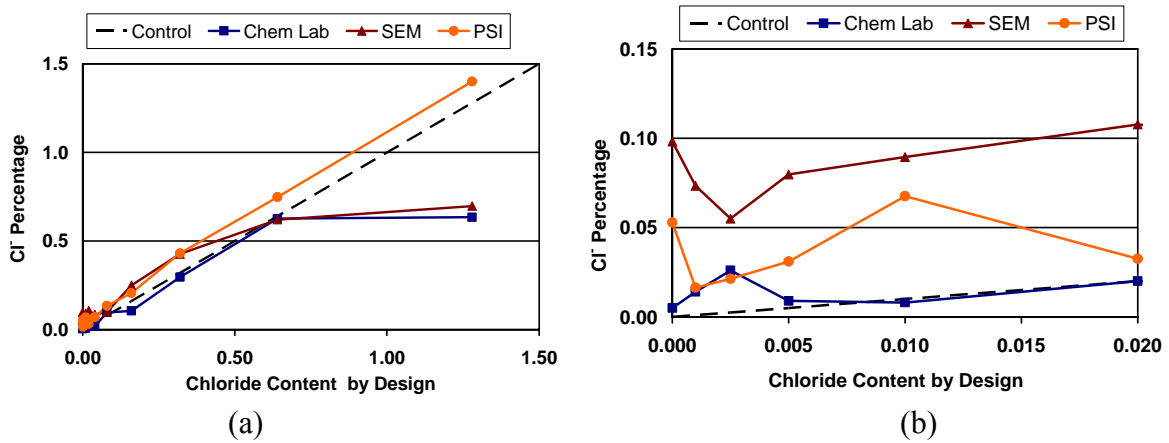


Figure 52 – Comparison of pilot study results (a) all test results  
(b) results showing only low chloride content

## 4 ALTERNATIVE TECHNIQUES AND INSTRUMENTATION

### 4.1 MICHIGAN TECH UNIVERSITY

Michigan Tech University (MTU) under the supervision of Dr. Larry Sutter and Dr. Karl Peterson routinely uses microscopy to determine chloride contamination of concrete. One of their specialties is the performance of chloride profiles for several state departments of transportation. Dr. Sutter's new approach to profiling involves using an x-ray microscope, which is similar to the EDS system on an SEM, but uses x-ray fluorescence for characterization instead of photon energy.

Tanya Reidhammer and Kerry Siebein traveled to MTU to work with Dr. Sutter and learn about using the SEM for chloride profiling. Some of the major topics covered during the visit to MTU were how to properly prepare a cement and concrete sample, the use of the x-ray microscope for chloride profiling, and how to use mineral standards as references for EDS analysis.

### 4.2 MATERIALS

As suggested by NIST, a high shear mixer was used to make the chloride standard cement mixes that were taken to MTU for testing. Table 34 shows the three different concentrations of sodium chloride that were dissolved in water and mixed with cement maintaining a w/cm of 0.35. The final samples were approximately 2-in. thick and 3-in. diameter discs. These mixes are referred to as the UF cement standards.

Table 34 - Mixture designs for chloride UF cement standards at 0.35 w/c, where bg = background chlorides

Mixture	Cl- Design	NaCl Weight (g)	Cement Weight (g)	Water Weight (g)	Cl- Calculated (wt %)
5111	bg + 400ppm	1.0551	591.811	207.134	0.0856
5112	bg + 3200ppm	4.2202	589.466	206.313	0.3256
5113	bg + 12800ppm	16.8810	580.088	203.031	1.2855

Several additional concrete samples were also taken to MTU for profiling and comparison. The sample in specific comparison was CPR 11C, which the FDOT had profiled through chemical titration (FM5-516) to a depth of approximately 2 in. with the results shown in Table 35.

Table 35 - FDOT chloride profile results for CPR 11C CPR Project, T259 Samples, 1 year exposure in G109 Room Unit Weight 2856 lbs/cy T259 (1/4" slices)

Profile		CPR11C		
Slice	Mid-depth	Cl (lbs/cy)	Cl (wt %)	Cl (ppm)
I	0.125	14.678	0.381	3762.625
II	0.375	4.761	0.123	1220.456
III	0.625	1.420	0.037	364.009
IV	0.875	0.468	0.012	119.969
V	1.125	0.237	0.006	60.754
VI	1.375	0.226	0.0066	57.934
VII	1.625	0.190	0.005	48.705
VIII	1.875	0.205	0.005	52.551

#### 4.3 SAMPLE PREPARATION

Sample preparation varied depending on the size and shape of the specimen. The sample prep for the cylinders is described in Appendix A. The following steps were used for the CPR sample and the UF cement standards.

Each sample was marked with a template to create an approximate 2-in. x 1-in. rectangle, referred to as a billet, and then cut on a kerosene-cooled trim saw as shown in Figure 53.

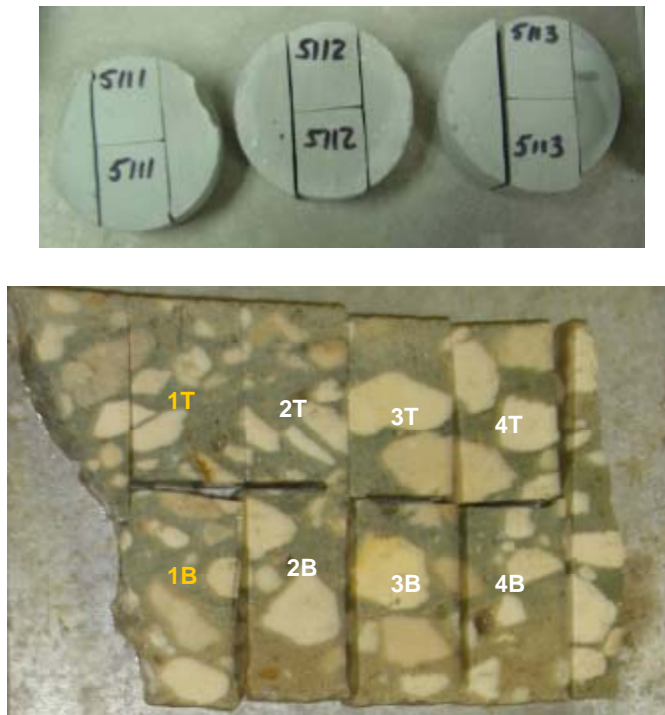


Figure 53 - Cement standards and CPR sample cut to billet size

Once cut, the billet was rinsed with clean kerosene and given a quick blast of compressed air to remove the kerosene from the holes and cracks. Each top side was marked and labeled as shown above. All billets were then transferred to 50°C oven to dry overnight. Due to cracking of the cement standards, they were further cut down to obtain the optimum sample surface possible.

When dry, the billets were epoxied onto a clear petrographic slide with JB Kwik epoxy. Figure 54 shows a few of the epoxied billets drying on a transparency film. The epoxy cured in approximate 15 minutes, in which the samples were then ready to be ground flat.



Figure 54 - Epoxied billets on petrographic slides

The next step of sample preparation was to ensure the flatness of the sample surface. Each billet was placed face down in a dish of kerosene (Figure 55) to break down the mineral oil faster, which was used to cool the grinder. The INGRAM thin section grinder, shown below in Figure 56, used a 60 grit wheel to grind the surfaces flat and a vacuum system to hold the slide to the arm. Once the surface was flat, the samples were placed in a 50°C oven overnight to dry.



Figure 55 - Billets in kerosene dish waiting to be ground flat



Figure 56 - INGRAM thin section grinder with vacuum held sample

The billets were then ready to be profiled using the x-ray microscope. Appendix A describes the extensive preparation necessary if the samples were to be analyzed using the SEM.

#### 4.4 CHLORIDE PROFILING

MTU used a Horiba XGT 2000 x-ray microscope for their chloride profiling. The filament in this case was Rhodium, the beam spot size was 100 microns while the voltage was set at 30keV and 1mA.

The instrument was calibrated with manganese (Mn), copper (Cu), and aluminum (Al) samples. Each sample was scanned 3 times, alternating between Cu and Al for 100 seconds each

and then once more for 300 seconds. The spectrums were then averaged and compared to the known peak energy of sample. The Mn sample was then scanned for 100 seconds. Here the FWHM was compared to its known value.

The calibration advised by Horiba calls for a Cu-Al alloy. MTU chose to use separate samples of copper and aluminum as an equivalent to calibrate their system.

A top and bottom piece from each sample was chosen for profiling. Prior to placing the sample in the XGT, each sample was scanned into Photoshop at a 600 dpi resolution. A 339 x 1017 pixel area is then placed around the image as shown in Figure 57a. The image was then split into 3 equal 339 x 339 pixel images, each of which covers the area of one scan for the XGT. A green 2x2 dot was placed in the center of the image, as part of the macro in Photoshop, as a reference on the sample to center the microscope and ensure the correct area of scanning.

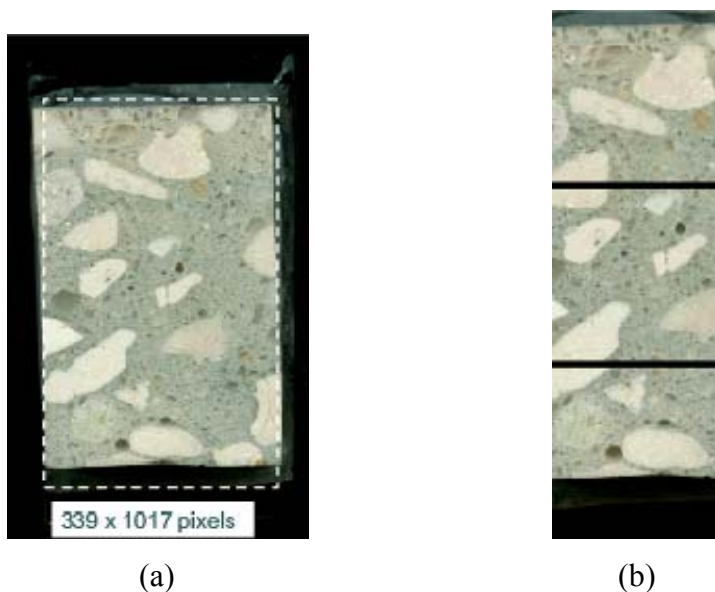


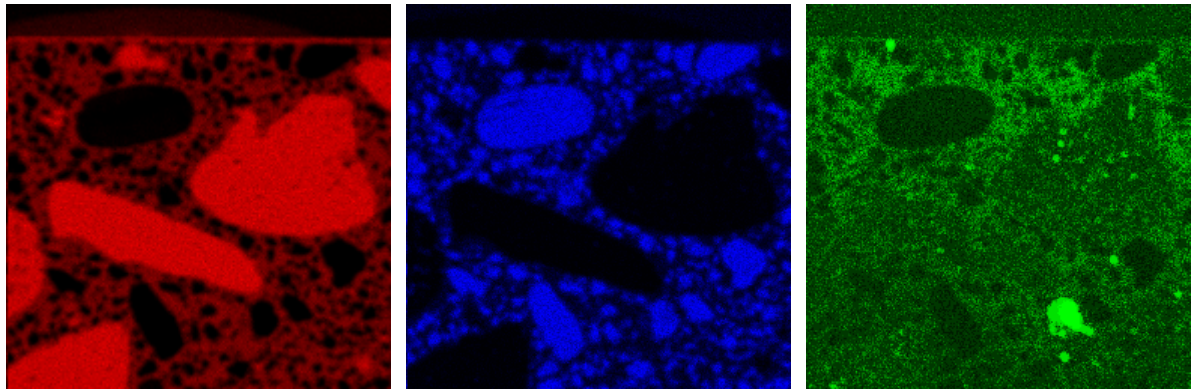
Figure 57 - CPR sample (a) Photoshop scan of CPR-1T billet before profiling and (b) after macro program split image into 3 equal parts - 339x339 pixels each

The CPR sample 1T (Figure 53) was placed in the XGT under vacuum. The XGT system was set to take elements maps for Mg, Si, S, Cl, K, Ca, Ti, Mn, Fe, and Rh at a resolution of 256x256 and collected for 3150 seconds. Element maps followed by multipoint spectrum analysis were taken for each section, top, middle and bottom. The maps were always taken under vacuum for better resolution; where as the multipoint analysis was done in atmospheric pressure, which was said to make the Rh-L peak negligible. This was important because the Rh-L peak has a slight overlap with the Cl-K peak. However, the fact that the release of the vacuum

caused the Rh-L peak to become negligible was a cause of concern for the intensity and drop in the chloride peak. If the release of vacuum to atmospheric pressure allows one peak to drop, or become negligible, it will have the same affect on all the peaks. This may affect the accuracy of the chloride counts per second during the multi-point analysis, but MTU did not feel that the difference was enough to be concerned about.

Figure 58 shows the three most important element maps, Ca, Si, and Cl, for the three sections of CPR 1T. The Ca map was used to determine where the cement was located, the Si map to identify the aggregate and the Cl map to identify the chlorides. The calcium map, being the most important since it identifies the paste, was used for the multipoint selection as shown in Figure 59. The points were chosen to be isolated in the paste as much as possible, avoiding any aggregate or air void, keeping three points in one horizontal line. Twenty-four points were taken for the top section of the sample, eighteen points for the middle and twelve points for the bottom section. At each selected point, a 100 second spectrum was collected and saved for later analysis.

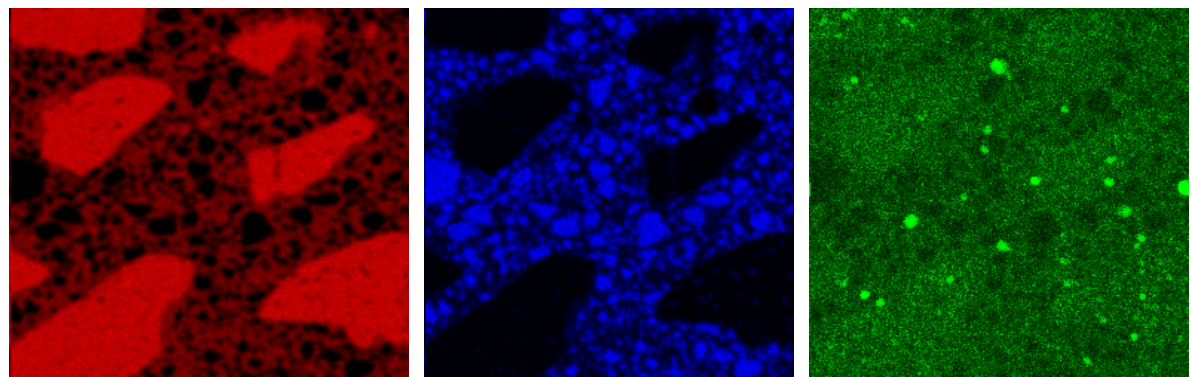
The cement paste standards were analyzed in a similar manner, except that the samples were much smaller than a normal size billet, due to some sample prep issues. The pastes were also made to have uniform chloride content (shown to be true by Figure 60(a)), so the profile was not the concern other than to ensure uniformity in the mix. The area of the sample was almost equivalent to one section (339x339), therefore a set of element maps were taken and then 24 points were used to get the best representative chloride content, as shown in Figure 60(b) for sample 5111.



Top Ca map

Top Si map

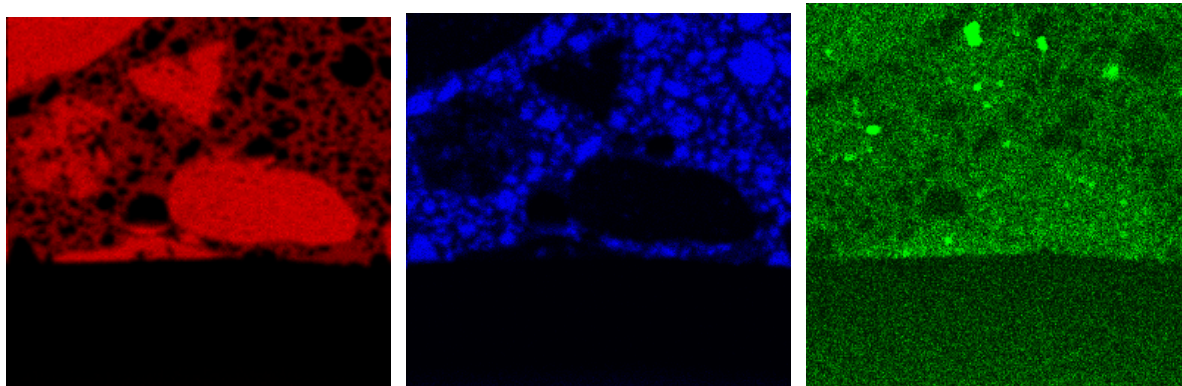
Top Cl map



Middle Ca map

Middle Si map

Middle Cl map



Bottom Ca map

Bottom Si map

Bottom Cl map

Figure 58 – Calcium, silicon, and chloride element map for the top, middle and bottom sections of CPR 11C sample 1T

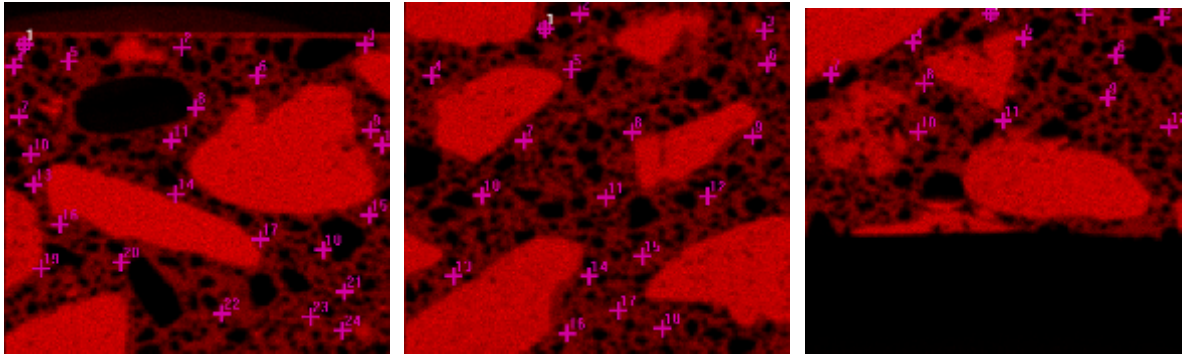


Figure 59 - Multipoint maps referencing the calcium element map for CPR 11C

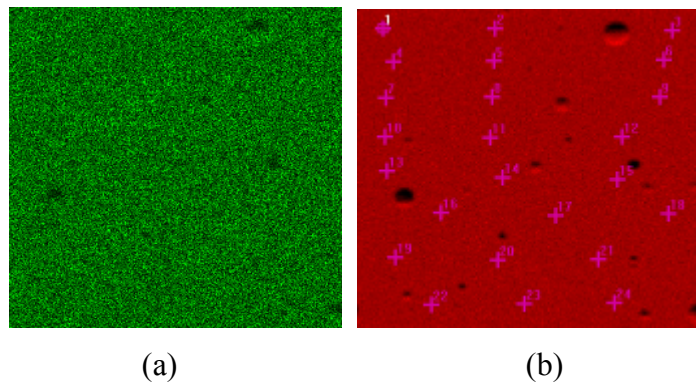


Figure 60 - Cement standard 5111 (a) Chloride element map, which helps confirm the uniformity of the mixture and (b) the calcium map used to place 24 points on the sample for the multipoint analysis

#### 4.5 RESULTS AND CALIBRATION

The depth of each point in Figure 59 was determined using Scion image software (Figure 61). Reference locations were identified and measured (Table 36) and were then used to create a continuous sample from the three sections – top, middle and bottom (Table 37). Each image had a small overlap that corresponded with the next, i.e. the bottom of the top image overlapped the top of the middle image, etc. Using the overlapping Scion position values, the gaps between the images were taken into account during calculations to find a more accurate depth throughout the sample. The calculations that were used to find the adjusted values were as follows:

$$\text{Top adjusted values} = \text{Raw coordinate} - \text{Y coordinate of the top surface}$$

Middle adjusted values = Raw coordinate – Y coordinate of the top surface +  
Y coordinate of the top/mid matching point from the top image –  
Y coordinate of the top/mid matching point from the mid image

Bottom adjusted values = Raw coordinate + Top Y coordinate adjustment for btm image

Top Y coordinate adjustment for btm image =  $b - a - c - e + d$

[Total of depth of top and middle image minus the overlapping gaps]

Once all the coordinates had been corrected, the spectrum data from the multipoint analysis was copied from the XGT software into the spreadsheet and set-up for plotting depth in mm vs. Cl by wt% with results showed by Table 38 and Figure 62 and Figure 63.

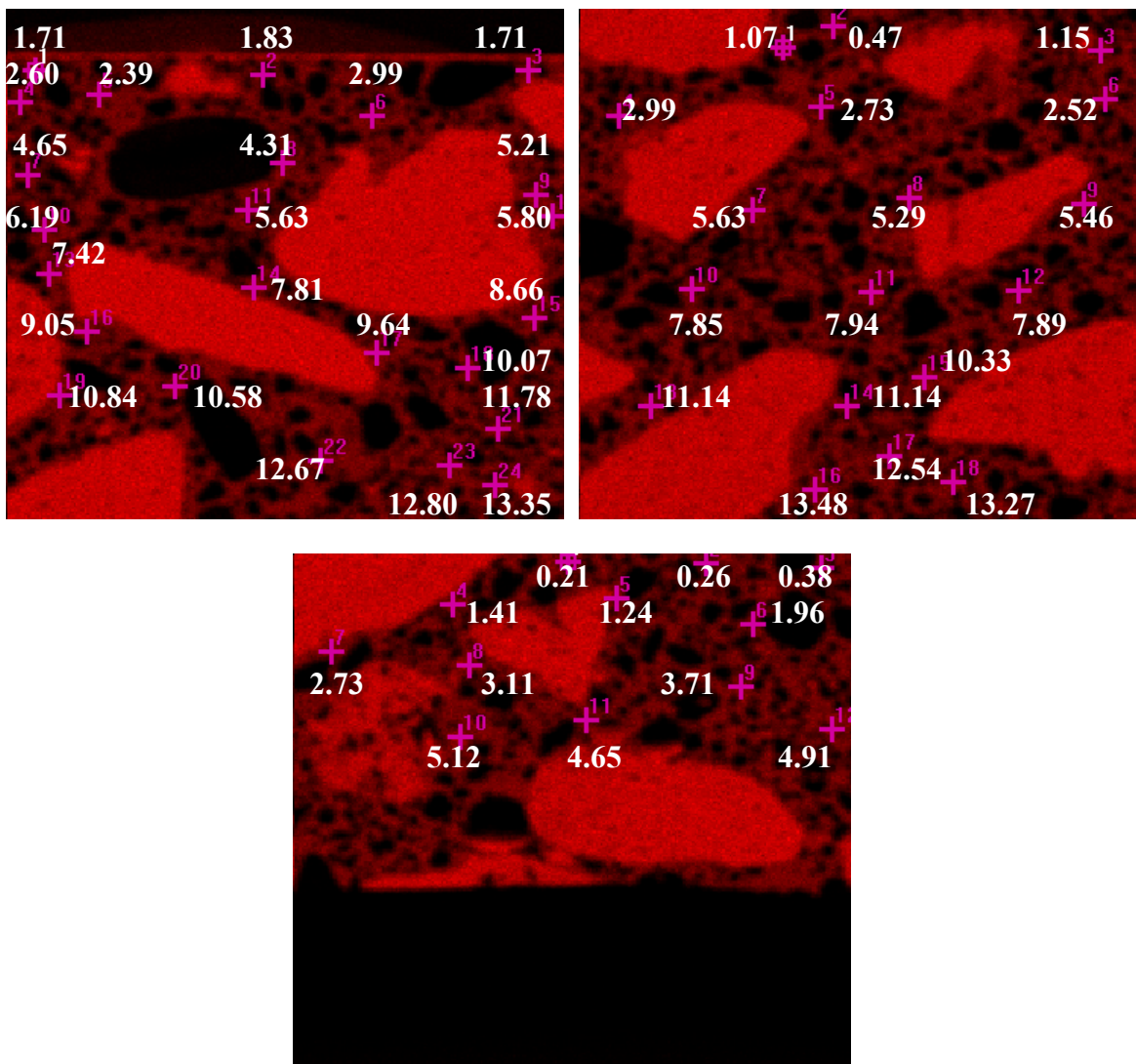


Figure 61 - Scion image position results for CPR11-C from the multipoint analysis maps

Table 36 – Reference Coordinates for Scion imaging (sample CPR11-C)

Y-coordinate location	Y-coordinate (mm)
top surface from top image (a)	1.24
top/mid matching point from top image (b)	14.12
top/mid matching point from mid image (c)	0.13
mid/btm matching point from mid image (d)	13.91
mid/btm matching point from bottom image (e)	0.13
adjustment for bottom image	26.53

Table 37 – Scion imaging position adjustment for sample CPR11-C.

Section	Scion Raw Data Position (mm)			Adjusted Position (mm)			Average (mm)
Top	1.71	1.83	1.71	0.47	0.59	0.47	0.51
	2.6	2.39	2.99	1.36	1.15	1.75	1.42
	4.65	4.31	5.21	3.41	3.07	3.97	3.48
	6.19	5.63	5.8	4.95	4.39	4.56	4.63
	7.42	7.81	8.66	6.18	6.57	7.42	6.72
	9.05	9.64	10.07	7.81	8.4	8.83	8.35
	10.84	10.58	11.78	9.6	9.34	10.54	9.83
	12.67	12.8	13.35	11.43	11.56	12.11	11.70
Middle	1.07	0.47	1.15	13.82	13.22	13.9	13.65
	2.99	2.73	2.52	15.74	15.48	15.27	15.50
	5.63	5.29	5.46	18.38	18.04	18.21	18.21
	7.85	7.94	7.89	20.6	20.69	20.64	20.64
	11.14	11.14	10.33	23.89	23.89	23.08	23.62
	13.48	12.54	13.27	26.23	25.29	26.02	25.85
Bottom	0.21	0.26	0.38	26.74	26.79	26.91	26.81
	1.41	1.24	1.96	27.94	27.77	28.49	28.07
	2.73	3.11	3.71	29.26	29.64	30.24	29.71
	5.12	4.65	4.91	31.65	31.18	31.44	31.42

Table 38 - XGT calculated chloride percentage for CPR11-C.

Cl Concentration (wt%)			Average (wt%)	Average Depth (mm)
1.45	1.47	1.04	1.32	0.51
1.04	1.68	1.31	1.34	1.42
1.05	1.18	1.27	1.17	3.48
0.91	0.98	1.18	1.02	4.63
0.67	0.72	0.86	0.75	6.72
0.35	0.70	0.55	0.53	8.35
0.14	0.16	0.36	0.22	9.83
0.25	0.05	0.09	0.13	11.70
0.02	0.01	-0.02	0.00	13.65
-0.03	0.00	0.02	0.00	15.50
0.00	-0.02	0.00	-0.01	18.21
-0.05	0.02	-0.05	-0.03	20.64
0.02	-0.01	0.00	0.01	23.62
0.02	-0.01	-0.03	-0.01	25.85
-0.04	-0.08	-0.04	-0.05	26.81
0.02	-0.04	-0.02	-0.02	28.07
0.01	0.02	-0.02	0.00	29.71
0.05	-0.03	0.01	0.01	31.42

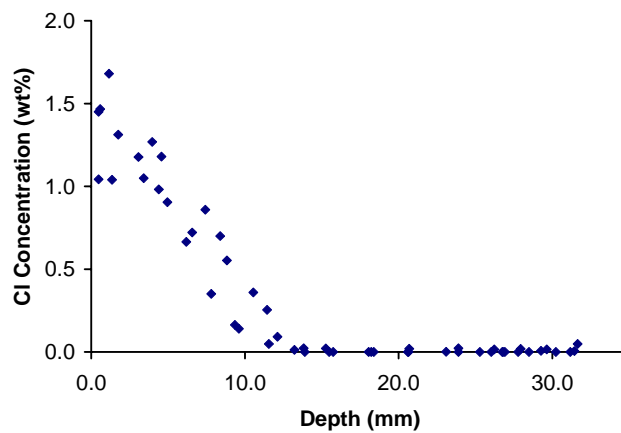


Figure 62 - Chloride concentration data for CPR11-C using the XGT software.

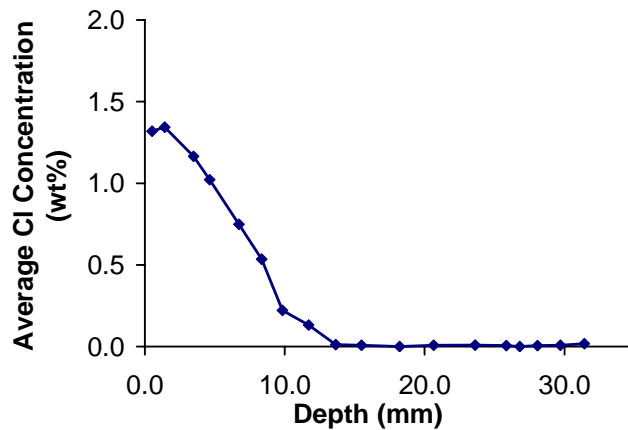


Figure 63 - Chloride concentration data for CPR11-C using the 0.35 w/cm calibration constants.

The cement standards 5111, 5112, and 5113 samples were mapped the same as the CPR sample. The biggest difference with these samples was that they consisted purely of cement paste; therefore it was not necessary to be as careful with the point placement as with a concrete sample. The samples were also small enough that the equivalent to one image (top, middle or bottom) covered the whole sample. Few, if any point adjustments had to be made for these samples. The chloride results for the UF standards 5111, 5112 and 5113 were 0.12, 0.42, and 2.6 wt% chlorides respectively. These averages were much higher than the design of the standards and the results of the wet chemistry, 0.087, 0.33, and 1.30 wt% chlorides respectively. The discrepancy brought attention to the way the system was calibrated to calculate the chloride content. The XGT software allowed the user to input calibrations constants for this type of calculation. The plots that were used to obtain the constants are in Appendix D.

MTU typically used a w/cm of 0.45 or 0.50 for their mixes. Therefore, the standards that MTU had calibrated their system to were 0.45 and 0.5 w/cm mortar samples with varied amounts of chlorides. The 0.45 w/cm constants were from 6 different concentrations of chlorides, whereas the 0.5 w/cm used 3 different types of salts ( $MgCl(H_2O)_6$ ,  $NaCl$ , and  $CaCl(H_2O)_2$ ) each at 6 different concentrations. These salts are similar to the content in the de-icing salts used on bridges. Each one of the samples was profiled as described above and plotted as weight percent chlorides vs. cps. The three curves were plotted together in Figure 64 and indicate the suspected effect due to the 0.35 w/c. Since UF only had three samples to test, the curve was not complete until a later date. Therefore, the calibration curve was created using UF standards 5111, 5112 and 5113. This calibration curve could then be used to analyze samples with 0.35

w/cm. Appendix D shows a more in depth view of the data and calculations of each w/cm calibration.

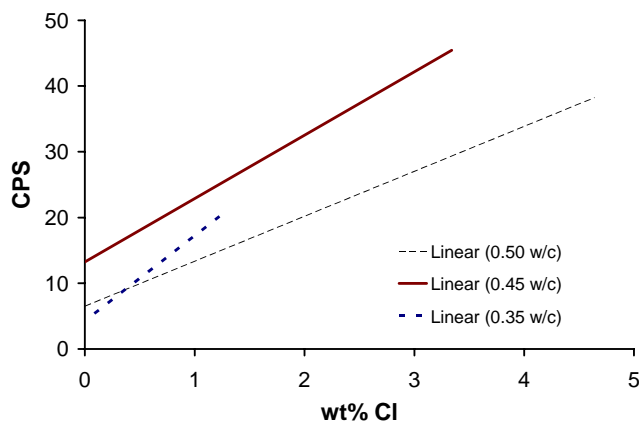


Figure 64 - Linear trends of the average chlorides by wt% for each w/cm – 0.35, 0.45, 0.50. Data from MTU salt calibration mortars and UF neat paste samples (5111, 5112, and 5113)

The new calibration constants were then placed into the XGT software and the chloride concentrations were then recalculated. Table 39 shows the effect the correct w/cm calibration constants had on the results.

Table 39 - Comparison of chloride content in ppm using the original 0.45 w/cm calibration constants compared to the adjusted 0.35 w/cm calibration constants and the wet chemistry results.

Standard	Design Cl (ppm)	Wet Chemistry (ppm)	0.45 Calibration		0.35 Calibration	
			(ppm)	Difference	(ppm)	Difference
5111	800	867	1200	+38%	1290	+49%
5112	3200	3330	4200	+26%	2870	-14%
5113	12800	12970	26000	+200%	12900	0%

The University of Florida in conjunction with the FDOT made more cement chloride samples ranging from 0% (no addition of chlorides to cement) to 3.0% Cl by weight. These samples were prepared and sent to MTU to complete the calibration curve previously started with samples 5111, 5112, and 5113. The completed 0.35 w/cm calibration curve is shown in Figure 65 in comparison to the 0.45 and 0.50 w/cm curves from MTU. As indicated by the plot,

the relationship is not linear to the water/cement ratio, possibly giving a relationship to the porosity of the paste and the chloride content of the sample.

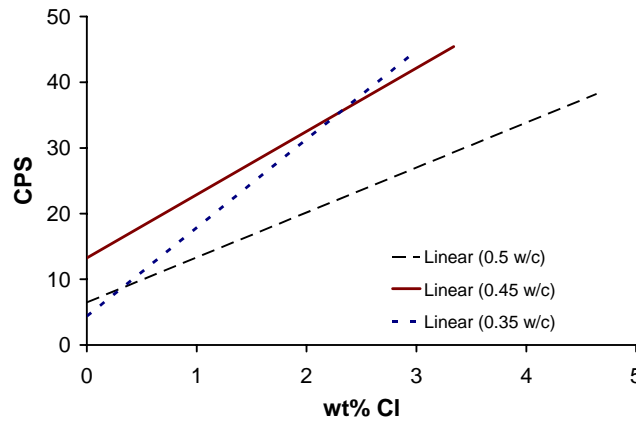


Figure 65 - Complete calibration curve comparison for 0.35, 0.45 and 0.50 w/cm ratios for the Horiba XGT 5000

CPR11-C has been previously profiled using wet chemistry (FM5-516). Using the wet chemistry profile data and the XGT profile data, a comparison was made between the two techniques (Figure 66). One key difference between the techniques was that the wet chemistry used milled layers of concrete. This includes the aggregate as well as the paste, whereas the x-ray microscope gave the ability to avoid the large aggregate and analyze the paste. Staying primarily in the paste area, the concentrations results from the x-ray microscope were higher than that of the wet chemistry which was diluted from the presence of the aggregate. An attempt to compensate for the aggregate dilution of chloride content with an estimated value of 33% by volume, the XGT profile was divided by three and then re-plotted against the wet chemistry profile in Figure 67.

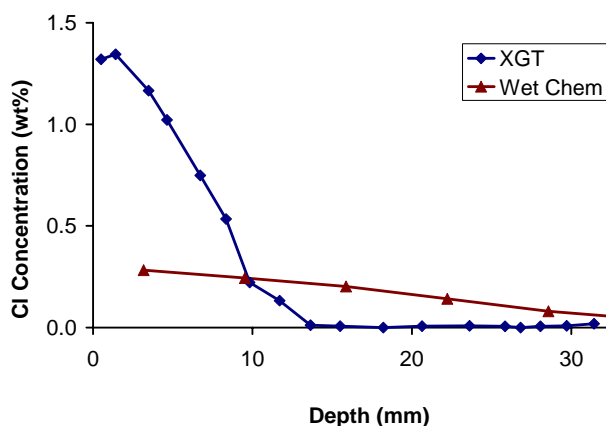


Figure 66 - Chloride profile comparison for CPR 11C sample 1T using XGT versus the wet chemistry profile

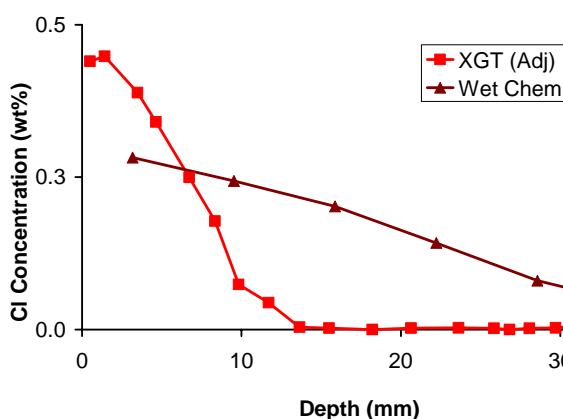


Figure 67 - Chloride profiles for CPR11-C sample 1T after the XGT profile had been adjusted for aggregate content for a better comparison to the wet chemistry titration profile, which contains a mixture of paste and aggregate for its sample.

Figure 67 shows that the XGT chloride profile is initially steeper than that of the wet chemistry profile and then becomes shallower at approximately 10 mm as the concentrations fall below the resolution capabilities of the x-ray microscope. The XGT allows the chloride concentrations to be determined closer to the edge of the sample, which appears to have a peak in concentration that may not be practical to detect with wet chemistry techniques. Furthermore, the lower values measured with wet chemistry may reflect the diluting effect of the aggregate. The more detail available in the beginning depths, the closer the chloride penetration and migration can be tracked.

#### 4.6 ALTERNATIVE APPROACH

A Phillips XL40 environmental scanning electron microscope (ESEM) was used to analyze the samples to determine its effectiveness at detecting chlorides. After some added sample preparation, as described in Appendix A, the three cement samples and appropriate mineral standards (Willimite for beam current and Scapulite for chlorides) were placed in the ESEM chamber and evacuated. EDS analysis was done by means of an EDAX system equipped with Phoenix software. The system settings were set as follows:

- RZAF list: Si, Ca, CL, Al, Mg, S, K, Ti, Mn, Fe (common elements found in cement)
- Background: manual
- Factors: Pure
- Quantification: ZAF correction, Type – elements, no normalization
- Standard: pure

The following steps were used to set up the EDS software:

- Place the beam over the Willimite sample using the ESEM
- Collect a spectra for 100 seconds
- Make a note of Zn peak value in cps
- Move the beam to the area of interest on the sample
- Collect spectra for 100 seconds
- Input previously noted beam current into Phoenix software
- Remove background from spectra with built-in routine
- Run *QUANT* (built into software)
- Save spectra and quantification results and record chloride wt%
- Repeat as needed

Table 40 shows the results of the ESEM chloride concentration determination (quantification with and without standards). The microscopy results are compared to the wet chemistry results in terms of percent difference. Statistical significance of the data can be improved if at least 30 spots are used. The results from the EDS indicated that the technique overestimated the chloride content at the lower contents for both with and without standards.

Even at the lower contents, however, EDS with standards provides comparable results, all within 23% of the wet chemistry. It is not clear, however, if the difference is due to the averaging effect of the wet chemistry test method or just systematic differences. More work is needed to determine correct settings, standards (mineral or otherwise), and sample preparation to determine the nature of the differences in the measurement.

Table 40 - Chloride concentration comparison (wt %) for EDS quantification with and without standards

Sample	Wet Chemistry	EDS w/Standards		EDS w/o standards		Number of spots analyzed
		(%wt)	Difference	(%wt)	Difference	
5111	0.0867	0.106	+22%	0.32	+369%	9
5112	0.333	0.339	+2%	0.89	+267%	9
5113	1.30	1.60	+23%	4.21	+324%	14

The typical list of minerals and their reference element(s) are listed in Table 41. One area that may need additional work is that of using a mineral – a combination of elements – as a standard for a single element. The general comments about the differences in the minerals and the actual composition of the cement or concrete were the following:

- Pure formulations of single crystalline structures typically found in cement paste are difficult to fabricate. Because of low demand for these standards and the difficulty in fabrication cement pure standards are not readily available commercially.
- ZAF factors must be close to 1.00 for the element of interest.
- Standards should contain the element of interest in the same or similar atomic proportions as that of the sample.
- The reference minerals have been found to work well with the quantification software.

Table 41 - List of typical minerals used as reference standards by MTU for compositional quantitative analysis by EDS

<b>Mineral</b>	<b>Formula</b>	<b>Element Reference</b>
Quartz	SiO <sub>2</sub>	Si
Amelia Albite	NaAlSi <sub>3</sub> O <sub>8</sub>	Al, Na
Nuevo Garnet	(Mg, Fe, Ca) <sub>3</sub> Al <sub>2</sub> (SiO <sub>4</sub> ) <sub>3</sub>	Fe, Mn
Diopside	CaMgSi <sub>2</sub> O <sub>6</sub>	Mg or Brucite
Fosterite	Mg <sub>2</sub> SiO <sub>4</sub>	Mg
Woolastinite	CaSiO <sub>3</sub>	Ca
Orthoclase	KAlSi <sub>3</sub> O <sub>8</sub>	K
Chalcopyrite	CuFeS <sub>2</sub>	S
Scapolite	(Na, Ca) <sub>4</sub> [Al <sub>3</sub> Si <sub>9</sub> O <sub>24</sub> ]Cl	Cl
Durango Apatite	Ca <sub>5</sub> (PO <sub>4</sub> ) <sub>3</sub> (F,Cl,OH)	P
Ilmenite	Fe <sup>++</sup> TiO <sub>3</sub>	Ti

## 5 SENSITIVITY STUDY

Currently, the FDOT is using FM5-516 (wet-chemistry) to determine the chloride content of a pulverized concrete sample or cement powder. The test method involves the acid digestion of free chloride ions within a sample. The software program, “Chloride 2000”, calculates the chloride content in weight percent, parts per million (ppm), lbs/yd<sup>3</sup>, or Kg/m<sup>3</sup>. The resolution of the result is equivalent to 1ppm.

Realizing that this resolution was impractical for the SEM/EDS, the goal of 33.3ppm was set for the pilot study. The idea that 3 grams of powder is diluted with 100ml of solution during the testing method of FM5-516, 33.3ppm was considered as an acceptable sensitivity level for any replacement test. After reviewing the data from the EDS the sensitivity of the analysis process was only 1000ppm. At this point, the possibility of using WDS was considered, since WDS is capable of resolving the chloride content to 200ppm.

The idea of using the SEM/WDS technique to determine the chloride content of contaminated concrete for 200ppm and above and wet-chemistry for 100ppm and below is proposed. This idea is also reinforced by the scope of FM5-516 which states that “the method is applicable to chloride contents lower than 100 part per million”. A sensitivity analysis on bulk diffusion samples that have been exposed to chlorides for 364 days was done. Chloride profiles with at least eight readings and the background content (taken prior to exposure) were determined by the wet-chemistry method. Using Fick’s Second Law, two different diffusion coefficients were calculated. The first diffusion coefficient included a complete set of data points, where as the second coefficient only included the values above 200ppm and the same value for the background chloride content. The fitted curves for sample CPR11 are shown in Figure 68 and Figure 69 (the rest of the plotted data are shown in Appendix D). Table 42 shows the results of each of the calculated diffusion coefficient.

The diffusion coefficients calculated from the profiles using only data 200 ppm and above combined with the background data have given accurate results. A maximum difference of 1.33% was found between the two sets of data. Therefore, using the SEM/WDS combined with wet-chemistry as a complete method of chloride analysis is reasonable.

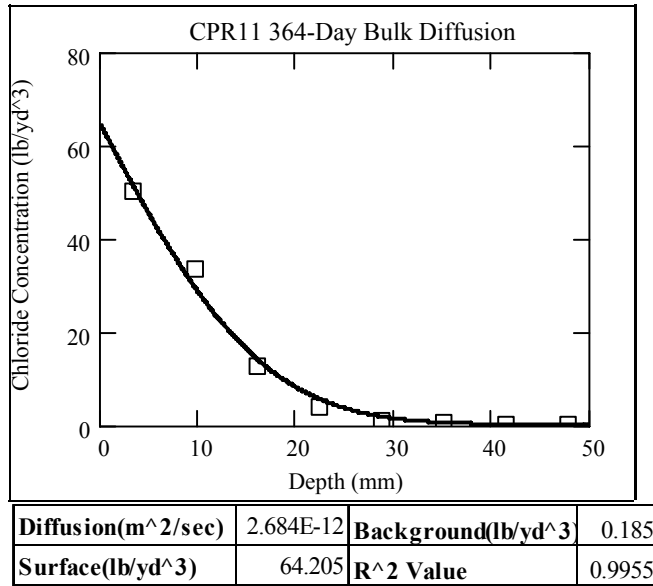


Figure 68 - Fitted chloride profile for sample CPR11 using a full set of results

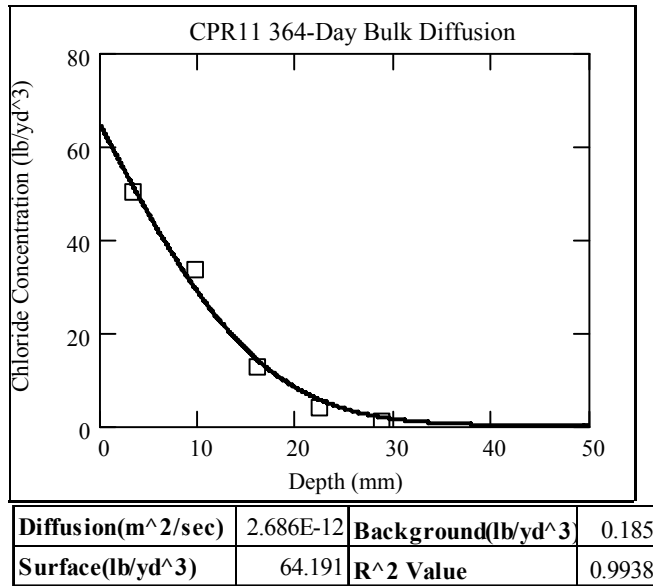


Figure 69 - Fitted chloride profile for sample CPR 11 using data points from 200ppm (0.80 lb/yd<sup>3</sup>) and above and the background chloride value

Table 42 - Diffusion coefficients for bulk diffusion samples using complete set of chloride profile results versus only using results 200ppm and above

Mixture	364-Day Bulk Diffusion Results (m <sup>2</sup> /sec)		Difference (%)
	Complete Set of Results	Only Cl Results of 200ppm and Above	
CPR1	1.853E-11	1.853E-11	0.00 (*)
CPR2	4.435E-12	4.449E-12	0.32
CPR3	9.916E-12	9.916E-12	0.00 (*)
CPR4	1.256E-12	1.255E-12	0.08
CPR5	5.025E-12	5.025E-12	0.00 (*)
CPR6	4.777E-12	4.8E-12	0.48
CPR7	2.057E-12	2.057E-12	0.00 (*)
CPR8	2.853E-12	2.858E-12	0.18
CPR9	1.1E-12	1.098E-12	0.18
CPR10	2.425E-12	2.438E-12	0.54
CPR11	2.684E-12	2.686E-12	0.07
CPR12	7.164E-12	7.164E-12	0.00 (*)
CPR13	1.005E-11	1.007E-11	0.20
CPR15	5.952E-12	5.952E-12	0.00 (*)
CPR16	5.801E-12	5.801E-12	0.00 (*)
CPR17	4.259E-12	4.262E-12	0.07
CPR18	2.258E-12	2.266E-12	0.35
CPR20	2.433E-12	2.428E-12	0.21
CPR21	2.405E-12	2.437E-12	1.33
(*) All the profile sample results were above 200ppm Cl content.			

## 6 CONCLUSIONS

The use of microscopic evaluation to determine quantitatively the chloride contamination of concrete was explored. The experimental program can be divided into three components. First, portland cement and water paste samples were prepared with a standard mortar mixer. The paste samples had predetermined quantities of chlorides mixed into the water. The hardened cement paste specimens were analyzed with variable pressure scanning electron microscope with energy dispersive spectroscopy analysis (VPSEM/EDS), X-ray fluorescence (XRF), and titration. It was found that a high shear mixer was needed to produce uniform distribution of chlorides in the hardened paste.

Next, paste samples were prepared with a high shear mixer. Two microscopy techniques were applied. The first was a technique observed while visiting Michigan Technological University (MTU), which was X-ray microscope with XRF (XGT/XRF). The second was an environmental scanning electron microscope with EDS analysis (ESEM/EDS).

Finally, chloride profiles were created from a chloride contaminated specimen of concrete using both XGT/EDS and titration. The following are conclusions based on the development work:

### Cement paste sample analysis:

- SEM with EDS (using mineral standards) was able to measure chloride content that was within 23% of the titration values in quantities down to 800 ppm. SEM/EDS may not have the sensitivity needed to detect the level of chlorides needed for analysis of chloride contaminated concrete below these levels.
- Testing has indicated that detecting chloride content of levels down to 200 ppm using XGT/XRF is possible with careful calibration.

### Concrete Sample analysis:

- A sensitivity study of concrete samples exposed to chlorides for 1-year indicated that chloride concentrations less than 200ppm had negligible effect on the calculated diffusion coefficient.
- Calibrating to a higher w/cm than is contained in a concrete sample will cause the chloride concentration to appear larger than it is.

- XGT chloride profile shows chloride contents much higher than that of the titration. This is thought to be the diluting effect that the aggregate has on the titration results.

## 7 FUTURE RESEARCH

Microscopy techniques for quantitatively determining chloride contamination of concrete provide a useful and efficient tool for evaluating concrete mixtures for durability. The work performed as part of this research project was primarily exploratory to determine the feasibility of these techniques and identify the roadblocks to further development. The following are some suggested research focus areas that will further advance these methods:

- The advantage of using SEM and EDS to determine the chlorine concentration is the increased spatial resolution of the x-ray microanalysis measurements and the ability to determine where chlorides are located in the microstructure, which produces a distinct advantage over titration. Much of the research in concrete durability, however, has been based on titration measurements. It is imperative to explore the relationship of the microscopy measurements with that of the titration measurements.
- SEM/EDS quantitative measurements have practical detection limits of greater than 0.1wt% (1000 ppm). Microprobe (EPMA) with wavelength dispersive spectrometer (WDS) has practical detection limits of approximately 0.01 wt % (100 ppm). It is recommended that this technique be explored further to determine its applicability to low chloride contents.

## 8 REFERENCES

- Denes, T and A.D. Buck, "An Experiment to Investigate Chloride Intrusion on Construction Joints in Concrete"; *Cement, Concrete and Aggregates*, v. 9, n. 2, 1987, pp. 80-81.
- Goldstein, J., Newbury, D. E., Joy, D. C., Lyman, C. E., Echlin, P., Lifshin, E., Sawyer L.C., Michael, J.R., *Scanning Electron Microscopy and X-ray Microanalysis*, 3ed. Kluwer Academic, New York 2003, 689 pp.
- Rodriguez, O.G., "Influence of Cracks on Chloride Ingress into Concrete". Master's Thesis, University of Toronto, 2001.
- Sutter, L.L., T.J. Van Dam, K.R. Peterson, and A. Ganguly, "The X-Ray Microscope: A New Tool for Determining Chloride Ion Diffusion in Hardened Concrete", Proceedings of the Conference on Advances in Cement and Concrete, Copper Mountain, Colorado, August 10-14, 2003.
- Sutter, L.L., K.R. Peterson, T. J. Van Dam, "Applications of an X-Ray Analytical Microscope to the Analysis of Concrete." Proceedings of the 25th International Conference on Cement Microscopy, Richmond, Virginia. April 6-10, 2003.
- Thaulow, N. and Grell, B., *Micro Defects Influence on Chloride Ingress into Concrete, Phase 1.1: Preliminary Test on Chloride Ingress by Diffusion and Penetration*, Technical Report, Storebeltsforbindelsen A/S (Great Belt Link A/S), Copenhagen, April 1993.

## APPENDIX A – LABORATORY MIXTURE TESTING DATA

### PLASTIC PROPERTIES TESTS

Table 43 - Plastic Properties Test Results

Mixture	Density (lb/ft <sup>3</sup> )	Slump (in)	Air (%)	Bleed (%)	Initial Set (min)	Final Set (min)	Temp. (°F)	Air Temp. (°F)
CTRL1	145	5.75	2.0	0.00	300	395	81	75
CTRL2	145	6.00	1.5	0.10	330	400	84	75
SLAG1	144	6.50	1.1	0.19	340	430	81	75
SLAG2	144	6.00	1.0	0.17	355	460	81	75
SLAG3	146	6.50	0.6	0.27	300	445	80	75
META1	144	6.25	1.4	0.00	375	435	84	75
META2	144	7.25	1.5	0.00	390	470	80	75
META3	144	6.00	1.4	0.00	N/A	N/A	80	75
UFA1	146	5.75	0.6	0.55	375	465	78	75
UFA2	145	6.75	1.8	0.00	385	485	78	75
UFA3	144	8.00	1.6	0.00	400	480	78	75
SF1	143	6.25	2.3	0.00	370	445	76	75
SF2	143	6.00	2.3	0.00	385	465	76	75

### MECHANICAL PROPERTIES TESTS

Table 44 - Compressive Strength Test

Mixture	3—day (psi)	7—day (psi)	28—day (psi)	91—day (psi)	365—day (psi)
CTRL1	7,760	8,740	8,780	9,480	9,750
CTRL2	6,830	7,990	8,290	9,920	10,250
SLAG1	6,160	7,620	8,730	9,690	10,400
SLAG2	5,750	7,510	8,640	9,620	10,330
SLAG3	4,890	6,790	8,700	8,900	9,380
META1	7,770	8,860	8,860	9,650	10,170
META2	7,050	8,960	8,840	9,740	10,310
META3	7,300	8,960	8,960	9,810	10,590
UFA1	5,310	6,490	8,470	9,590	10,090
UFA2	5,650	6,770	8,780	9,480	10,090
UFA3	5,680	6,790	8,730	9,590	10,110
SF1	6,170	7,280	8,950	9,680	10,240
SF2	6,230	7,830	9,180	9,730	10,340

Table 45 – Flexural Strength for Initial Series of Mixtures

<b>Mixture</b>	<b>3—day (psi)</b>	<b>7—day (psi)</b>
CTRL1	1,021	1,139
CTRL2	993	1,043
SLAG1	976	1,086
SLAG2	977	1,092
SLAG3	984	1,006
META1	991	1,049
META2	1,132	1,079
META3	1,079	1,094
UFA1	817	1,051
UFA2	872	1,054
UFA3	922	1,045
SF1	1,009	1,028
SF2	1,051	1,154

Table 46 - Flexural Strength for Second Series of Mixtures

<b>Mixture</b>	<b>3—day (psi)</b>	<b>7—day (psi)</b>	<b>365—day (psi)</b>
CTRL1	1,021	1,139	1,121
CTRL2	993	1,043	1,165
SLAG1	976	1,086	1,145
SLAG2	977	1,092	1,238
SLAG3	984	1,006	1,242
META1	991	1,049	1,060
META2	1,132	1,079	1,122
META3	1,079	1,094	1,180
UFA1	817	1,051	1,057
UFA2	872	1,054	1,088
UFA3	922	1,045	1,132
SF1	1,009	1,028	1,139
SF2	1,051	1,154	1,208

Table 47 - Averaged Flexural Strength for All Mixtures

Mixture	3—day (psi)	7—day (psi)	365—day (psi)
CTRL1	987	1049	1,121
CTRL2	964	1024	1,165
SLAG1	886	1033	1,145
SLAG2	922	1043	1,238
SLAG3	906	997	1,242
META1	901	954	1,060
META2	1,008	1029	1,122
META3	964	1003	1,180
UFA1	793	974	1,057
UFA2	834	977	1,088
UFA3	853	984	1,132
SF1	971	1022	1,139
SF2	994	1091	1,208

Table 48 - Modulus of Elasticity

Mixture	7—day (psi*10 <sup>6</sup> )	28—day (psi*10 <sup>6</sup> )	365—day (psi*10 <sup>6</sup> )
CTRL1	5.10	5.85	5.82
CTRL2	4.91	5.80	5.85
SLAG1	4.82	5.29	5.49
SLAG2	5.11	5.34	5.72
SLAG3	5.16	5.35	5.71
META1	5.18	5.86	5.88
META2	5.36	5.89	5.93
META3	5.52	5.88	5.80
UFA1	5.14	5.38	5.95
UFA2	4.87	5.09	5.68
UFA3	4.67	5.33	5.58
SF1	4.63	5.46	5.90
SF2	4.77	5.46	5.97

Table 49 - Poisson's Ratio

Mixture	7—day	28—day	365—day
CTRL1	0.258	0.278	0.273
CTRL2	0.179	0.281	0.183
SLAG1	0.260	0.261	0.204
SLAG2	0.282	0.256	0.313
SLAG3	0.253	0.263	0.297
META1	0.268	0.291	0.227
META2	0.259	0.255	0.212
META3	0.247	0.255	0.207
UFA1	0.242	0.243	0.263
UFA2	0.236	0.264	0.366
UFA3	0.243	0.252	0.219
SF1	0.227	0.259	0.276
SF2	0.247	0.259	0.219

Table 50 - Splitting Tensile Strength (psi)

Mixture	3—day	7—day	28—day	91—day	365—day
CTRL1	1,227	1,184	987	1,007	1,192
CTRL2	1,041	916	1,035	1,196	1,214
SLAG1	951	980	1,248	1,153	1,302
SLAG2	969	949	1,197	989	1,251
SLAG3	1,021	848	892	962	1,058
META1	1,235	1,189	1,085	915	999
META2	1,191	1,259	1,300	1,304	966
META3	1,306	1,064	1,425	1,300	932
UFA1	936	757	812	1,015	794
UFA2	770	1,078	1,079	1,118	953
UFA3	572	1,040	1,057	1,026	819
SF1	1,213	1,131	987	1,107	749
SF2	1,224	1,208	977	1,193	834

**DURABILITY TESTS**

Table 51 - Linear Shrinkage, Volume of Voids, Absorption, and Permeability

<b>Mixture</b>	<b>Shrinkage (%)</b>	<b>Voids (%)</b>	<b>Absorption (%)</b>	<b>Kp (ft*10<sup>-10</sup>/hr)</b>
CTRL1	0.0360	13.9	6.31	8.89
CTRL2	0.0330	13.8	6.30	8.97
SLAG1	0.0307	13.6	6.20	9.81
SLAG2	0.0247	13.1	5.92	3.77
SLAG3	0.0270	14.5	6.66	4.97
META1	0.0243	15.0	6.92	4.45
META2	0.0210	15.0	6.89	7.06
META3	0.0227	15.5	7.14	10.63
UFA1	0.0330	14.2	6.52	5.45
UFA2	0.0207	13.9	6.34	8.03
UFA3	0.0193	14.3	6.56	1.01
SF1	0.0287	13.6	6.31	6.28
SF2	0.0253	13.3	6.18	4.34

Table 52 - Sulfate Expansion (%)

<b>Mixture</b>	<b>Concrete Expansion</b>	<b>Mortar Expansion</b>
CTRL1	0.0179	0.0361
CTRL2	0.0143	0.0320
SLAG1	0.0158	0.0348
SLAG2	0.0147	0.0316
SLAG3	0.0260	0.0353
META1	0.0142	0.0254
META2	0.0137	0.0245
META3	0.0123	0.0250
UFA1	0.0167	0.0337
UFA2	0.0127	0.0297
UFA3	0.0083	0.0275
SF1	0.0102	0.0195
SF2	0.0100	0.0213

Table 53 - Surface Resistivity

<b>Mixture</b>	<b>3 day</b>	<b>7 day</b>	<b>28 day</b>	<b>91 day</b>	<b>364 day</b>
CRTL1	8	9	13	16	17
CRTL2	7	8	13	30	69
SLAG1	6	10	25	43	80
SLAG2	6	11	29	55	92
SLAG3	6	11	28	42	72
META1	8	29	57	75	136
META2	8	34	61	94	177
META3	9	31	82	105	186
UFA1	5	7	25	75	169
UFA2	6	8	29	86	*200
UFA3	6	7	32	96	*200
SF1	7	14	78	140	*200
SF2	6	15	93	175	*200

Table 54 - Rapid Migration Test

<b>Mixture</b>	<b>28 day</b>	<b>56 day</b>	<b>91 day</b>
CTRL1	0.029	0.029	0.021
CTRL2	0.025	0.020	0.014
SLAG1	0.016	0.014	0.010
SLAG2	0.016	0.015	0.009
SLAG3	0.017	0.017	0.010
META1	0.013	0.011	0.007
META2	0.008	0.009	0.006
META3	0.009	0.007	0.005
UFA1	0.019	0.014	0.006
UFA2	0.015	0.010	0.008
UFA3	0.017	0.012	0.005
SF1	0.009	0.007	0.006
SF2	0.008	0.005	0.004

*RELATIVE HUMIDITY IN DRY CURING ROOM*

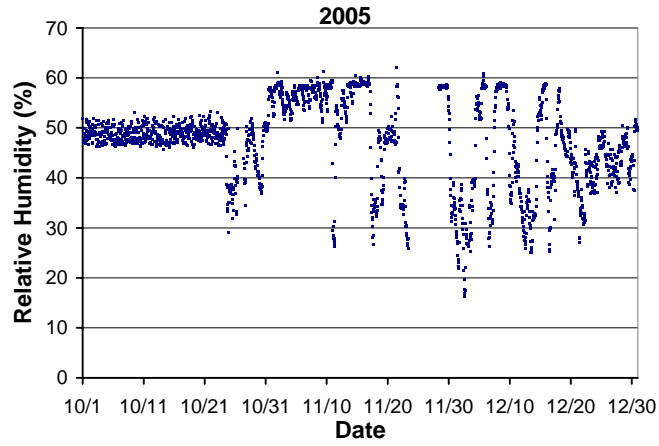


Figure 70 - Relative Humidity in Dry Curing Room 2005

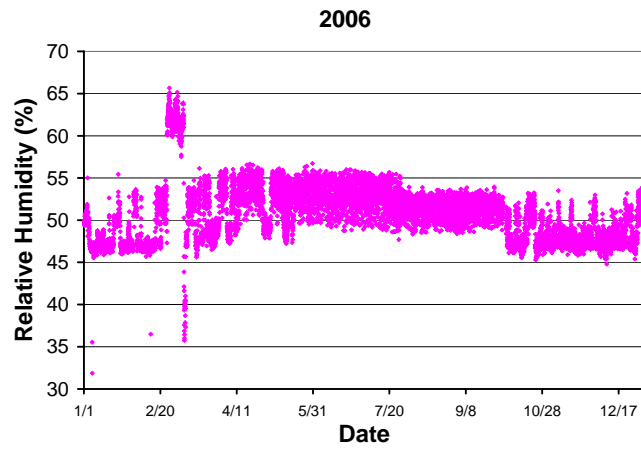


Figure 71 - Relative Humidity in Dry Curing Room 2006

TEMPERATURE IN DRY CURING ROOM

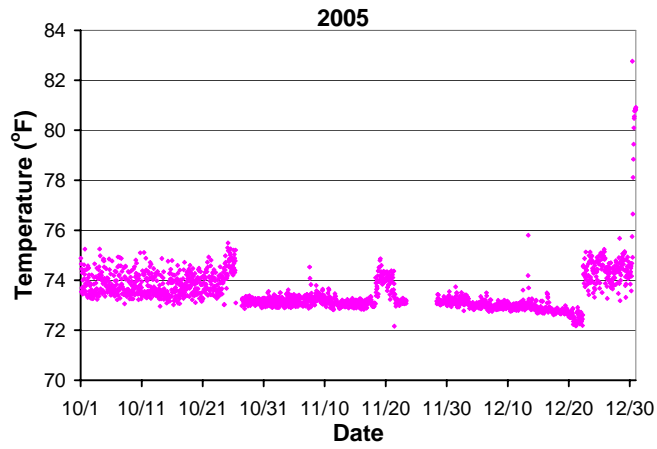


Figure 72 - Temperature in Dry Curing Room 2005

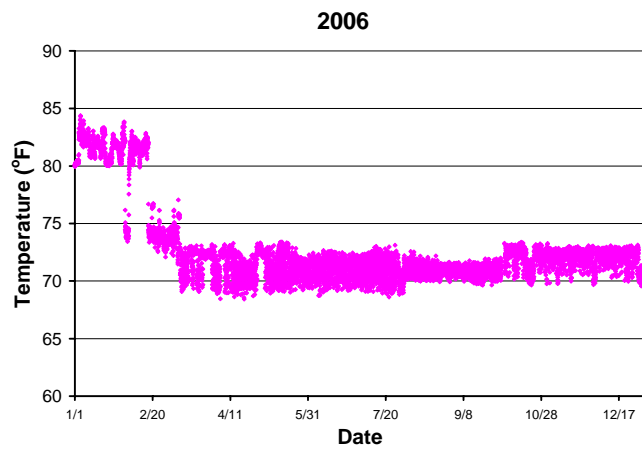


Figure 73 - Temperature in Dry Curing Room 2006

## CORROSION OF EMBEDDED STEEL REINFORCEMENT

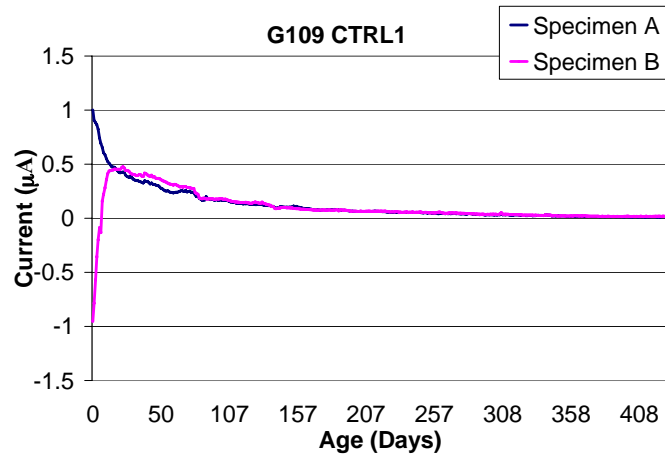


Figure 74 - Control Mixture 1

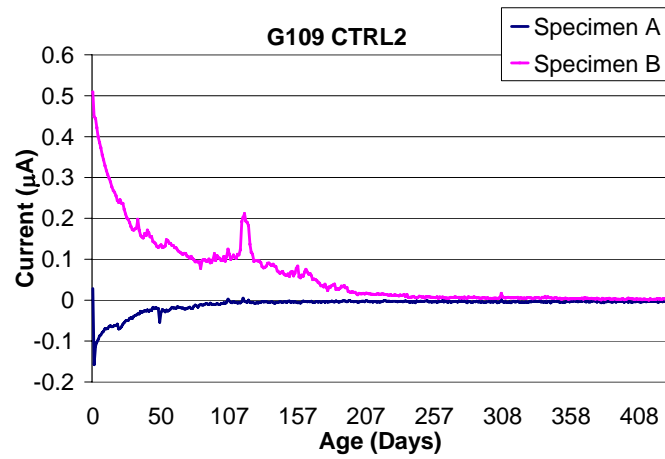


Figure 75 - Control Mixture 2

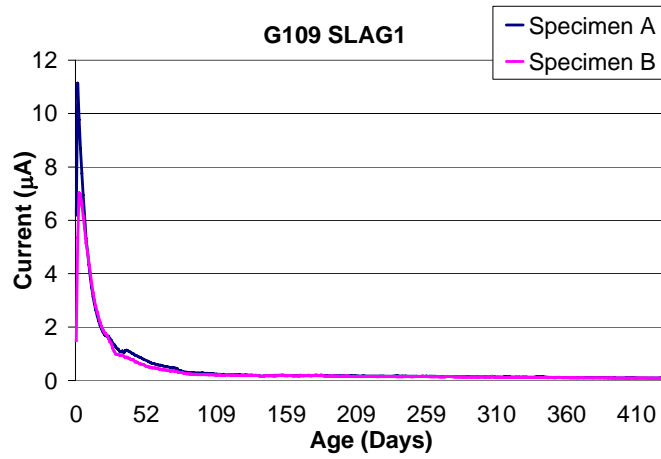


Figure 76 - Slag Mixture 1

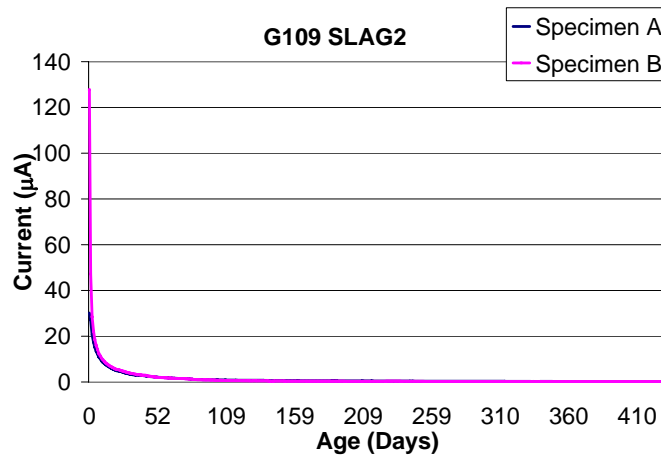


Figure 77 - Slag Mixture 2

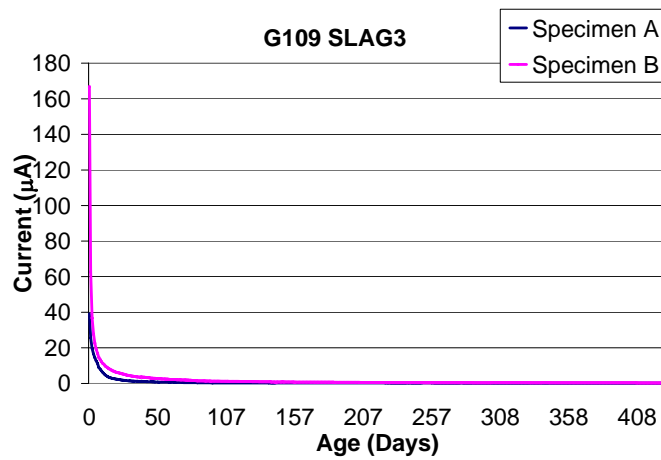


Figure 78 - Slag Mixture 3

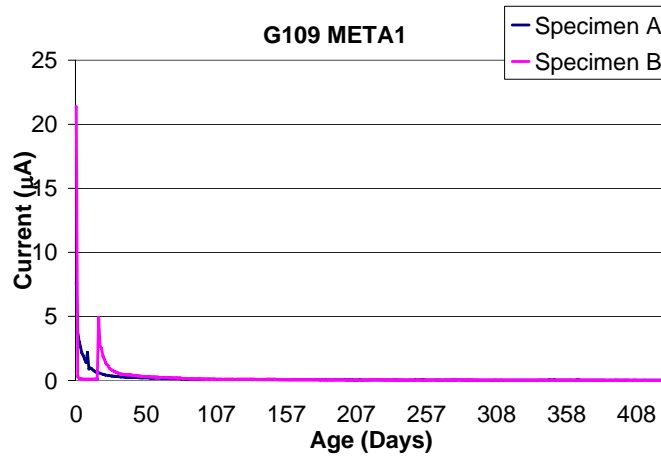


Figure 79 - Metakaolin Mixture 1

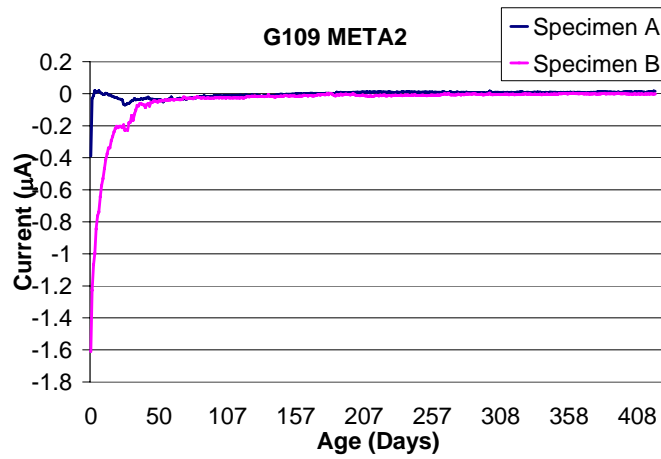


Figure 80 - Metakaolin Mixture 2

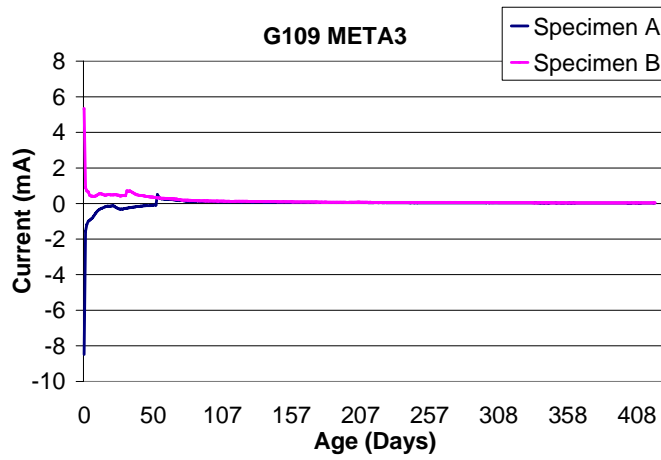


Figure 81 - Metakaolin Mixture 3

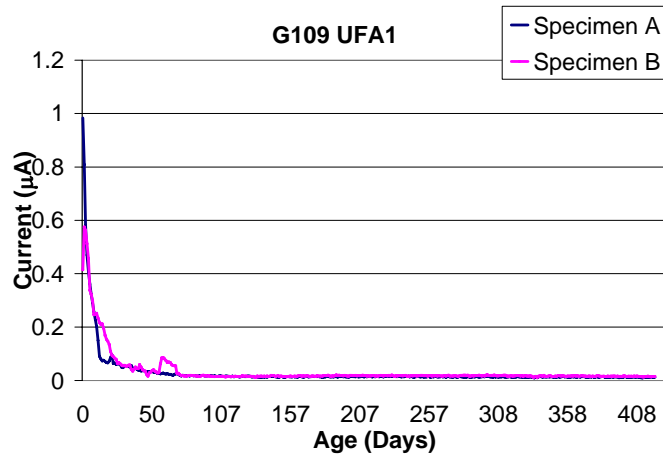


Figure 82 - Ultra Fine Fly Ash Mixture 1

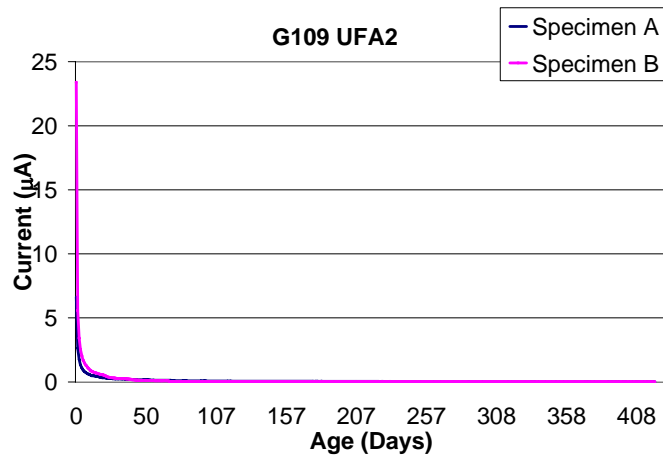


Figure 83 - Ultra Fine Fly Ash Mixture 2

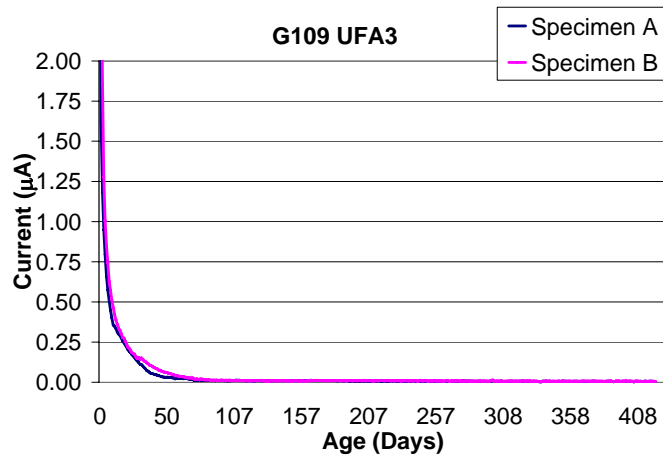


Figure 84 - Ultra Fine Fly Ash Mixture 3

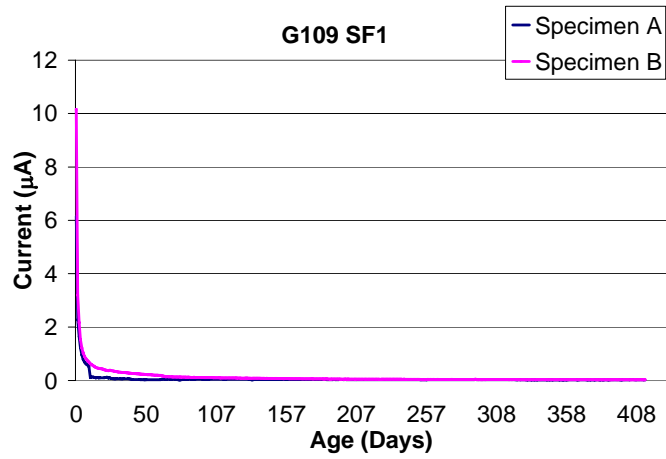


Figure 85 - Silica Fume Mixture 1

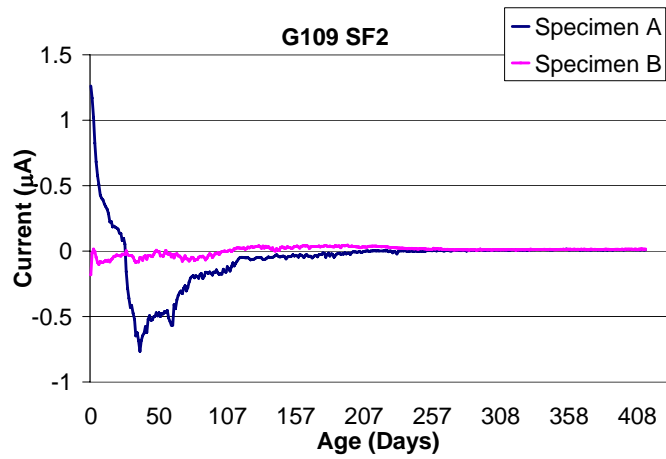


Figure 86 - Silica Fume Mixture 2

## APPENDIX B – LABORATORY MIXTURE NORMALIZED DATA

### *COST*

Table 55 - Material Cost

	<b>Cost (\$/Ton)</b>	<b>Relative Cost</b>
Cement	95	1.000
Fly Ash	42	0.442
Slag	90	0.947
Metakaolin	480	5.053
Ultrafine Fly Ash	1000	10.526
Silica Fume	600	6.316

### *MECHANICAL TESTS*

Table 56 - Normalized Mechanical Test Results

	<b>Compressive Strength</b>	<b>Flexural Strength</b>	<b>Modulus of Elasticity</b>	<b>Shrinkage</b>
CRTL1	1.000	1.000	1.000	1.000
CTRL2	0.956	1.092	0.993	0.917
SLAG1	0.978	1.049	0.905	0.852
SLAG2	0.986	1.043	0.914	0.685
SLAG3	1.065	1.132	0.914	0.750
META1	0.983	1.086	0.951	0.676
META2	0.974	1.056	1.008	0.583
META3	0.967	1.041	1.006	0.630
UFA1	0.988	1.084	0.921	0.917
UFA2	1.000	1.081	0.871	0.574
UFA3	0.989	1.091	0.912	0.537
SF1	0.979	1.108	0.934	0.796
SF2	0.974	0.987	0.926	0.704

**DURABILITY TESTS**

Table 57 - Normalized Durability Test Results

	<b>Surface Resistivity</b>	<b>RMT</b>	<b>Voids</b>	<b>Absorption</b>	<b>Sulfate Expansion</b>
CRTL1	1.000	1.000	1.000	1.000	1.000
CTRL2	0.511	0.563	0.993	0.997	0.886
SLAG1	0.360	0.303	0.977	0.982	0.963
SLAG2	0.285	0.320	0.941	0.938	0.874
SLAG3	0.369	0.281	1.046	1.054	0.977
META1	0.208	0.167	1.082	1.096	0.666
META2	0.167	0.136	1.078	1.092	0.609
META3	0.149	0.117	1.119	1.131	0.715
UFA1	0.208	0.141	1.026	1.033	0.932
UFA2	0.181	0.262	0.999	1.005	0.729
UFA3	0.163	0.130	1.029	1.038	0.786
SF1	0.111	0.143	0.980	1.000	0.540
SF2	0.089	0.092	0.960	0.978	0.591

**SUMMARY**

Table 58 - Summary of All Tests

<b>Mixture</b>	<b>Cost</b>	<b>Mechanical Tests</b>	<b>Durability Tests</b>	<b>Equation Value</b>
CRTL1	1.000	1.000	1.000	1.000
CTRL2	0.900	0.989	0.790	0.881
SLAG1	0.886	0.946	0.717	0.826
SLAG2	0.884	0.907	0.672	0.787
SLAG3	0.881	0.965	0.745	0.847
META1	1.224	0.924	0.644	0.814
META2	1.305	0.905	0.616	0.801
META3	1.386	0.911	0.646	0.826
UFA1	1.852	0.977	0.668	0.910
UFA2	2.043	0.881	0.635	0.874
UFA3	2.233	0.882	0.629	0.891
SF1	1.272	0.955	0.555	0.786
SF2	1.378	0.898	0.542	0.768

## APPENDIX C – SAMPLE PREPARATION FOR XGT AND SEM ANALYSIS

The following is the procedure followed by Michigan Tech to prepare a sample for the SEM or X-ray Microscope from a 4 in. x 4 in. cylinder.

ALWAYS use gloves and safety precautions (eye protection and face masks) for many of the steps use products that can be harmful to the body

Each cylinder is marked with a ruler in sections of approximately 0.25in. to 0.5in. thick



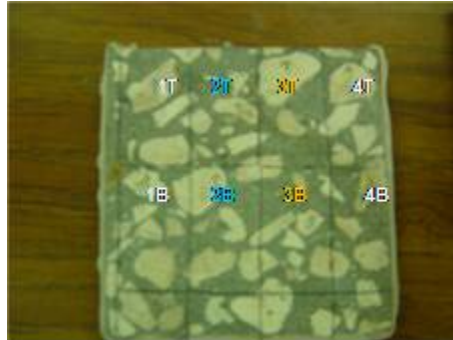
➤ The cylinder is then placed into large diamond bladed section saw, cooled by kerosene



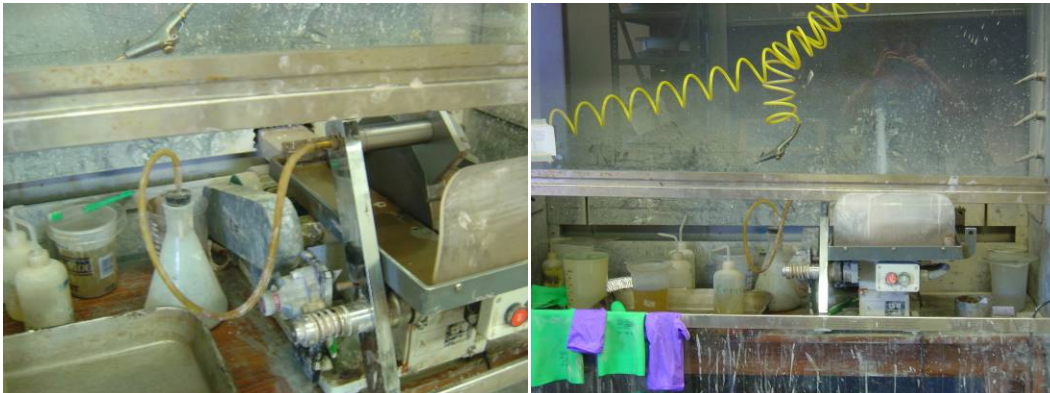
- Each slice takes approximately 1 hour to cut
- After each slice is cut, brush clean with a toothbrush and rinse with kerosene
- Place the slices in a 50°C oven to dry overnight

*Each slice of the cylinder is now cut into billet size samples*

- Each billet should be approximately 2in. x 1in. with the long dimension oriented along the length of the cylinder



- For each marked section:
  - Mark each billet with an arrow to indicate the top and a label which indicates the position of each within the core (make a key or take photos to help keep records.)
  - Cut billets with a small section saw
  - Rinse with kerosene
  - Blow with compressed air to remove the excess kerosene and grit in voids
  - Re-label the billets (location and top), for the kerosene may fade the original labels





- Place the billets in a 50°C oven overnight to dry (a convection oven is preferable if available – the sample will dry faster)

*The samples are now ready to be epoxied to clear petrographic slides*

- Prepare labels on thin paper strips for each sample with the sample name and any other pertinent information needed to identify the billet
- Epoxy the billets
  - JB Quick is a two part epoxy that is mixed just prior to application according to the direction on the package
  - A piece of mylar is placed on the work surface to prevent epoxying any samples to the workbench
  - A thin layer of epoxy is applied to the underside of the billet
  - The appropriate label is placed on the epoxy in such a way that it will help with the identification of the orientation of the billet, i.e. reading upright will give you the correct top and bottom of sample
  - A glass slide is then placed on top of the epoxy and pressed lightly to ensure even distribution of epoxy without spreading it too thin
  - CAUTION: The cure time for the JB Weld epoxy is approximately 5-10 minutes

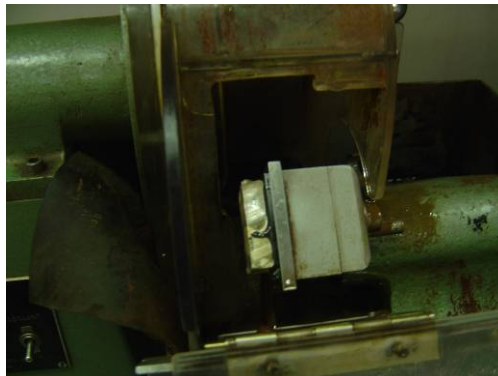


*The billet surface can now be ground flat*

- Place the billets face down in a shallow dish
  - Put a thin layer of kerosene on the bottom of the dish – enough to just cover the surface of the billet
  - This will help break down the mineral oil that is used during this step



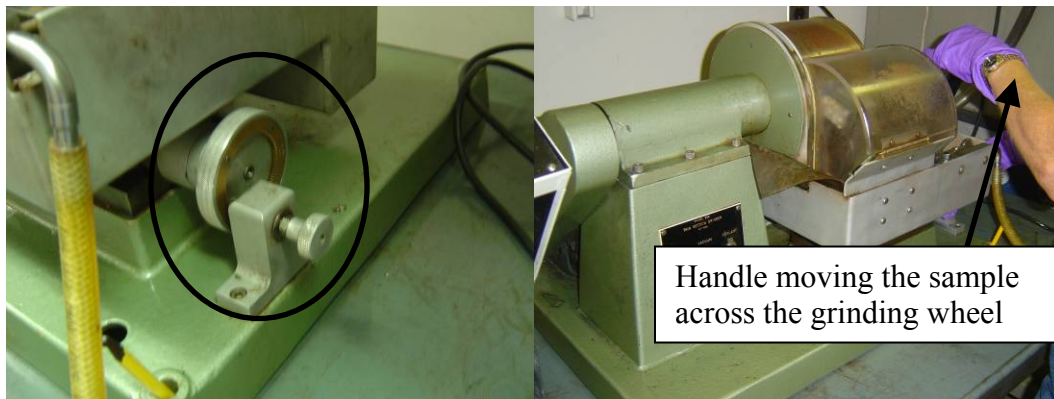
- The next few steps will use an INGRAM Thin Section Grinder
- Place the slide side of the sample against the holder and turn on the vacuum system, which holds the sample in place



- Turn on the pump system – this will circulate mineral oil through the system to help prevent the surface from accumulating too much heat



- Pull the splash guard down and turn the grinder on
- There is a dial on the lower right side of the grinder marked in increments equaling one degree for each. Moving the dial clockwise moves the holder toward the wheel.
  - Slowly rotating the wheel toward the grinding wheel, move the handle up and down until you hear the surface just hit the surface of the sample



- Once part of the surface hits the grinding wheel (indicated by sound), move the arm slowly back and forth approximately 2-3 times
- Now move the dial on the right side of the grinder 5 notches (5 degrees) clockwise
- Moving the arm slowly back and forth another few times
- Repeat the last two steps until the grinding wheel is making contact with the entire face of the billet

- Once this happens, move the surface across the grinding wheel 5 times slowly and advance the sample forward – repeat 8 times
- Rinse clean with kerosene to help break down the mineral oil and blow compressed air across the sample to help flush out the small particles in the voids
- Allow to dry overnight in a 50°C oven

### **Samples ready for XGT analysis (2 day sample preparation)**



### **Sample preparation for the SEM continues with more grinding and polishing**

The surface of the billet coming out of the INGRAM requires further polishing to ensure a flat and polished surface to analyze the sample correctly with the SEM

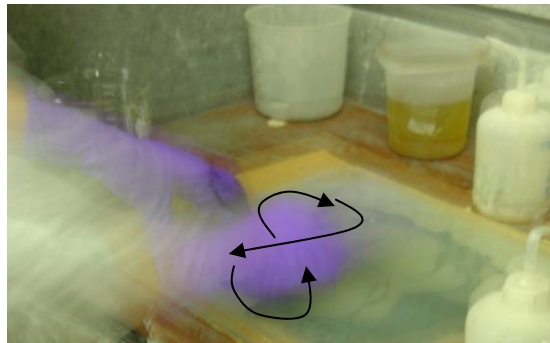
Depending on the number of samples you have – this part of the process may take many days to finish. On average the polishing process takes an extra 3 days, yielding approximately 6 samples when done manually.

#### *Grinding*

- Grind surface with abrasive powder on glass plate → 400, 600, 1000 grit powder
  - Place a teaspoon of powder in the middle of the glass plate and add small amount of kerosene to create an abrasive slurry



- Place billet face down in the slurry and make figure 8's through the powder
  - Keep an even pressure through the sample so the whole surface gets ground evenly



- Be aware that the slurry will spread out and it may need to be re-supplied through the process
  - Rinse the billet with kerosene and check to see if the entire surface has made contact with the grit – use the reflection of the light off the surface to determine if it has been ground evenly
- Between each grit size, rinse the sample with kerosene and use compressed air to remove excess grit from the surface

### *Polish*

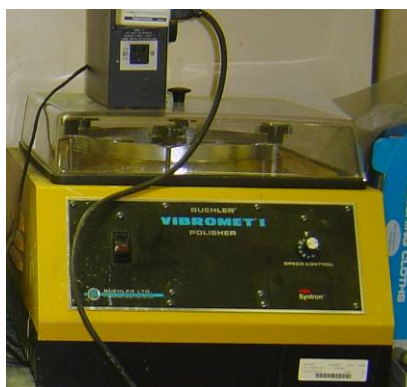
- Place the billets in an ultrasonic kerosene bath for one minute



- Polish each sample using a polishing wheel at 250 rpm (Buehler 10" PowerPro Wheel) with 9 $\mu$ m, 6  $\mu$ m, 1  $\mu$ m diamond pastes lubricated with kerosene
  - These samples can be done manually or with the power head attachment
  - Polish each for approximately 2-3 minutes for each diamond paste using the ultrasonic cleaner between each step



- Using a 0.25 $\mu$ m diamond paste and kerosene slurry – place samples on a vibratory polisher for a 2 hours (Buehler Vibromet)



- Clean in ultrasonic cleaner again
  
- Place in 50C oven over-night to dry

*Final SEM prep*

- Place billets in an ultrasonic ethanol bath for approximately 5 minutes
  - This will allow the sample to dry out completely
  
- Place the samples in a carbon coater and carbon coat each sample

**SAMPLES NOW READY FOR SEM ANALYSIS**

*Equipment list*

- **Ovens** – regular, convection (capable of holding a temperature of 50°C consistently)
- **Saws** – Large diamond saw, sectioning saws
- **Polishers** – automated polishing wheel, vibratory polisher
- **Thin Section Grinder**
- **Glass plates** (or automatic grinder/polisher)
- **Microscopes** – SEM and/or X-ray Microscope
- **Fume Hoods** - with air and water
- **Ultrasonic cleaners**
- **Carbon Coater**

*Consumables:*

- **Epoxy**
  - JB KWIK
- **Coolants**

- Kerosene
- Mineral Oil (Crystal Plus Oil 70 FG)
- **Ethanol**
- **Powder Grit**
  - 400, 600, 800, 1000
- **Diamond Paste**
  - 9, 6, 1, 0.25 micron
- **Petrographic Slides**

## APPENDIX D - PILOT STUDY SEM/EDS DATA

Table 59 Overall results of the pilot study mixes – average CI by Wt%

Mix	CI (Wt%)
A	0.11%
B	0.24%
C	0.06%
D	0.63%
E	0.10%
F	0.08%
G	0.70%
H	0.09%
I	0.08%
J	0.10%
K	0.07%
L	1.73%

### Data for the individual points of each sample for each mix:

12 mixes total (A-L): 3 samples/mix (i.e. A1, A2, A3)\* 12 CI%/sample = 36 CI%/Mix

### Layout of pilot study samples

1	2	3	4
5	6	7	8
9	10	11	12

Mix	Location on sample												Ave Cl% per sample
	1	2	3	4	5	6	7	8	9	10	11	12	
A1	0.06%	0.17%	0.23%	0.22%	0.04%	0.06%	0.14%	0.21%	0.10%	0.09%	0.17%	0.26%	0.15%
A2	0.08%	0.10%	0.07%	0.00%	0.07%	0.04%	0.09%	0.18%	0.12%	0.04%	0.04%	0.10%	0.08%
A3	0.13%	0.10%	0.06%	0.07%	0.05%	0.17%	0.11%	0.11%	0.07%	0.12%	0.10%	0.08%	0.10%
B1	0.26%	0.22%	0.26%	0.29%	0.33%	0.37%	0.32%	0.25%	0.19%	0.32%	0.34%	0.37%	0.29%
B2	0.23%	0.30%	0.23%	0.00%	0.13%	0.24%	0.25%	0.25%	0.25%	0.15%	0.32%	0.32%	0.22%
B3	0.15%	0.24%	0.25%	0.18%	0.19%	0.18%	0.27%	0.27%	0.25%	0.20%	0.16%	0.18%	0.21%
C1	0.00%	0.03%	0.04%	0.08%	0.08%	0.10%	0.00%	0.09%	0.08%	0.04%	0.00%	0.09%	0.05%
C2	0.07%	0.14%	0.00%	0.16%	0.10%	0.05%	0.00%	0.12%	0.00%	0.06%	0.03%	0.09%	0.07%
C3	0.05%	0.00%	0.11%	0.05%	0.00%	0.00%	0.00%	0.07%	0.00%	0.07%	0.08%	0.10%	0.04%
D1	0.55%	0.55%	0.51%	0.57%	0.59%	0.64%	0.71%	0.60%	0.65%	0.46%	0.57%	0.53%	0.58%
D2	0.42%	0.54%	0.60%	1.00%	0.66%	0.61%	0.68%	0.65%	0.62%	0.64%	0.68%	0.63%	0.64%
D3	0.71%	0.64%	0.64%	0.61%	0.78%	0.57%	0.62%	0.66%	0.75%	0.73%	0.67%	0.61%	0.67%
E1	0.05%	0.07%	0.05%	0.19%	0.18%	0.10%	0.14%	0.06%	0.23%	0.15%	0.10%	0.08%	0.12%
E2	0.16%	0.18%	0.00%	0.00%	0.08%	0.17%	0.11%	0.14%	0.08%	0.04%	0.05%	0.09%	0.09%
E3	0.05%	0.08%	0.10%	0.13%	0.05%	0.00%	0.09%	0.00%	0.08%	0.15%	0.11%	0.10%	0.08%
F1	0.13%	0.13%	0.10%	0.09%	0.14%	0.00%	0.04%	0.11%	0.09%	0.13%	0.06%	0.09%	0.09%
F2	0.06%	0.13%	0.04%	0.00%	0.00%	0.14%	0.05%	0.07%	0.05%	0.05%	0.00%	0.06%	0.05%
F3	0.08%	0.07%	0.18%	0.04%	0.10%	0.12%	0.13%	0.04%	0.16%	0.03%	0.08%	0.08%	0.09%
G1	0.76%	0.73%	0.76%	0.75%	0.79%	0.37%	0.74%	0.80%	0.79%	0.74%	0.72%	0.79%	0.73%
G2	0.69%	0.71%	0.68%	1.00%	0.76%	0.69%	0.75%	0.77%	0.76%	0.81%	0.73%	0.77%	0.76%
G3	0.65%	0.59%	0.64%	0.71%	0.62%	0.61%	0.70%	0.67%	0.54%	0.51%	0.47%	0.64%	0.61%
H1	0.00%	0.00%	0.14%	0.09%	0.22%	0.11%	0.06%	0.00%	0.10%	0.09%	0.06%	0.09%	0.08%
H2	0.07%	0.05%	0.08%	0.07%	0.07%	0.10%	0.07%	0.05%	0.00%	0.15%	0.11%	0.15%	0.08%
H3	0.16%	0.11%	0.12%	0.06%	0.13%	0.14%	0.09%	0.13%	0.10%	0.07%	0.11%	0.07%	0.11%
I1	0.09%	0.08%	0.00%	0.09%	0.10%	0.14%	0.09%	0.07%	0.18%	0.12%	0.00%	0.13%	0.09%
I2	0.06%	0.10%	0.03%	0.00%	0.11%	0.00%	0.00%	0.07%	0.06%	0.11%	0.09%	0.13%	0.06%
I3	0.10%	0.10%	0.11%	0.06%	0.06%	0.12%	0.12%	0.03%	0.00%	0.16%	0.15%	0.00%	0.08%
J1	0.00%	0.00%	0.11%	0.13%	0.07%	0.07%	0.15%	0.03%	0.00%	0.11%	0.07%	0.10%	0.07%

Mix	Location on sample												Ave Cl% per sample
	1	2	3	4	5	6	7	8	9	10	11	12	
J2	0.12%	0.00%	0.06%	0.06%	0.08%	0.12%	0.05%	0.10%	0.08%	0.06%	0.18%	0.17%	0.09%
J3	0.24%	0.14%	0.14%	0.11%	0.13%	0.16%	0.08%	0.10%	0.17%	0.06%	0.12%	0.16%	0.13%
K1	0.18%	0.07%	0.07%	0.09%	0.15%	0.00%	0.06%	0.03%	0.00%	0.03%	0.11%	0.00%	0.07%
K2	0.07%	0.07%	0.08%	0.00%	0.10%	0.15%	0.03%	0.15%	0.10%	0.06%	0.05%	0.07%	0.08%
K3	0.05%	0.00%	0.08%	0.12%	0.04%	0.06%	0.08%	0.06%	0.09%	0.06%	0.13%	0.08%	0.07%
L1	0.37%	0.40%	0.42%	0.34%	0.38%	0.46%	0.34%	0.39%	0.40%	43.00%	0.34%	0.34%	3.93%
L2	0.47%	5.00%	0.57%	0.47%	0.63%	0.61%	0.61%	0.31%	0.39%	0.35%	0.16%	0.15%	0.81%
L3	0.42%	0.50%	0.48%	0.53%	0.48%	0.42%	0.42%	0.45%	0.39%	0.44%	0.51%	0.47%	0.46%

Table 60 - University of Florida Cement Paste Standards – 0.35 w/c

5111		5112		5113	
cps/mA	known wt% Cl	cps/mA	known wt% Cl	cps/mA	known wt% Cl
6.11	0.0867	8.02	0.333	22.34	1.297
6.52	0.0867	7.56	0.333	20.53	1.297
5.9	0.0867	7.84	0.333	19.17	1.297
5.75	0.0867	7.58	0.333	22.14	1.297
5.92	0.0867	7.74	0.333	20.21	1.297
5.62	0.0867	8.07	0.333	19.99	1.297
6.55	0.0867	8.76	0.333	21.73	1.297
5.93	0.0867	8.26	0.333	21.04	1.297
6.18	0.0867	7.8	0.333	20.26	1.297
5.87	0.0867	7.75	0.333	21.86	1.297
5.65	0.0867	8.16	0.333	21.27	1.297
5.88	0.0867	8.48	0.333	20.13	1.297
5.62	0.0867	7.61	0.333	21.77	1.297
5.86	0.0867	8.28	0.333	20.36	1.297
5.7	0.0867	7.58	0.333	20.08	1.297
5.44	0.0867	8.09	0.333	21.8	1.297
5.98	0.0867	8.5	0.333	21.18	1.297
5.41	0.0867	8.22	0.333	22.04	1.297
6.51	0.0867	8.98	0.333	22.9	1.297
5.55	0.0867	7.43	0.333	21.96	1.297
5.44	0.0867	7.56	0.333	20.94	1.297
5.89	0.0867	7.66	0.333	23.4	1.297
6.17	0.0867	7.51	0.333	20.38	1.297
5.91	0.0867	7.67	0.333	21.55	1.297
<b>Average</b>	<b>5.89</b>	<b>7.96</b>	<b>0.333</b>	<b>21.21</b>	<b>1.297</b>

Table 61 - Michigan Tech University Cement Standards:  
0.45 w/c: 6 different chloride concentrations

<b>STD</b>	<b>Wt% Cl</b>	<b>X1 [cps/mA]</b>
1	0	12.00
2	0	11.99
3	0	12.07
4	0.22	13.25
5	0.22	13.00
6	0.22	13.21
7	0.44	21.04
8	0.44	20.89
9	0.44	20.89
10	0.87	21.41
11	0.87	21.29
12	0.87	21.35
13	1.72	31.04
14	1.72	31.08
15	1.72	30.35
16	3.34	45.05
17	3.34	45.07
18	3.34	43.93

Table 62 - Michigan Tech University Cement Standards:  
 0.50 w/c: 3 different salts at 6 different concentrations each

STD	Wt% Cl	X1 [cps/mA]
NaCl	0	4.62
	0.2	7.92
	0.4	9.67
	0.8	13.61
	1.57	21.45
	3.06	31.25
CaCl	0	4.70
	0.32	7.25
	0.63	9.09
	1.25	13.65
	2.44	21.30
	4.64	34.24
MgCl	0	4.65
	0.12	6.22
	0.23	7.74
	0.46	11.38
	0.9	16.89
	1.76	19.72

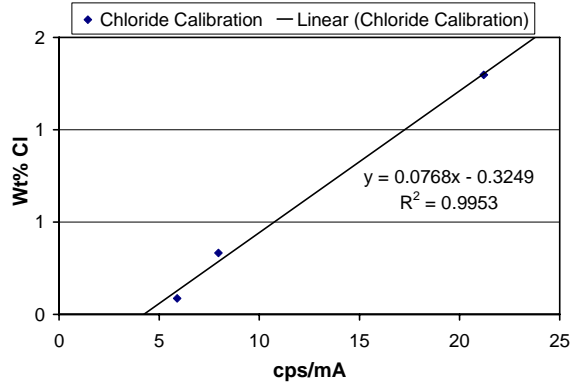


Figure 87 - Calibration curve for UF 0.35 w/c standards  
(Calibration constants: A = 0.0768, B = -0.3249)

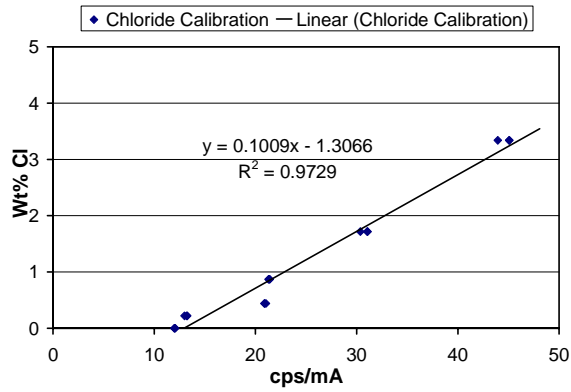


Figure 88 Calibration curve for MTU 0.45 w/c standards  
(Calibration constants: A = 0.1009, B = -1.3066)

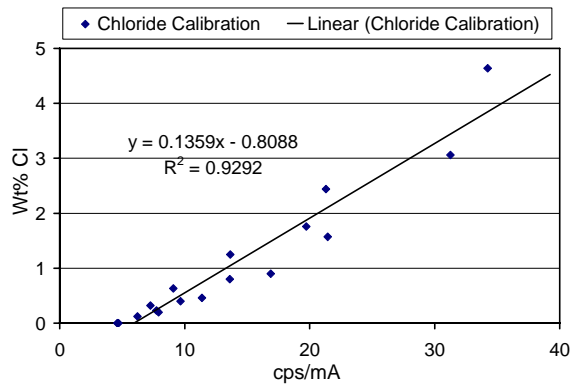


Figure 89 - Calibration curve for MTU 0.50 w/c standards  
(Calibration constants: A = 0.1359, B = -0.8088)

### Complete set of data for UF standards

Total of 11 mixes completed at a later date by MTU

CTL		Mix 4		5111		Mix 6	
wt% Cl	cps						
0	4.840	0.04	4.60	0.08	6.110	0.16	6.690
0	4.660	0.04	4.93	0.08	6.520	0.16	6.370
0	4.740	0.04	4.81	0.08	5.900	0.16	6.520
0	4.190	0.04	5.03	0.08	5.750	0.16	6.480
0	5.010	0.04	4.98	0.08	5.920	0.16	7.380
0	4.540	0.04	5.06	0.08	5.620	0.16	6.940
0	4.600	0.04	5.32	0.08	6.550	0.16	6.090
0	4.470	0.04	5.41	0.08	5.930	0.16	6.460
0	4.590	0.04	5.60	0.08	6.180	0.16	7.200
0	4.620	0.04	2.26	0.08	5.870	0.16	7.030
0	4.380	0.04	5.16	0.08	5.650	0.16	6.960
0	4.720	0.04	5.27	0.08	5.880	0.16	6.240
0	4.100	0.04	5.30	0.08	5.620	0.16	6.660
0	4.310	0.04	4.98	0.08	5.860	0.16	7.030
0	4.390	0.04	5.50	0.08	5.700	0.16	6.850
0	4.920	0.04	5.18	0.08	5.440	0.16	6.310
0	4.020	0.04	5.45	0.08	5.980	0.16	6.840
0	4.690	0.04	5.54	0.08	5.410	0.16	7.210
0	4.440	0.04	5.23	0.08	6.510	0.16	6.630
0	4.580	0.04	5.02	0.08	5.550	0.16	7.210
0	4.700	0.04	4.68	0.08	5.440	0.16	6.680
0	4.310	0.04	4.91	0.08	5.890	0.16	6.980
0	4.550	0.04	5.17	0.08	6.170	0.16	6.640
0	4.580	0.04	5.41	0.08	5.910	0.16	7.060
0	4.540	0.04	5.03	0.08	5.890	0.16	6.769
Average	4.540	Average	5.033	Average	5.890	Average	6.769

**Complete set of data for UF standards**

Total of 11 mixes completed at a later date by MTU

5112		Mix 8		5113		Mix 10	
wt% Cl	cps	wt% Cl	cps	wt% Cl	cps	wt% Cl	cps
0.32	8.020	0.64	13.650	1.28	22.340	1.5	25.920
0.32	7.560	0.64	12.810	1.28	20.530	1.5	6.030
0.32	7.840	0.64	12.180	1.28	19.170	1.5	19.350
0.32	7.580	0.64	13.050	1.28	22.140	1.5	24.590
0.32	7.740	0.64	12.480	1.28	20.210	1.5	24.860
0.32	8.070	0.64	13.510	1.28	19.990	1.5	23.880
0.32	8.760	0.64	12.540	1.28	21.730	1.5	25.790
0.32	8.260	0.64	12.590	1.28	21.040	1.5	25.370
0.32	7.800	0.64	13.210	1.28	20.260	1.5	22.580
0.32	7.750	0.64	14.150	1.28	21.860	1.5	18.710
0.32	8.160	0.64	13.010	1.28	21.270	1.5	25.490
0.32	8.480	0.64	13.540	1.28	20.130	1.5	25.420
0.32	7.610	0.64	13.120	1.28	21.770	1.5	21.210
0.32	8.280	0.64	14.240	1.28	20.360	1.5	10.230
0.32	7.580	0.64	13.820	1.28	20.080	1.5	24.720
0.32	8.090	0.64	13.760	1.28	21.800	1.5	24.810
0.32	8.500	0.64	14.290	1.28	21.180	1.5	25.290
0.32	8.220	0.64	13.230	1.28	22.040	1.5	23.720
0.32	8.980	0.64	13.210	1.28	22.900	1.5	24.180
0.32	7.430	0.64	11.990	1.28	21.960	1.5	25.340
0.32	7.560	0.64	13.290	1.28	20.940	1.5	22.010
0.32	7.660	0.64	12.370	1.28	23.400	1.5	24.160
0.32	7.510	0.64	13.650	1.28	20.380	1.5	23.750
0.32	7.670	0.64	14.110	1.28	21.550	1.5	25.050
0.32	7.963	0.64	13.242	1.28	21.210	1.5	22.603
Average	7.963	Average	13.242	Average	21.210	Average	23.861

**Complete set of data for UF standards**

Total of 11 mixes completed at a later date by MTU

Mix 11		Mix 12		Mix 13	
wt% Cl	cps	wt% Cl	cps	wt% Cl	cps
2	32.490	2.5	40.230	3	45.630
2	30.420	2.5	37.750	3	49.480
2	30.580	2.5	39.320	3	39.510
2	29.640	2.5	39.650	3	44.450
2	31.330	2.5	39.540	3	39.920
2	31.440	2.5	9.820	3	38.020
2	31.920	2.5	40.050	3	51.630
2	29.730	2.5	39.670	3	40.780
2	32.070	2.5	34.950	3	47.140
2	30.260	2.5	38.340	3	40.560
2	30.570	2.5	37.190	3	56.560
2	29.490	2.5	39.270	3	40.980
2	30.960	2.5	44.660	3	40.410
2	32.080	2.5	40.520	3	51.520
2	31.530	2.5	37.840	3	52.850
2	30.150	2.5	39.200	3	39.650
2	31.210	2.5	42.180	3	38.950
2	31.870	2.5	36.340	3	59.260
2	31.020	2.5	42.710	3	52.860
2	29.810	2.5	40.840	3	38.720
2	31.710	2.5	36.830	3	45.100
2	29.880	2.5	38.680	3	36.920
2	30.670	2.5	40.440	3	40.700
2	30.210	2.5	41.750	3	36.690
2	30.877	2.5	38.240	3	44.512
Average	30.877	Average	39.425	Average	44.512

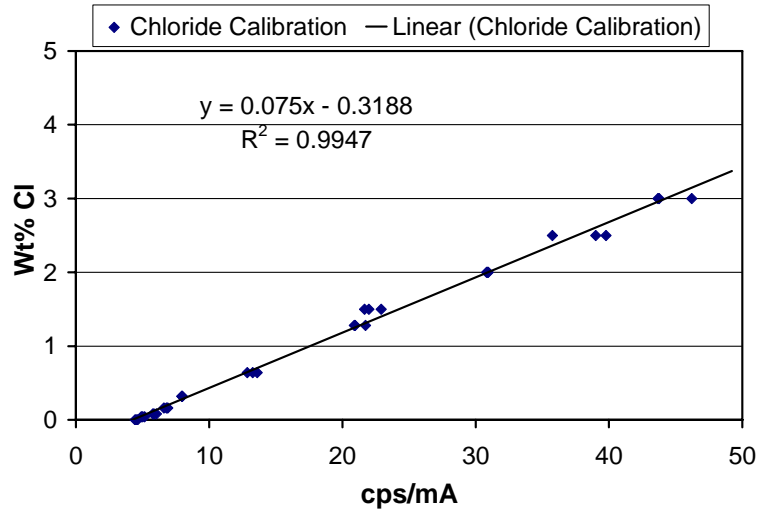
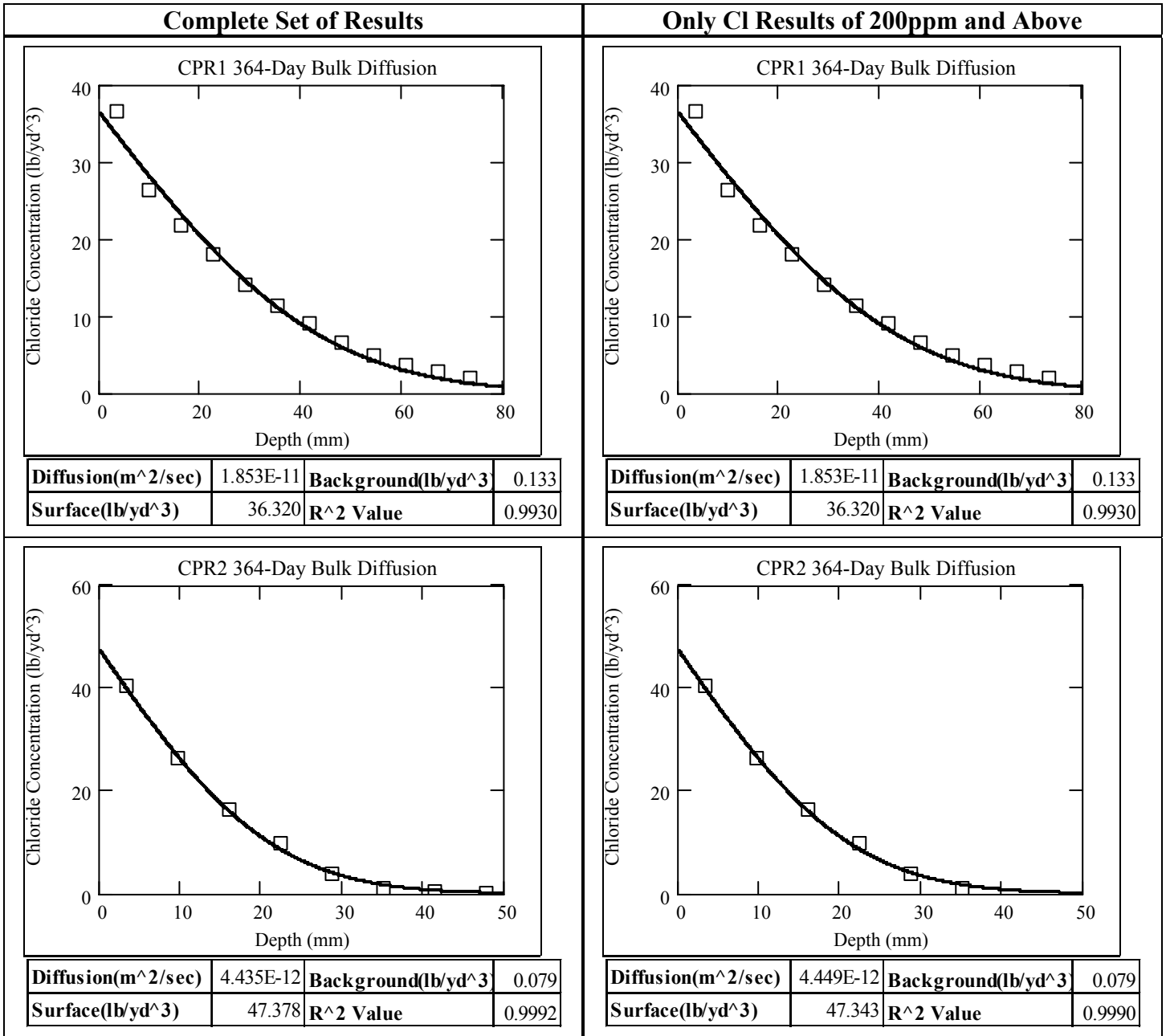
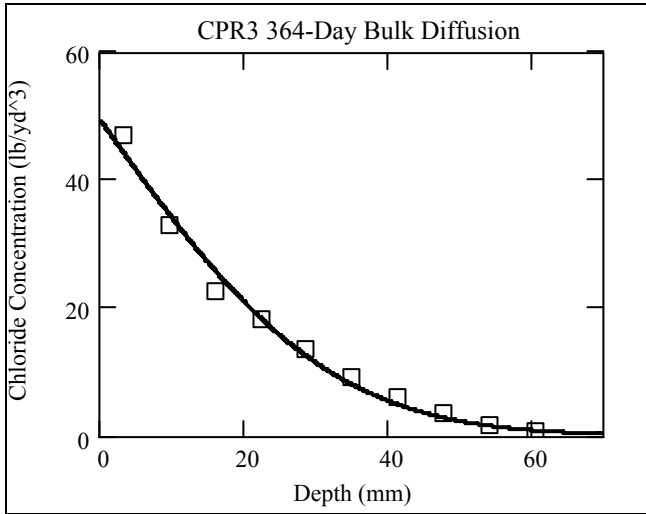


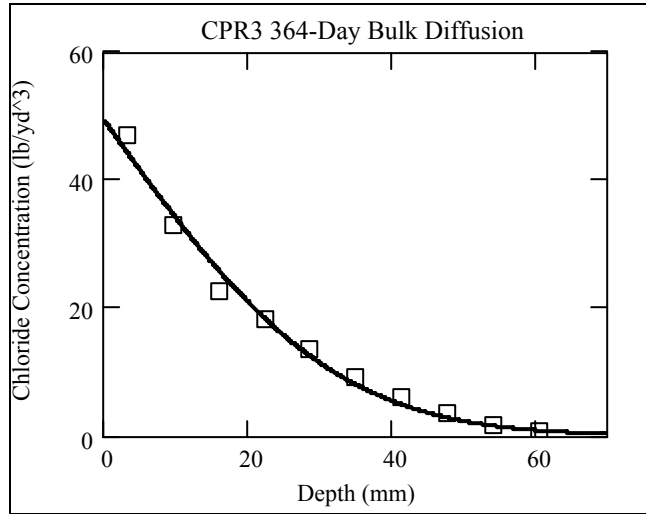
Figure 90 - Calibration curve for full set of 0.35 w/c standards  
 (Calibration Constants A = 0.075, B = -0.3188) Comparison of the calibration curves with full  
 data set for 0.35 w/c from UF

## Sensitivity Study Plots



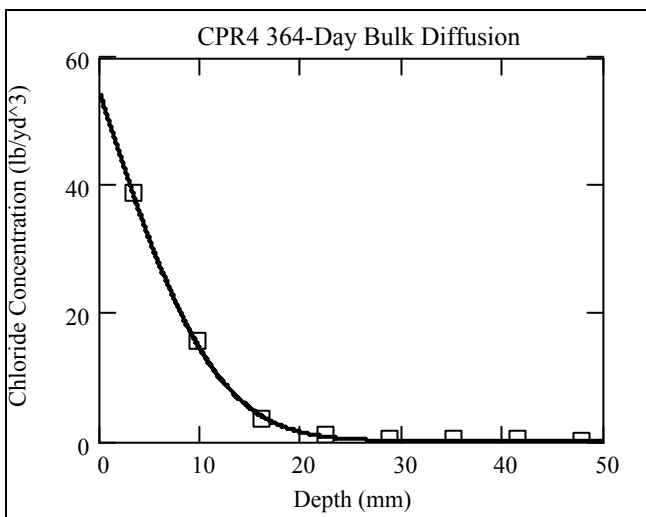


<b>Diffusion(m<sup>2</sup>/sec)</b>	9.916E-12	<b>Background(lb/yd<sup>3</sup>)</b>	0.125
<b>Surface(lb/yd<sup>3</sup>)</b>	49.334	<b>R<sup>2</sup> Value</b>	0.9941



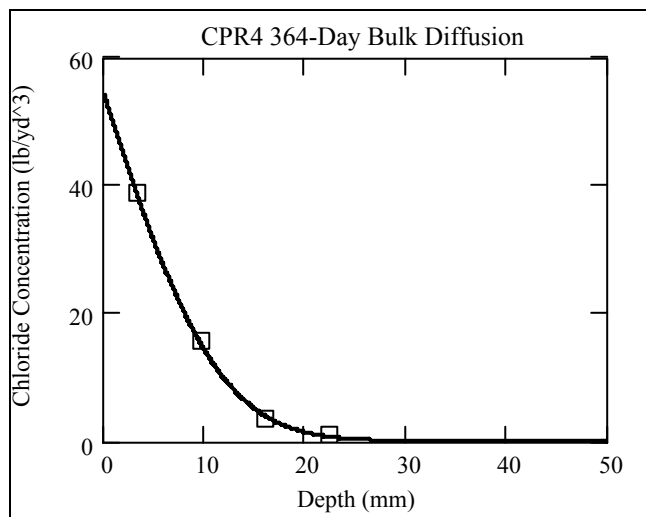
<b>Diffusion(m<sup>2</sup>/sec)</b>	9.916E-12	<b>Background(lb/yd<sup>3</sup>)</b>	0.125
<b>Surface(lb/yd<sup>3</sup>)</b>	49.334	<b>R<sup>2</sup> Value</b>	0.9941

**Complete Set of Results**

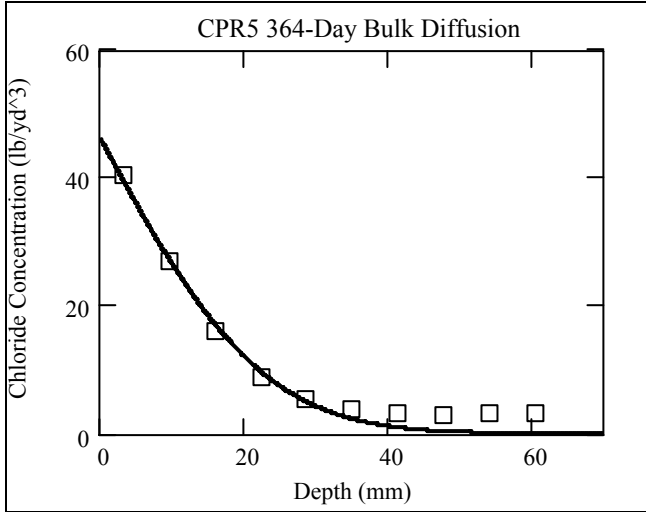


<b>Diffusion(m<sup>2</sup>/sec)</b>	1.256E-12	<b>Background(lb/yd<sup>3</sup>)</b>	0.151
<b>Surface(lb/yd<sup>3</sup>)</b>	54.105	<b>R<sup>2</sup> Value</b>	0.9998

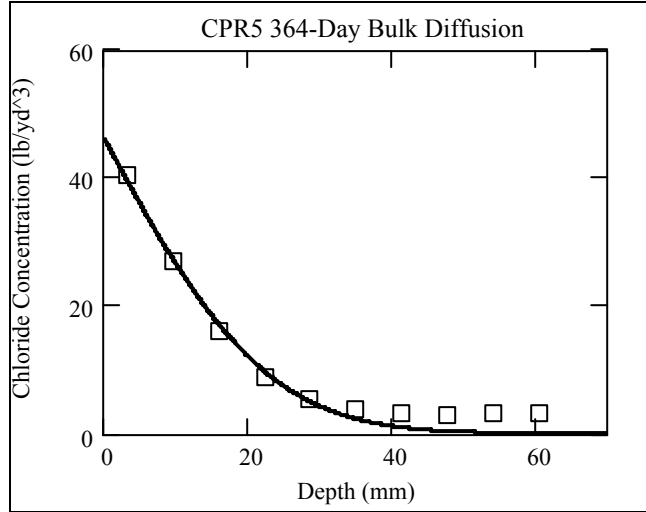
**Only CI Results of 200ppm and Above**



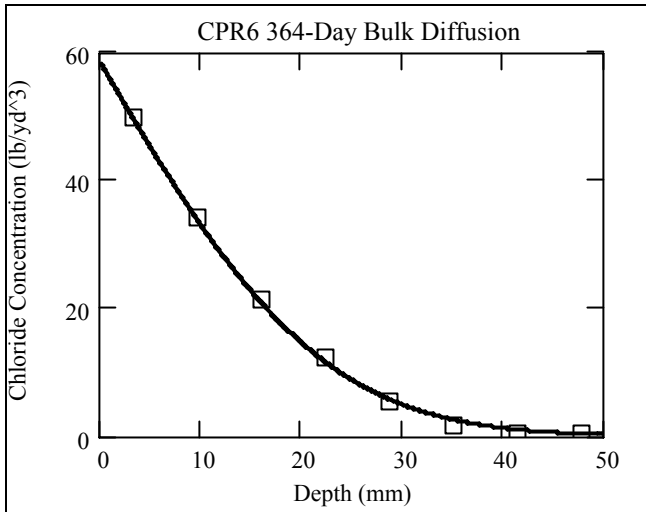
<b>Diffusion(m<sup>2</sup>/sec)</b>	1.255E-12	<b>Background(lb/yd<sup>3</sup>)</b>	0.151
<b>Surface(lb/yd<sup>3</sup>)</b>	54.118	<b>R<sup>2</sup> Value</b>	0.9997



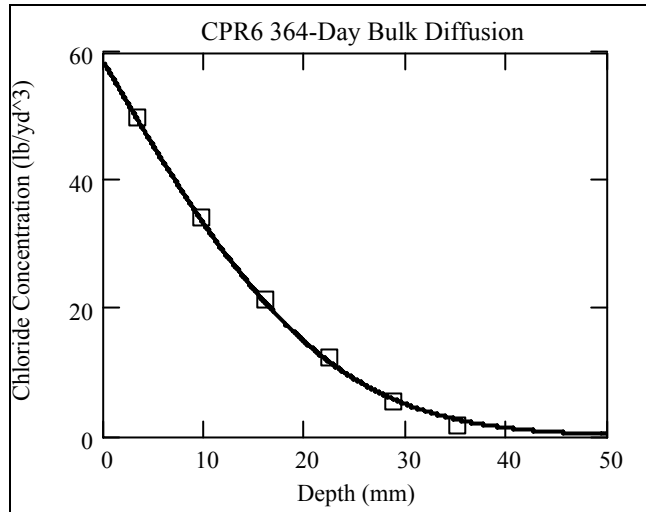
<b>Diffusion(m<sup>2</sup>/sec)</b>	5.025E-12	<b>Background(lb/yd<sup>3</sup>)</b>	0.140
<b>Surface(lb/yd<sup>3</sup>)</b>	46.159	<b>R<sup>2</sup> Value</b>	0.9947



<b>Diffusion(m<sup>2</sup>/sec)</b>	5.025E-12	<b>Background(lb/yd<sup>3</sup>)</b>	0.140
<b>Surface(lb/yd<sup>3</sup>)</b>	46.159	<b>R<sup>2</sup> Value</b>	0.9947



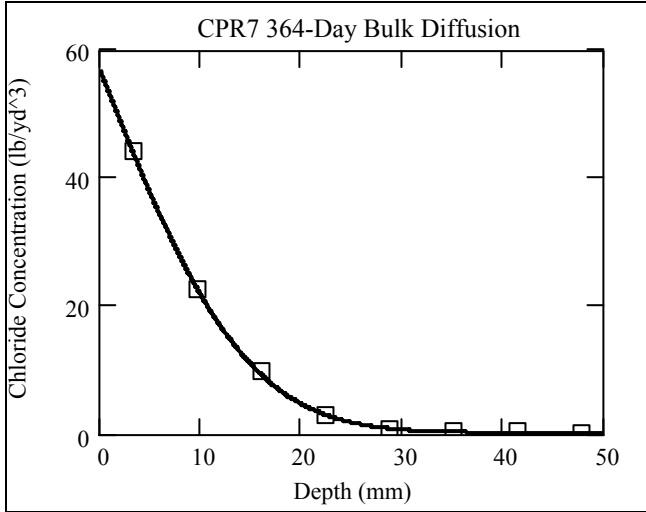
<b>Diffusion(m<sup>2</sup>/sec)</b>	4.777E-12	<b>Background(lb/yd<sup>3</sup>)</b>	0.107
<b>Surface(lb/yd<sup>3</sup>)</b>	58.364	<b>R<sup>2</sup> Value</b>	0.9996



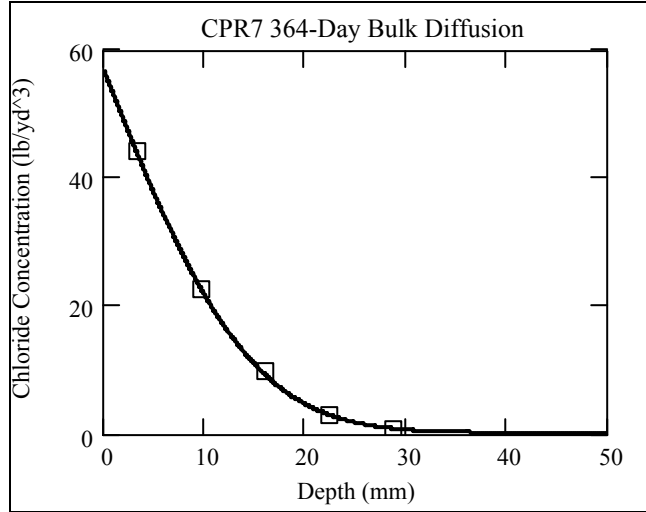
<b>Diffusion(m<sup>2</sup>/sec)</b>	4.800E-12	<b>Background(lb/yd<sup>3</sup>)</b>	0.107
<b>Surface(lb/yd<sup>3</sup>)</b>	58.299	<b>R<sup>2</sup> Value</b>	0.9996

**Complete Set of Results**

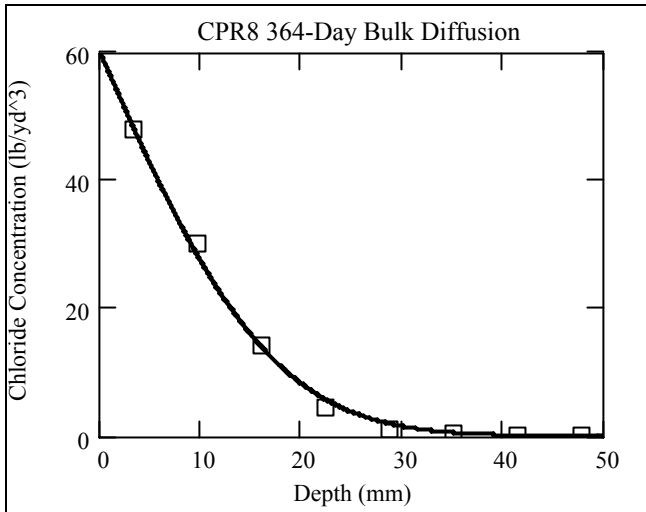
**Only CI Results of 200ppm and Above**



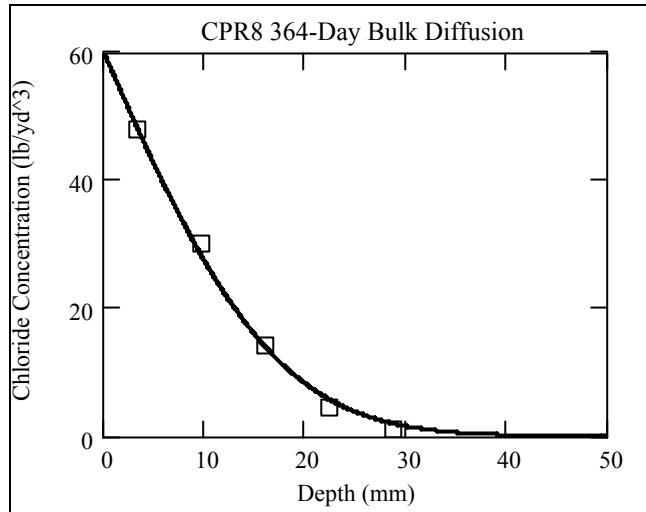
<b>Diffusion(m<sup>2</sup>/sec)</b>	2.057E-12	<b>Background(lb/yd<sup>3</sup>)</b>	0.233
<b>Surface(lb/yd<sup>3</sup>)</b>	56.651	<b>R<sup>2</sup> Value</b>	0.9999



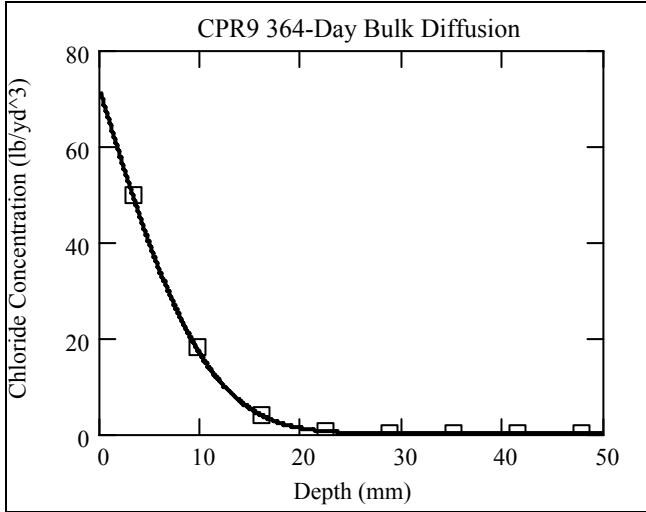
<b>Diffusion(m<sup>2</sup>/sec)</b>	2.057E-12	<b>Background(lb/yd<sup>3</sup>)</b>	0.233
<b>Surface(lb/yd<sup>3</sup>)</b>	56.654	<b>R<sup>2</sup> Value</b>	0.9999



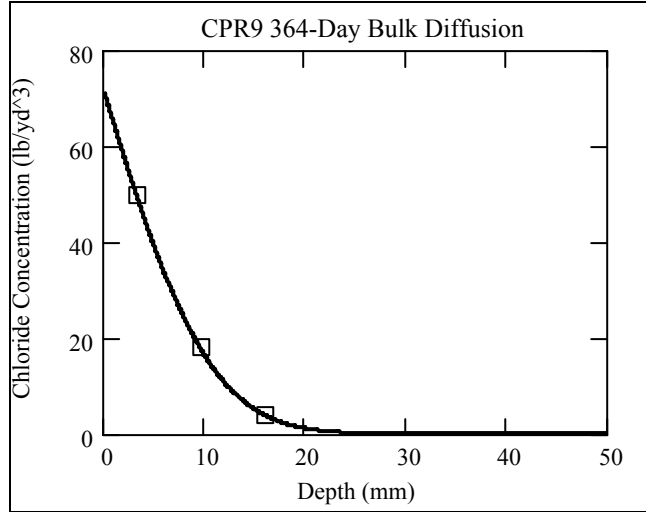
<b>Diffusion(m<sup>2</sup>/sec)</b>	2.853E-12	<b>Background(lb/yd<sup>3</sup>)</b>	0.096
<b>Surface(lb/yd<sup>3</sup>)</b>	59.827	<b>R<sup>2</sup> Value</b>	0.9987



<b>Diffusion(m<sup>2</sup>/sec)</b>	2.858E-12	<b>Background(lb/yd<sup>3</sup>)</b>	0.096
<b>Surface(lb/yd<sup>3</sup>)</b>	59.804	<b>R<sup>2</sup> Value</b>	0.9983



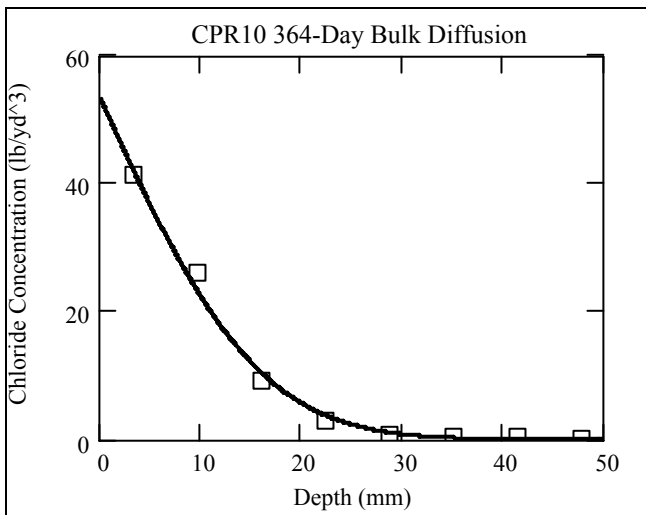
<b>Diffusion(m<sup>2</sup>/sec)</b>	1.100E-12	<b>Background(lb/yd<sup>3</sup>)</b>	0.075
<b>Surface(lb/yd<sup>3</sup>)</b>	71.043	<b>R<sup>2</sup> Value</b>	1.0000



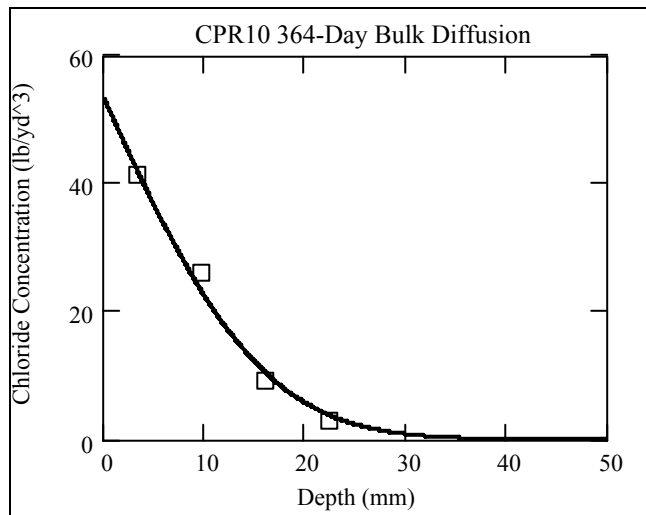
<b>Diffusion(m<sup>2</sup>/sec)</b>	1.098E-12	<b>Background(lb/yd<sup>3</sup>)</b>	0.075
<b>Surface(lb/yd<sup>3</sup>)</b>	71.077	<b>R<sup>2</sup> Value</b>	1.0000

**Complete Set of Results**

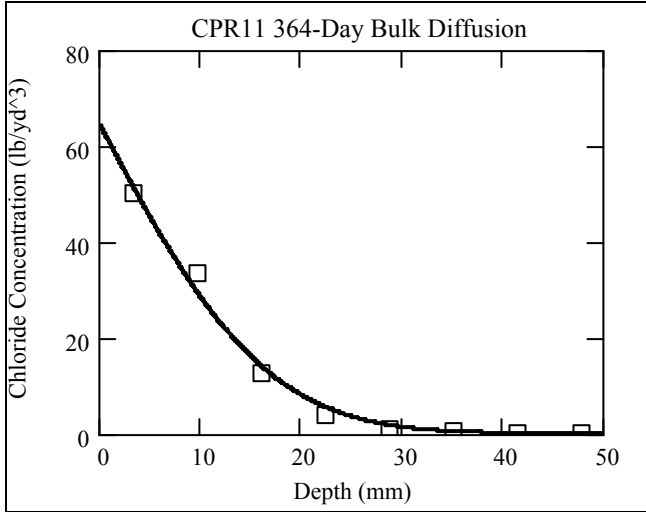
**Only CI Results of 200ppm and Above**



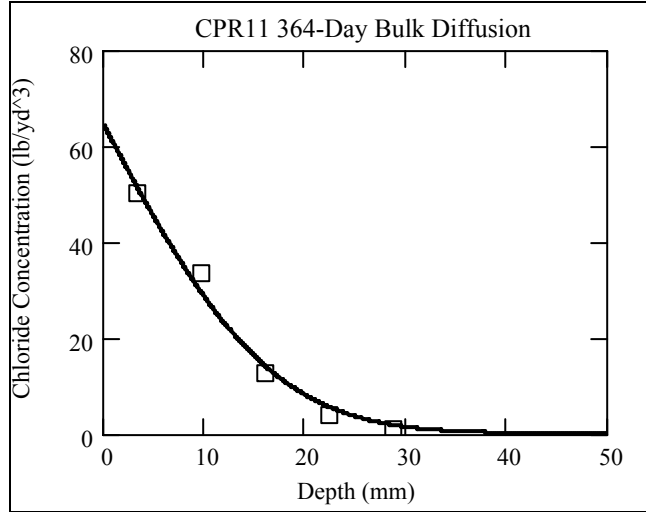
<b>Diffusion(m<sup>2</sup>/sec)</b>	2.425E-12	<b>Background(lb/yd<sup>3</sup>)</b>	0.074
<b>Surface(lb/yd<sup>3</sup>)</b>	53.269	<b>R<sup>2</sup> Value</b>	0.9970



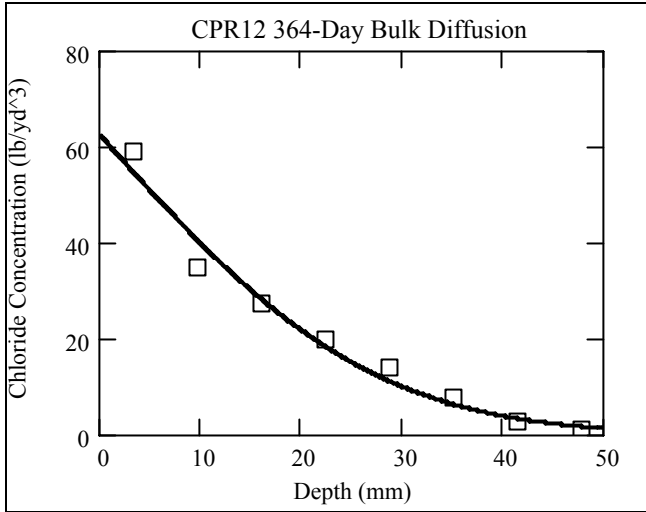
<b>Diffusion(m<sup>2</sup>/sec)</b>	2.438E-12	<b>Background(lb/yd<sup>3</sup>)</b>	0.074
<b>Surface(lb/yd<sup>3</sup>)</b>	53.202	<b>R<sup>2</sup> Value</b>	0.9950



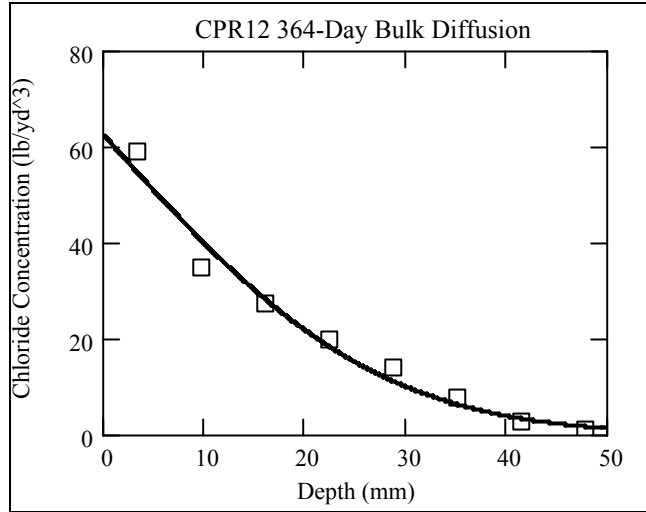
<b>Diffusion(m<sup>2</sup>/sec)</b>	2.684E-12	<b>Background(lb/yd<sup>3</sup>)</b>	0.185
<b>Surface(lb/yd<sup>3</sup>)</b>	64.205	<b>R<sup>2</sup> Value</b>	0.9955



<b>Diffusion(m<sup>2</sup>/sec)</b>	2.686E-12	<b>Background(lb/yd<sup>3</sup>)</b>	0.185
<b>Surface(lb/yd<sup>3</sup>)</b>	64.191	<b>R<sup>2</sup> Value</b>	0.9938



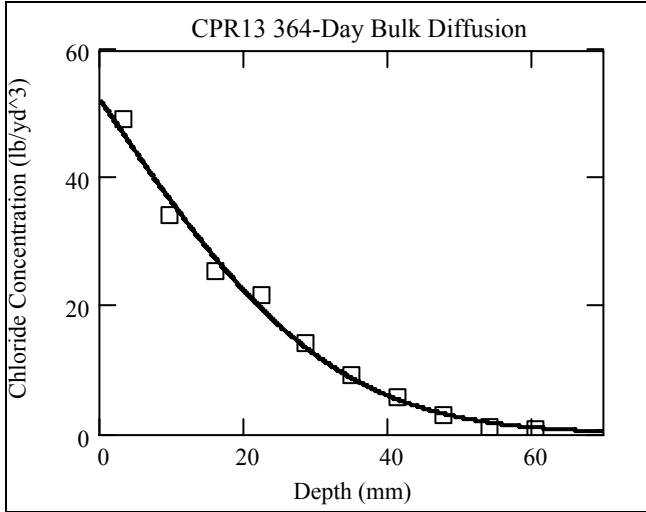
<b>Diffusion(m<sup>2</sup>/sec)</b>	7.164E-12	<b>Background(lb/yd<sup>3</sup>)</b>	0.141
<b>Surface(lb/yd<sup>3</sup>)</b>	62.262	<b>R<sup>2</sup> Value</b>	0.9879



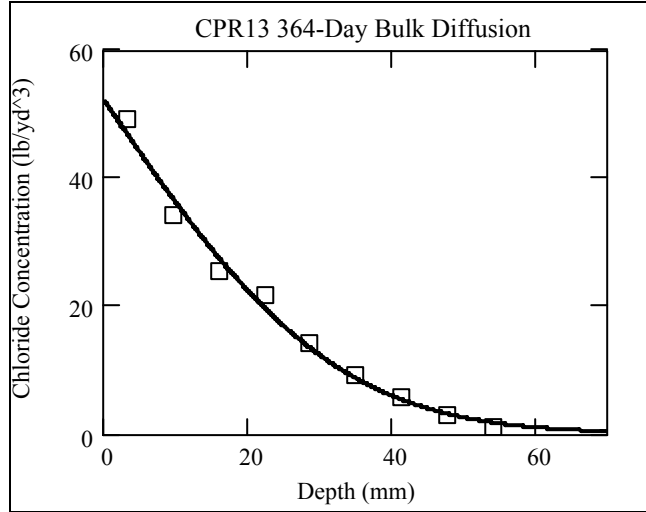
<b>Diffusion(m<sup>2</sup>/sec)</b>	7.164E-12	<b>Background(lb/yd<sup>3</sup>)</b>	0.141
<b>Surface(lb/yd<sup>3</sup>)</b>	62.262	<b>R<sup>2</sup> Value</b>	0.9879

**Complete Set of Results**

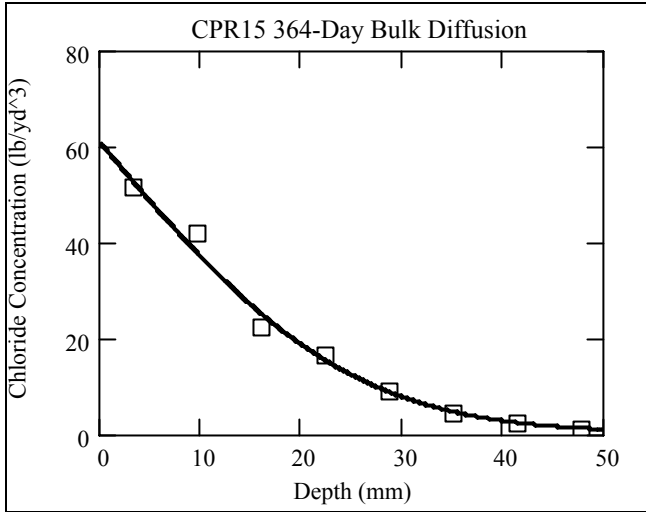
**Only CI Results of 200ppm and Above**



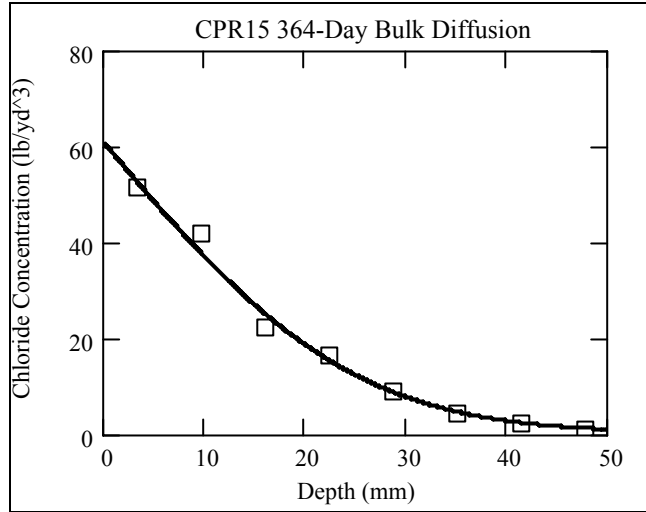
<b>Diffusion(m<sup>2</sup>/sec)</b>	1.005E-11	<b>Background(lb/yd<sup>3</sup>)</b>	0.178
<b>Surface(lb/yd<sup>3</sup>)</b>	52.174	<b>R<sup>2</sup> Value</b>	0.9954



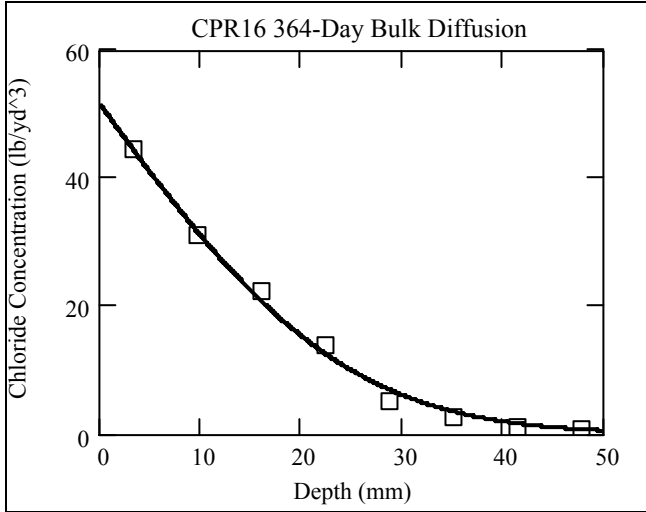
<b>Diffusion(m<sup>2</sup>/sec)</b>	1.007E-11	<b>Background(lb/yd<sup>3</sup>)</b>	0.178
<b>Surface(lb/yd<sup>3</sup>)</b>	52.156	<b>R<sup>2</sup> Value</b>	0.9948



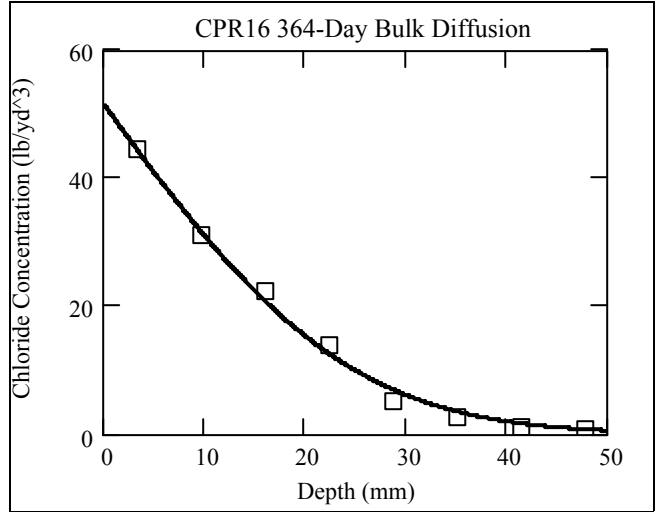
<b>Diffusion(m<sup>2</sup>/sec)</b>	5.952E-12	<b>Background(lb/yd<sup>3</sup>)</b>	0.515
<b>Surface(lb/yd<sup>3</sup>)</b>	60.714	<b>R<sup>2</sup> Value</b>	0.9940



<b>Diffusion(m<sup>2</sup>/sec)</b>	5.952E-12	<b>Background(lb/yd<sup>3</sup>)</b>	0.515
<b>Surface(lb/yd<sup>3</sup>)</b>	60.714	<b>R<sup>2</sup> Value</b>	0.9940



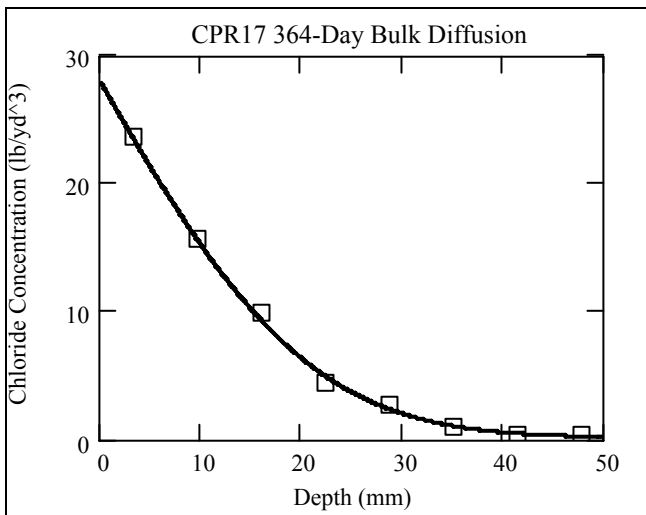
<b>Diffusion(m<sup>2</sup>/sec)</b>	5.801E-12	<b>Background(lb/yd<sup>3</sup>)</b>	0.126
<b>Surface(lb/yd<sup>3</sup>)</b>	51.412	<b>R<sup>2</sup> Value</b>	0.9978



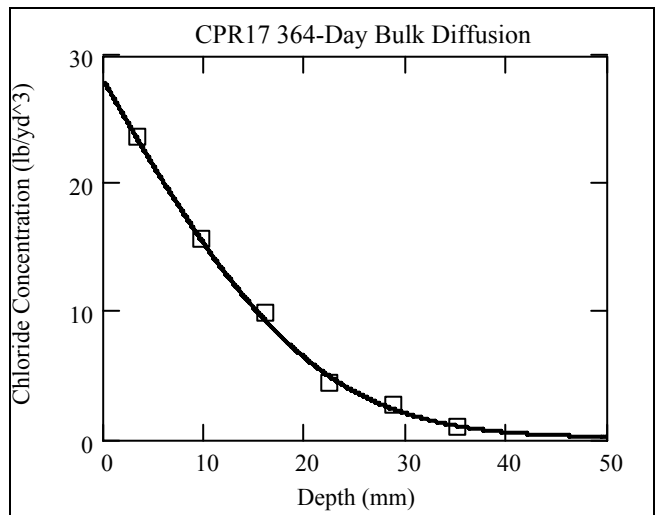
<b>Diffusion(m<sup>2</sup>/sec)</b>	5.801E-12	<b>Background(lb/yd<sup>3</sup>)</b>	0.126
<b>Surface(lb/yd<sup>3</sup>)</b>	51.412	<b>R<sup>2</sup> Value</b>	0.9978

**Complete Set of Results**

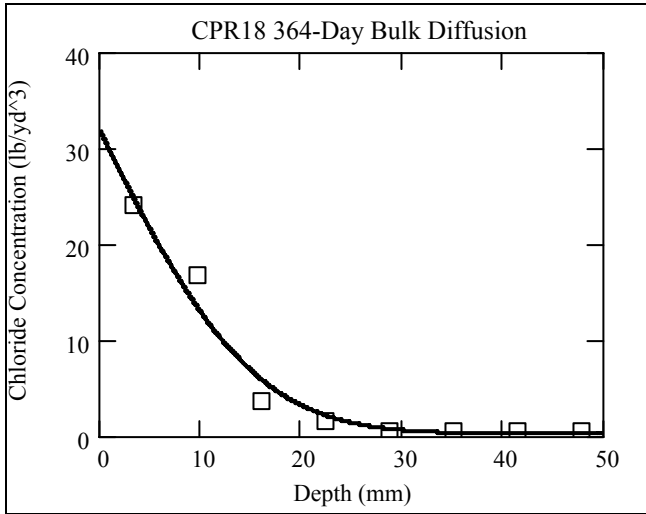
**Only CI Results of 200ppm and Above**



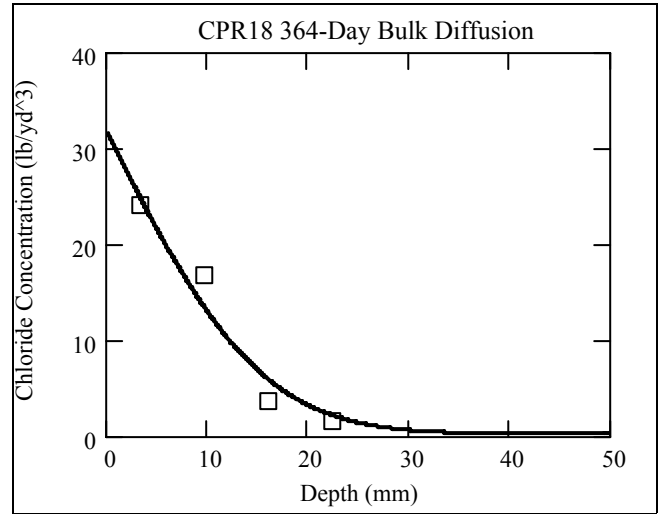
<b>Diffusion(m<sup>2</sup>/sec)</b>	4.259E-12	<b>Background(lb/yd<sup>3</sup>)</b>	0.179
<b>Surface(lb/yd<sup>3</sup>)</b>	27.940	<b>R<sup>2</sup> Value</b>	0.9992



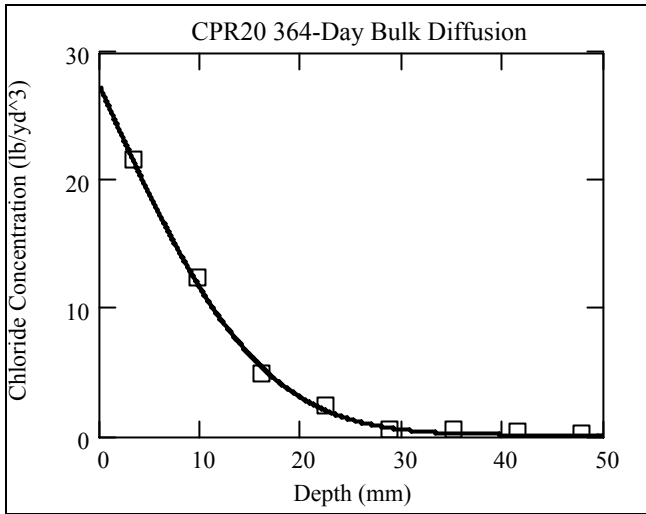
<b>Diffusion(m<sup>2</sup>/sec)</b>	4.262E-12	<b>Background(lb/yd<sup>3</sup>)</b>	0.179
<b>Surface(lb/yd<sup>3</sup>)</b>	27.936	<b>R<sup>2</sup> Value</b>	0.9990



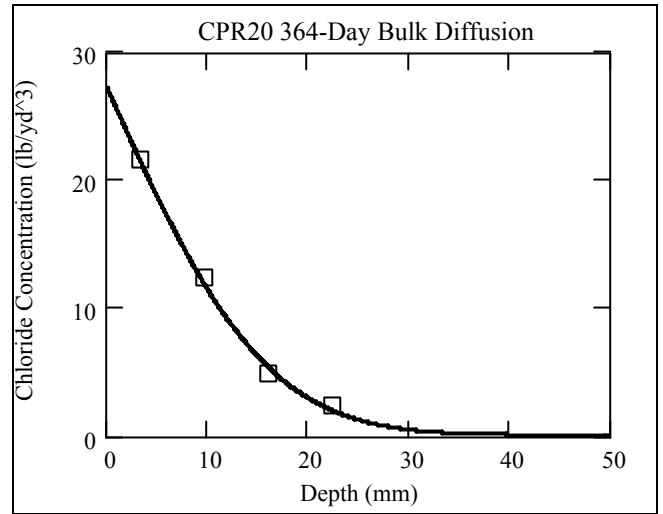
<b>Diffusion(m<sup>2</sup>/sec)</b>	2.258E-12	<b>Background(lb/yd<sup>3</sup>)</b>	0.259
<b>Surface(lb/yd<sup>3</sup>)</b>	31.681	<b>R<sup>2</sup> Value</b>	0.9855



<b>Diffusion(m<sup>2</sup>/sec)</b>	2.266E-12	<b>Background(lb/yd<sup>3</sup>)</b>	0.259
<b>Surface(lb/yd<sup>3</sup>)</b>	31.656	<b>R<sup>2</sup> Value</b>	0.9765



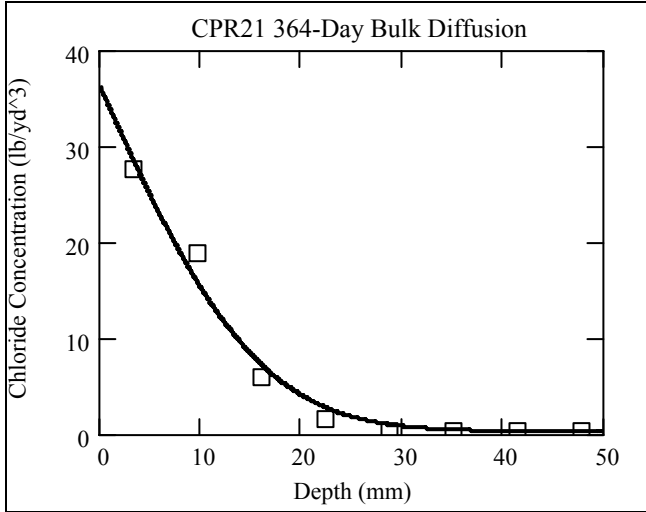
<b>Diffusion(m<sup>2</sup>/sec)</b>	2.433E-12	<b>Background(lb/yd<sup>3</sup>)</b>	0.119
<b>Surface(lb/yd<sup>3</sup>)</b>	27.193	<b>R<sup>2</sup> Value</b>	0.9992



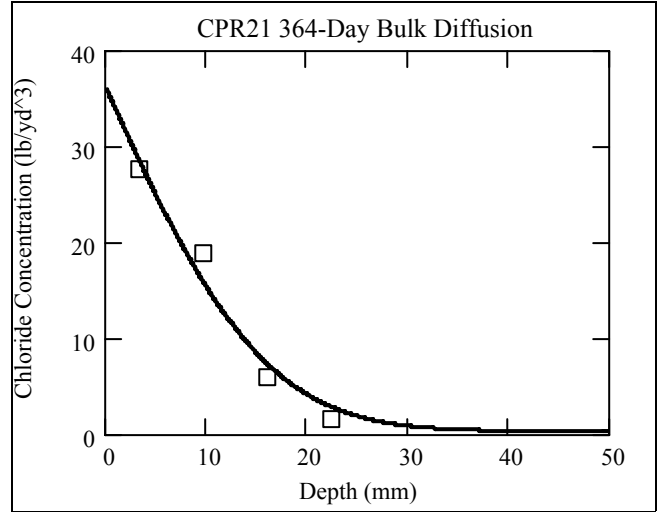
<b>Diffusion(m<sup>2</sup>/sec)</b>	2.428E-12	<b>Background(lb/yd<sup>3</sup>)</b>	0.119
<b>Surface(lb/yd<sup>3</sup>)</b>	27.209	<b>R<sup>2</sup> Value</b>	0.9987

**Complete Set of Results**

**Only CI Results of 200ppm and Above**



<b>Diffusion(m<sup>2</sup>/sec)</b>	2.405E-12	<b>Background(lb/yd<sup>3</sup>)</b>	0.316
<b>Surface(lb/yd<sup>3</sup>)</b>	36.086	<b>R<sup>2</sup> Value</b>	0.9912



<b>Diffusion(m<sup>2</sup>/sec)</b>	2.437E-12	<b>Background(lb/yd<sup>3</sup>)</b>	0.316
<b>Surface(lb/yd<sup>3</sup>)</b>	35.976	<b>R<sup>2</sup> Value</b>	0.9850